The Effect of Thermo-mechanical Treatments on the Micro-structure and Mechanical Properties of High Strength Low Alloy Steels Micro-alloyed With Vanadium.

A thesis
presented for the Degree of
Master
of
Mechanical Engineering
in the University of Canterbury
by

Ian George Trippner.

University of Canterbury,
Christchurch, New Zealand.
1990.

Acknowledgments.

I wish to express my sincere gratitude to Professor L.A. Erasmus, my supervisor, for his patient guidance and assistance throughout the years of work on this project. His help as a teacher and friend will never be forgotten.

I would further like to extend my thanks to all the staff of the Mechanical Engineering Department of the University of Canterbury, may of whom have been like family members to me.

This project was sponsored by Pacific Steel Ltd. of Auckland, New Zealand. I wish to thank Pacific Steel Ltd. for their generous assistance during the preparation of the samples for this work, and the Harold A. Longden Memorial Scholarship for the years 1987 and 1988. Special thanks to Mr N.M. Corry, Technical Services Manager and his staff.

I would finally like to thank all my friends, their names too many to mention, who have also supported me during the course of this project. Special thanks to my wife, Siang Lin.

Abstract.

A series of vanadium micro-alloyed high strength low alloy steels were tested to evaluate the effect thermo-mechanical treatments had on their mechanical properties. The properties under consideration were the mechanical strengths and strain ageing propensity, as defined by the standard tensile test, and the fracture mode transition temperaure, as defined by the Charpy impact test. Ferrite grain size was also evaluated, as was the portion of the interstitial nitrogen in the steel which was present in the form of a micro-alloy precipitate. Cooling rate was found to be the most significant factor in determining the ferrite grain size of the steel. Steel chemistry was found to be the primary factor in determining precipitation strengthening, this being independent of thermo-mechanical history. Carbon rich vanadium carbo-nitride precipitates in the steel were found to coarsen more rapidly than nitrogen rich precipitates, and a vanadium to nitrogen atomic ratio of less than 2:1 was, therefore, required to avoid loss of precipitation strengthening as a result of this effect. The effect of vanadium carbo-nitride precipitates on the fracture mode transition temperature of the steel was found to be essentially independent of cooling rate. It was dependent on the vanadium concentration of the steel, and on whether the carbo-nitride precipitates were coherent or non-coherent with the ferrite lattice. Strain ageing was found to be significantly reduced (less than 15 MPa) if the atomic ratio of vanadium to nitrogen was greater than 1.8:1. The fine precipitate present in the samples were found to be dissolved by standard acid dissolution nitrogen analysis techniques. As a result of this an alternate analysis technique was developed and shown to be more accurate in determining the concentration of nitrogen rich precipitates in the steel samples.

Contents.

List of Figures.

List of Tables.

Chapter 1.

Micro-alloying of Steel.

In a historical review of the micro-alloying of steel, Woodhead [1] states that the term "Micro-alloy" was first used in 1962 by Noren. The 25 years since then have seen a multitude of publications produced on the topic, together with a greater understanding of the principles involved, such that micro-alloyed steels now constitute a significant part of world steel production. It cannot be said, however, that knowledge associated with the micro-alloying of steel is complete.

Woodhead [1] draws a distinction between High Strength Low Alloy steels and micro-alloyed steels. HSLA steels are defined as those with yield strengths significantly greater than a mild (low carbon) steel, typically 250 MPa, but posses a wide range of compositions and micro-structures. For example, air cooled bainitic steels, and quenched and tempered martensitic steels containing alloy additions of between 0.5 and 3 wt. % are classified as HSLA steels. By comparison, micro-alloyed steels contain only small alloy additions, each typically less than 0.1% by weight, but again have mechanical properties superior to those of mild steel. A ferrite/pearlite micro-structure is typical, though acicular ferrite and dual phase micro-structures may also be produced. The distinction between micro-alloyed and HSLA steels is not generally clear, however, with different authors relating the < 0.1 wt. % definition to both micro-alloyed steels [2] and HSLA steels [3,4]. In this thesis micro-alloyed steels will be considered by Woodhead's definition.

Micro-alloying can have a significant influence on the properties of a steel. When combined with accurately controlled thermo-mechanical processing, a steel with a yield strength of greater than 500 MPa can be produced with good toughness, and possessing reasonable formability and weldability [5].

Titanium, niobium and vanadium are the three most commonly used micro-alloying elements. They form very stable carbides and nitrides which may precipitate in the austenite and/or ferrite phase, depending upon their relative solubilities and the thermo-mechanical history of the steel. Figure 1.1 [6] shows the relative solubilities of these micro-alloy carbides and nitrides in austenite (and also in ferrite for VC and VN). They are in the form of solubility product (as an atomic percent) plotted against inverse temperature, producing a linear relationship.

Precipitation in the austenite phase produces two main effects. Firstly, a fine dispersion of precipitates prevents temperature induced grain growth. During hot rolling the presence of these precipitates will allow a successively finer austenite grain size to be attained, and maintained. A fine austenite grain size assists in obtaining a fine ferrite grain size, and thus enhanced mechanical properties in the steel. Secondly, precipitation on dislocations in the austenite may retard recrystallisation, such that at lower hot rolling temperatures a severely elongated austenite grain structure is obtained. This structure also leads to a fine ferrite grain size after transformation. One or both of these effects may be used to reduce the austenite grain size before transformation to ferrite.

Precipitation in the ferrite phase, or at the phase interface during transformation from austenite

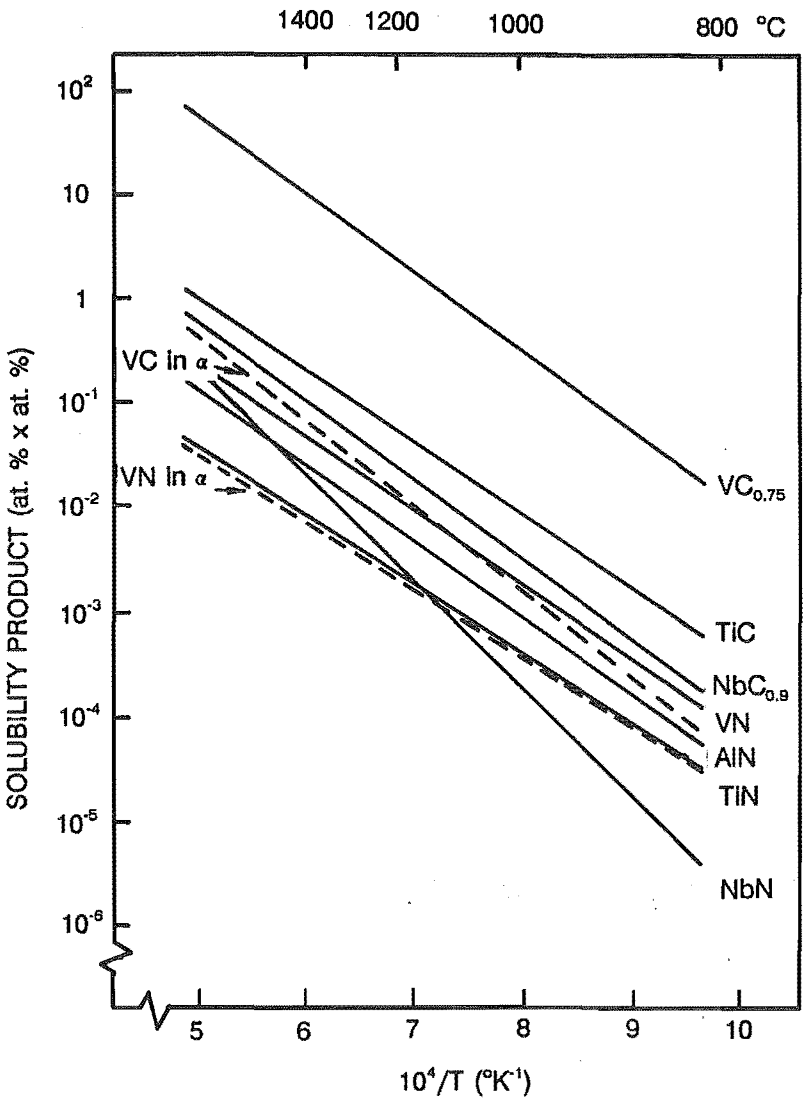

Figure 1.1 The solubility product of micro-alloy carbides and nitrides in austenite and ferrite [6].

to ferrite (interphase precipitation) causes an increase in the yield strength of the steel, by increasing the resistance to dislocation motion.

Precipitation is a complex topic which is still not fully understood. (For example, an appreciable effort is still aimed at evaluating the structure and composition of interphase precipitates). Each micro-alloying element has specific precipitation preferences, and thus must be considered separately [4,7,8,9,10]. This includes both their effects on processing [11] and the resulting structure - property relationships [12].

Other micro-alloying elements may also be added to steel to enhance its properties. Calcium, caesium, zirconium, (and titanium) are used for sulphide shape control to enhance the formability of the steel. Boron and molybdenum promote the formation of bainite or acicular ferrite in steels.

Further information about HSLA steels, and the general micro-alloying of low carbon steel can be obtained from one or more of the many good publications on the subject [13,14,15,16]. These publications include details about precipitation and the effects of controlled rolling and accelerated cooling on the final microstructure and mechanical properties of the steel. They also discuss the production processes used, and the post-production use of quenched and tempered steels, acicular ferrite and bainitic steels, dual phase steels, as well as ferrite/pearlite steels. Inclusion shape control is also covered.

This thesis is primarily concerned with micro-alloying with vanadium. The greater solubility of its carbides and nitrides in the austenite phase, when compared to titanium or niobium (see figure 1.1), means that for a similar micro-alloy addition, vanadium is retained in solution in the austenite to a lower temperature. This allows precipitation of carbides and nitrides to be induced in both the austenite and ferrite phase, depending on mechanical property requirements. For a quenched and tempered steel, a vanadium micro-addition remains dissolved at lower solution temperatures, before quenching, increasing the hardenability of the steel [17]. In a low carbon steel, however, increasing the hardenability of the steel is undesirable, as the presence of martensitic or bainitic phases reduce ductility and formability. Precipitation of vanadium nitride and carbide (face centered cubic [18] precipitates formed by a supersaturation of vanadium and nitrogen or carbon, respectively, in the iron matrix) in both the austenite and ferrite phases is preferable. If this precipitation is fine, with a high volume fraction, grain size control and precipitation hardening of the steel can be achieved.

A micro-addition of vanadium is not always sufficient to improve the mechanical properties of low carbon steel. The chemical composition of the steel, and its thermo-mechanical history also affect the formation of vanadium nitride and carbide, and thus the mechanical properties of the steel.

The aim of this work is to examine, in detail, relationships between the final mechanical properties of a vanadium micro-alloyed low carbon steel and its chemistry and thermo-mechanical history. Once defined, these relationships will allow primary factors controlling the mechanical properties to be isolated, and, therefore, applied to the production of a vanadium micro-alloyed low carbon steel, so as to achieve optimum mechanical properties at minimum production cost.

Chapter 2.

Micro-alloying of Steel With Vanadium.

2.1 Solubility and Composition of Precipitates Formed in a Vanadium Micro-alloyed Low Carbon Steel on Cooling from the Austenite Phase.

A variety of similar expressions for the solubility of vanadium nitride and vanadium carbide in both austenite and ferrite phases in steel have been produced by different authors. These are shown in figures 2.1 [19] and 2.2 [19], respectively. From these figures it can be seen that a) the solubility of both vanadium nitride and carbide decrease significantly during the phase change from austenite to ferrite, and b) the solubility of vanadium nitride in austenite is less than that of vanadium carbide in ferrite. This has been noted by Woodhead [18] (see figure 2.3 [18]).

Solubility curves in figures 2.1, 2.2 and 2.3 represent equilibrium reactions, for example:

$$[V] + [N] \rightleftharpoons [VN]$$

On re-heating a billet to 1300 °C it may take many hours to reach thermal equilibrium, and equilibrium between VN precipitates and vanadium and nitrogen in solution in he austenite. This time period is governed by the dimensions of the billet (governing time at temperature of the billet core), and the diffusion rate of vanadium and nitrogen in austenite. It is also affected by the size, and therefore the dissolution time of existing vanadium nitride precipitates.

The solubility of vanadium nitride in austenite has also been shown to increase with the steel's manganese content [7,20], due to the effect of manganese on the activity of nitrogen.

Vanadium carbide and vanadium nitride have face centered cubic structures, with similar lattice parameters, being ideally represented as VC and VN, respectively [18]. These structures often contain lattice defects, however, such that the true stoichiometry may range from $VX_{0.75}$ to VX (X=C,N). In steel, analysis of electron diffraction patterns produced by these precipitates (from extraction replicas or thin foil samples) show that the composition of vanadium carbide tends towards $VC_{0.75}$, whereas vanadium nitride tends towards VN [18]. Roberts and Sandberg [19], using a thermodynamic argument related to the activity of carbon in steel, suggest that vanadium carbide is better represented as VC than V_4C_3. Their analysis considered a vanadium micro-alloyed low carbon steel that is free from both nitrogen and vanadium nitride (Carbon 0.1 wt. %, Vanadium 0.1 wt. %). In austenite, they argued, any carbide formed would have a composition ranging between $VC_{0.92}$ and $VC_{0.96}$. In ferrite only a carbide of composition VC would be formed (the activity of carbon in ferrite being higher than the activity of carbon in austenite). They found that for a carbon concentration of 0.1 wt. % the activity of interstitial carbon in both austenite and ferrite would require a vanadium concentration of approximately 2 wt. % before any carbides with a composition of V_4C_3 were formed. This argument is perfectly feasible, considering the physical similarities of vanadium carbide and nitride precipitates, and the possible inaccuracies that would arise from their physical analysis, the size of these precipitates being measured in nanometres. For this reason both vanadium carbide and nitride will be considered to exist as VC and VN, respectively.

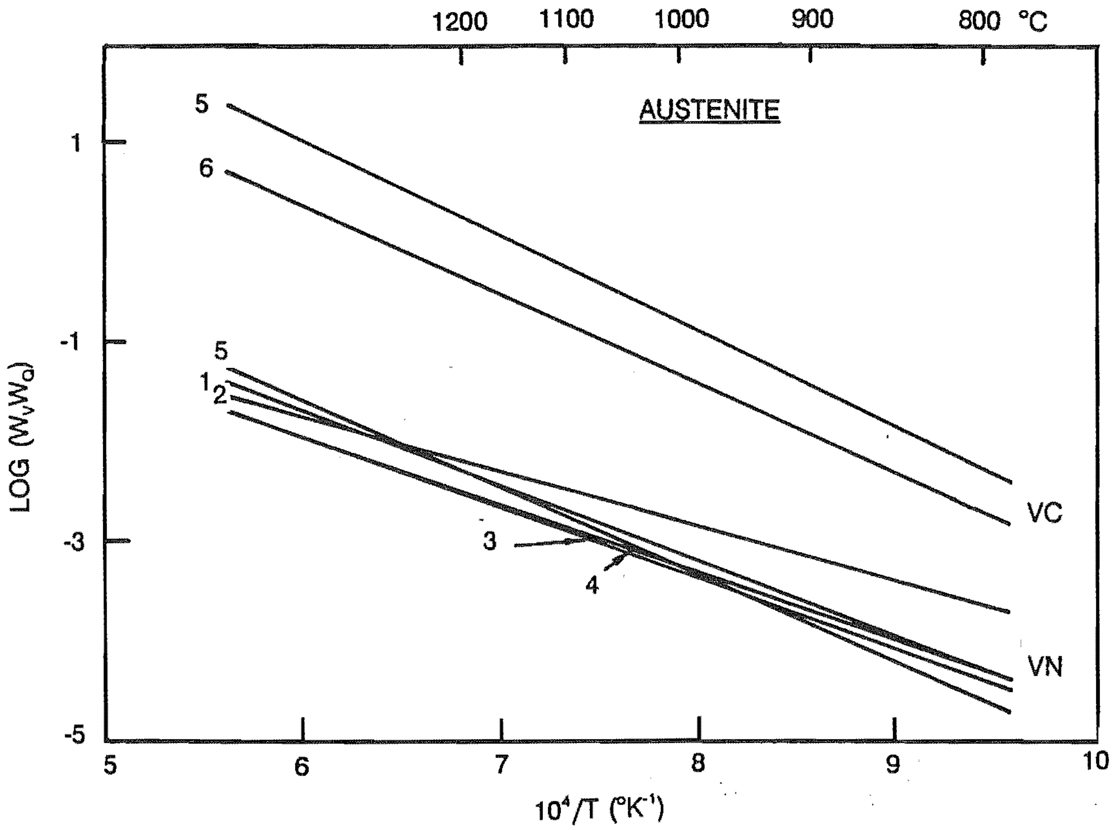

1 Irvine et. al.

2 Engineer

3 Konig et. al.

4 Frohberg & Graf

5 Narita

6 Bungardt et. al.

Figure 2.1 The solubility of vanadium nitride and vanadium carbide in austenite [19] (expressed as the log of a solubility product of weight percentage).

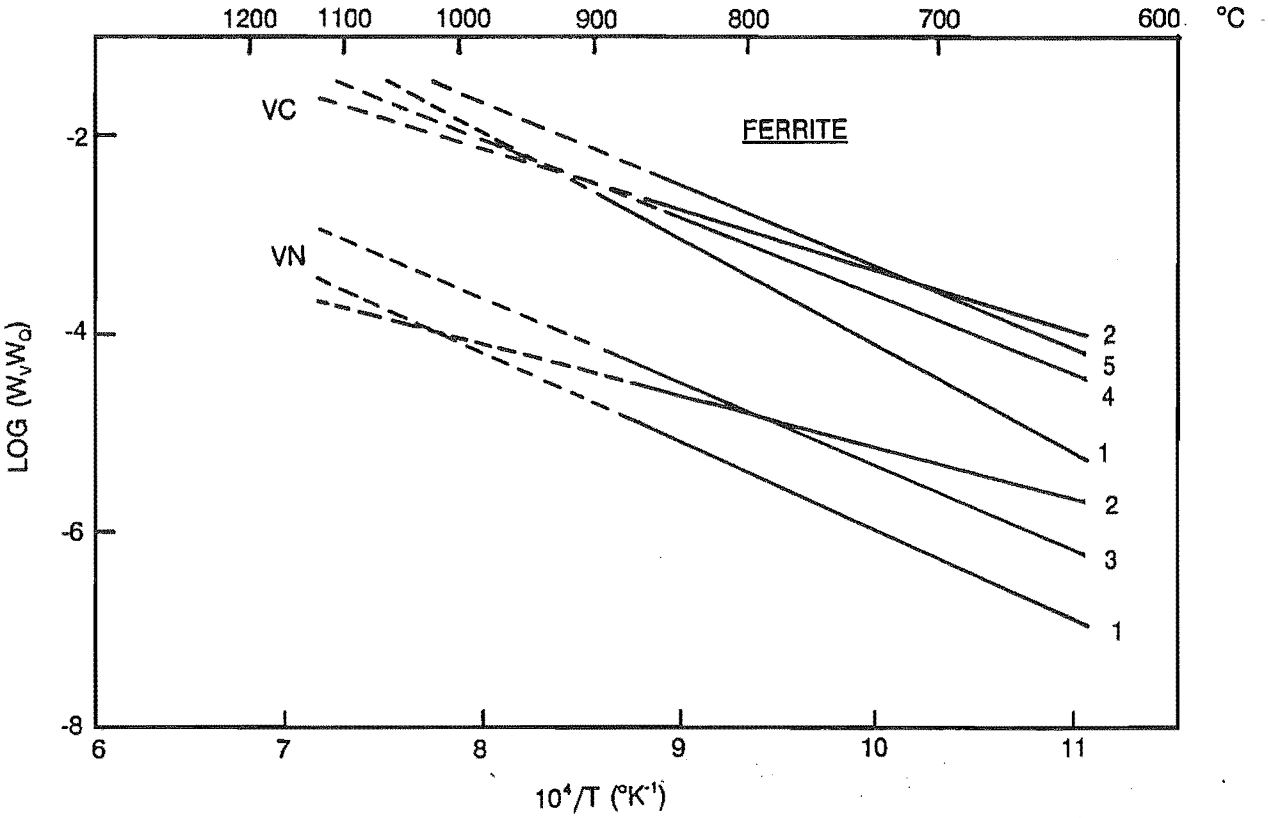

1 Calculated from solubility in austenite

2 Koyama et. al.

3 Frohberg & Graf

4 Sekine et. al.

5 Seriko et. al.

Figure 2.2 The solubility of vanadium nitride and vanadium carbide in ferrite [19] (expressed as the log of a solubility product of weight percentage).

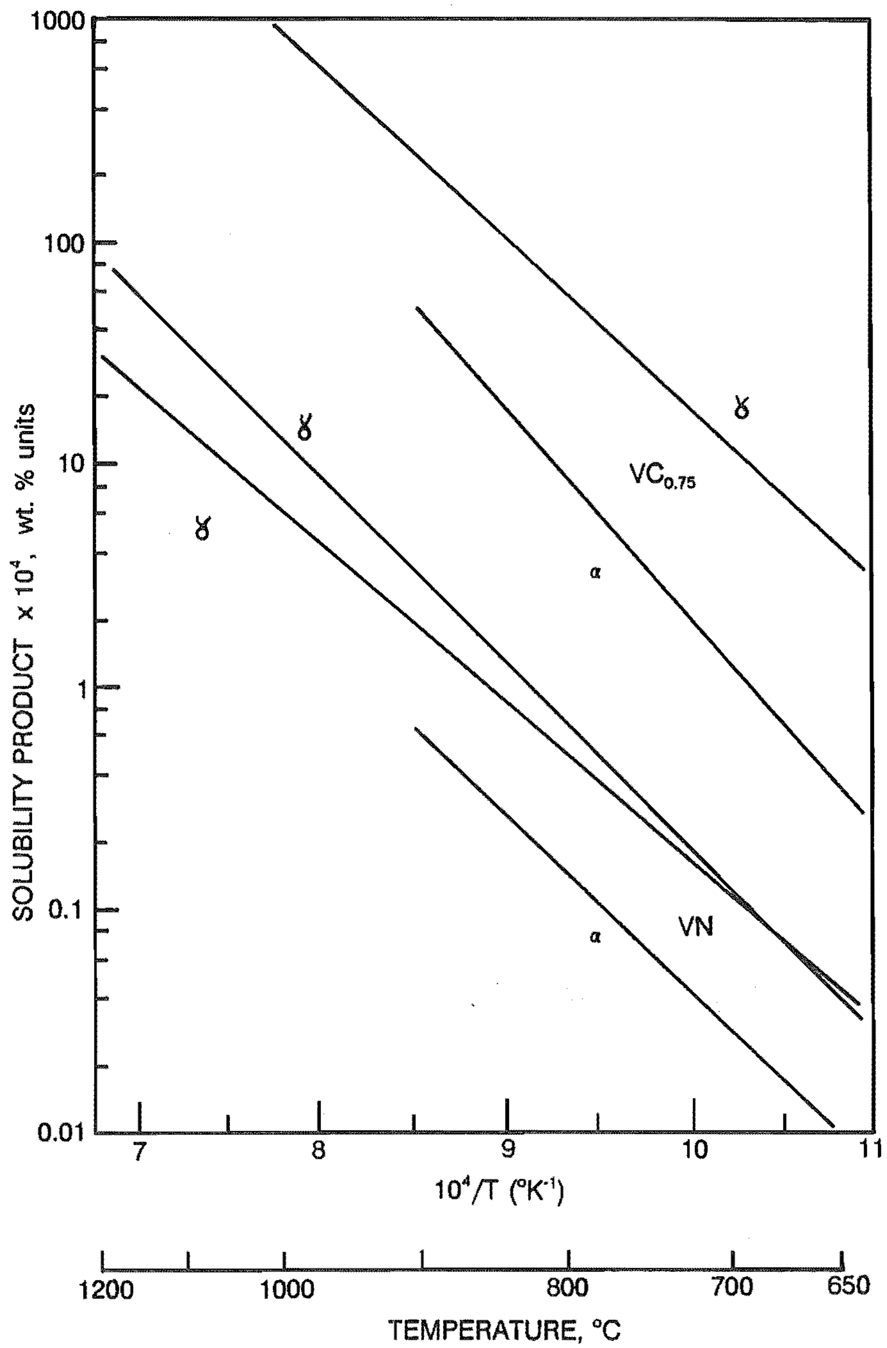

Figure 2.3 The relationship between the solubility of vanadium nitride and vanadium carbide in both austenite and ferrite [18].

Vanadium carbide and vanadium nitride are mutually soluble in both austenite and ferrite [18,19]. Precipitates formed on the cooling of a vanadium micro-alloyed steel will therefore be of the form VC_xN_y, where the ratio of "x" to "y" is dependent on the relative amounts of carbon and nitrogen in solution. Following the same argument outlined above, that is, vanadium carbide and nitride exist in a one to one atomic ratio (VC and VN, respectively), it will be assumed that $x+y=1$ [19]. The composition of the precipitate can therefore be defined as VC_xN_{1-x}. Any deviations from stoichiometry will be neglected.

For equilibrium precipitation in austenite, Roberts and Sandberg [19] found that the carbo-nitride formed is nitrogen rich ($x < 0.25$). For a typical vanadium micro-alloy addition of 0.1 wt. % this nitrogen rich carbo-nitride is formed at all temperatures in the austenite range unless the carbon concentration is high (> 0.2 %), as can be seen in figures 2.4 [19] and 2.5 [19]. In figure 2.4, considering austenite at a temperature of 900 °C, the value of "x" is plotted as a function of nitrogen concentration in solution (wt. %) for a steel containing 0.1 wt. % vanadium and carbon concentrations up to 0.5 wt. %. It can be seen that the initial nitrogen concentration of precipitates formed during the cooling of a vanadium micro-alloyed steel is high. For example, with carbon and nitrogen concentrations of 0.1 wt. % and 0.01 wt. %, respectively, and with 0.1 wt. % vanadium, the initial precipitate formed will have a value of "x" of approximately 0.07. As further precipitate forms its nitrogen content decreases, but only slightly. At the solubility limit, ie. the point where there is not enough vanadium in solution to form a precipitate at that temperature, the value of "x" is only 0.25.

Figure 2.5 is the same as figure 2.4, with the exception that it considers austenite at 800 °C. (Note: The data in this figure was generated mathematically, not experimentally. This explains why the austenite phase is present at 800 °C with carbon contents less than 0.2 wt. %). Comparing these figures, it can be seen that the carbon concentration of precipitates which are formed increases as the steel cools. The carbo-nitride precipitates can still be considered to be nitrogen rich, however.

As nitrogen rich VC_xN_{1-x} is formed, the concentration of carbon, with respect to nitrogen increases, such that the carbon concentration of the precipitate increases. The precipitation rate decreases however, as the concentration of vanadium in solution decreases. This situation becomes more complex in a multi-alloy system. In titanium - vanadium [21] and niobium - vanadium [22] micro-alloyed steels, for example, the precipitates formed are (Ti,V).(C,N) and (Nb,V).(C,N), respectively. All these elements are mutually soluble in austenite (and ferrite), and controlled by different solubility criteria. Figure 2.6 [23], considering a micro-alloy steel containing 0.07 wt. % titanium, 0.07 wt. % vanadium, 0.05 wt. % niobium, 0.07 wt. % carbon and 0.007 wt. % nitrogen, shows how complex precipitation in a multi-alloy system can be. When cooling this steel from 1700 °C, a titanium rich nitride will be the first precipitate to form at approximately 1650 °C. Precipitation of titanium rich nitride will continue as the steel cools, until a temperature of 1200 °C is reached, when a niobium rich nitride will also begin to form. Continuing along the horizontal axis, representing the cooling of the steel, a titanium rich carbide will be next to form, followed by a niobium rich carbide, a vanadium rich nitride and finally a vanadium rich carbide. Obviously, there is insufficient nitrogen in solution to form nitrides with all these elements, so the actual carbides and nitrides precipitated will depend on precipitation kinetics and the cooling rate of the steel. The vertical axis represents the amount of precipitate formed as the curves are followed during cooling. Though not accurate, this figure gives an indication as to how complex precipitation in a multi-alloy system can be. At any given temperature, multiple micro-alloy additions are competing for available carbon and nitrogen, and forming complex precipitates to overcome unfavourable precipitation kinetics.

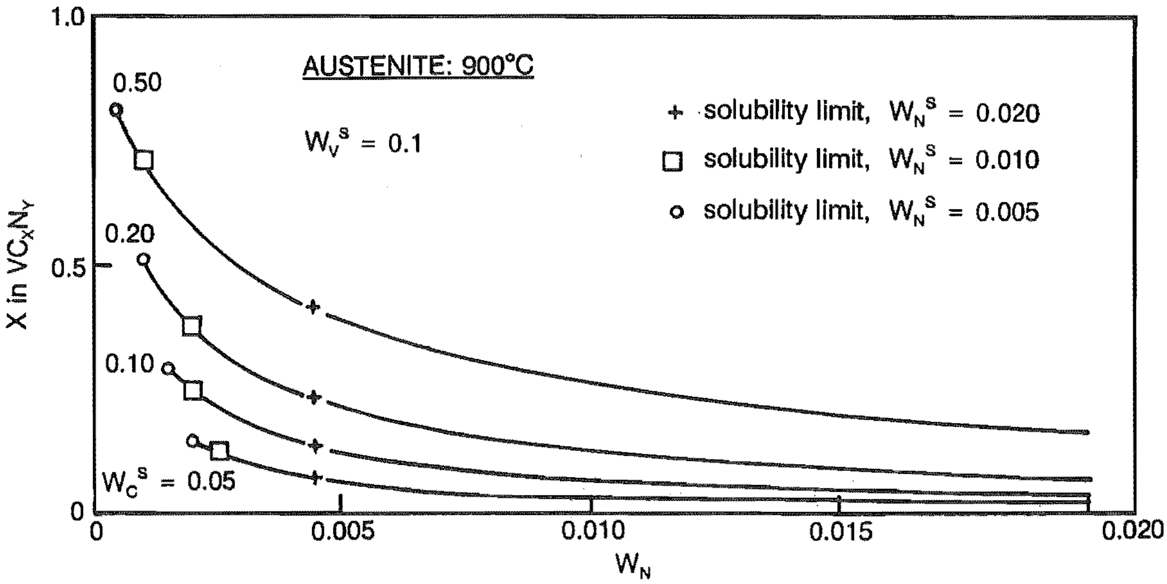

Figure 2.4 Composition of vanadium carbo-nitride precipitates, with respect to nitrogen content, in austenite at 900 °C [19].

W_V^S = wt. % vanadium in solution before start of precipitation.
W_N = wt. % nitrogen in solution.
W_N^S = wt. % nitrogen in solution before start of precipitation.
W_C^S = wt. % carbon in solution before start of precipitation.

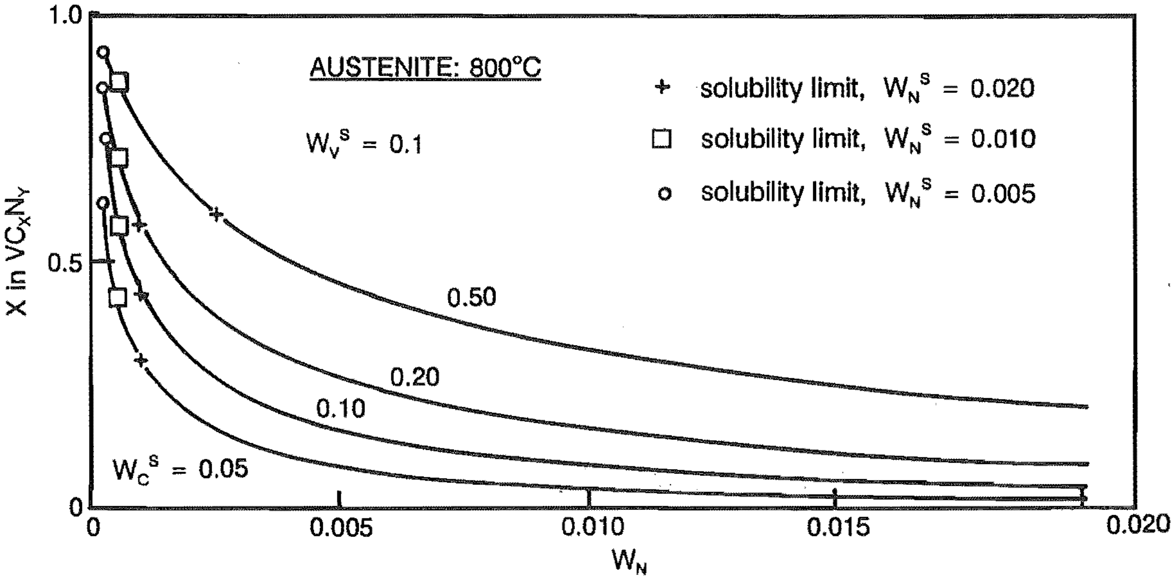

Figure 2.5 Composition of vanadium carbo-nitride precipitates, with respect to nitrogen content, in austenite at 800 °C [19].

W_V^S = wt. % vanadium in solution before start of precipitation.
W_N = wt. % nitrogen in solution.
W_N^S = wt. % nitrogen in solution before start of precipitation.
W_C^S = wt. % carbon in solution before start of precipitation.

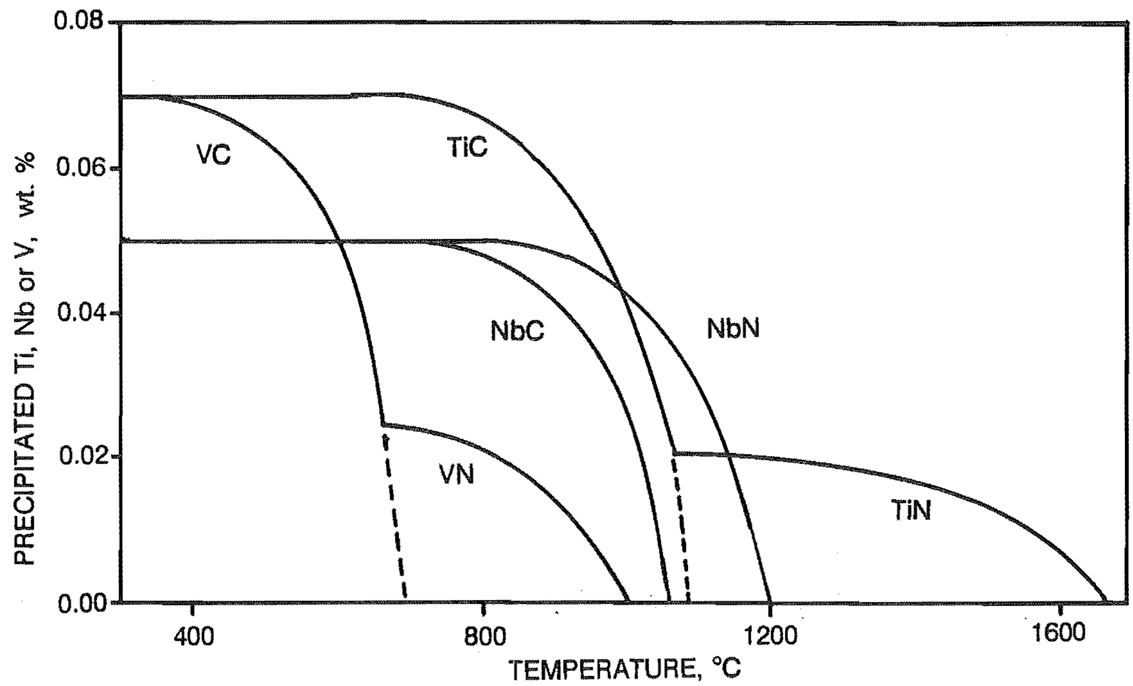

Figure 2.6 Solubility driven precipitation in a micro-alloy steel containing multiple alloy additions. Composition of precipitate fraction as a function of temperature [23].

The phase change from austenite to ferrite is accompanied by precipitation at the interphase boundary [18,19,24,25,26]. This is due to the decrease in the solubility of vanadium carbide and vanadium nitride in ferrite.

There has been some speculation as to the composition of interphase precipitates, this being related to which side of the interphase boundary the precipitates actually form.

Woodhead [18] suggests that interphase precipitation is essentially VC. Though sufficient nitrogen probably exists in solution to form a high nitrogen carbo-nitride, carbon is rejected to the austenite at the interphase boundary as pro-eutectoid ferrite is formed, increasing the local carbon concentration of the austenite, and therefore the driving force for the production of vanadium carbide. If Woodhead's [18] assumption is true, then the precipitates must be formed on the austenite side of the phase boundary. This being the case, Roberts and Sandberg [19] suggest that this interphase precipitation varies in concentration from VC to $VC_{0.5}N_{0.5}$. This is shown in figure 2.7 [19]. At a temperature of 700 °C, say, a vanadium micro-alloyed steel with a nitrogen concentration of 0.010 wt. % would be expected to form precipitates of approximate composition $VC_{0.55}N_{0.45}$ as it transforms from austenite to ferrite. "W_C", on the right vertical axis, represents the carbon concentration at the phase interface, this increasing as temperature decreases. The exponent symbolises that the carbon concentration is dependent on that of the austenite phase.

The presence of fine precipitates in the austenite phase would be expected to slow the progress of the interphase boundary. The austenite to ferrite phase change in micro-alloyed steels, however, does not appear to be retarded by interphase precipitation [27]. This implies that the precipitates are actually formed on the ferrite side of the interphase boundary. Baker [28] agrees with this conclusion, stating that precipitation in the ferrite phase would allow homogeneous nucleation to occur, accounting for the observed diffraction patterns from such precipitates. These diffraction patterns imply that the precipitates were coherent or partially coherent. If the dependent carbon concentration is that of ferrite, Roberts and Sandberg [19] argue that the precipitate will be nitrogen rich, as can be seen from figure 2.8 [19]. In the example mentioned above (700 °C, 0.010 wt. % nitrogen) the precipitate formed on the ferrite side of the interphase boundary would have an approximate composition $VC_{0.05}N_{0.95}$. The exponent symbol associated with "W_C", in this case, implies that the carbon concentration is dependent on that of the ferrite phase.

It can be seen that there is no clear agreement on the composition of interphase precipitates in a vanadium micro-alloyed steel. Considering that the maximum precipitation rate for vanadium nitride in ferrite has been found to occur at approximately 700 °C [5,29], it is possible that interphase precipitation is just a special case of general ferrite precipitation. The high diffusion rate at the interphase boundary, together with the high interstitial concentration, allows vanadium and nitrogen to form multiple pre-precipitation clusters rapidly, subsequently growing into precipitates in the ferrite phase. At normal air cooling rates these clusters/precipitates would have insufficient time to grow significantly, dissolve and diffuse through the ferrite matrix to a more favourable nucleation site, or undergo decomposition in the presence of a larger, more stable precipitate. This would leave fine precipitates in rows parallel to the position where the interphase boundary previously existed. Other precipitate morphologies mentioned by Honey-combe [2,27,30] are probably a function of other variables, such as cooling rate of the steel, the temperature of transformation, or the post transformation orientation of the ferrite matrix. This argument, being in agreement with that used by Baker [28] above, is the one which will be followed hereafter.

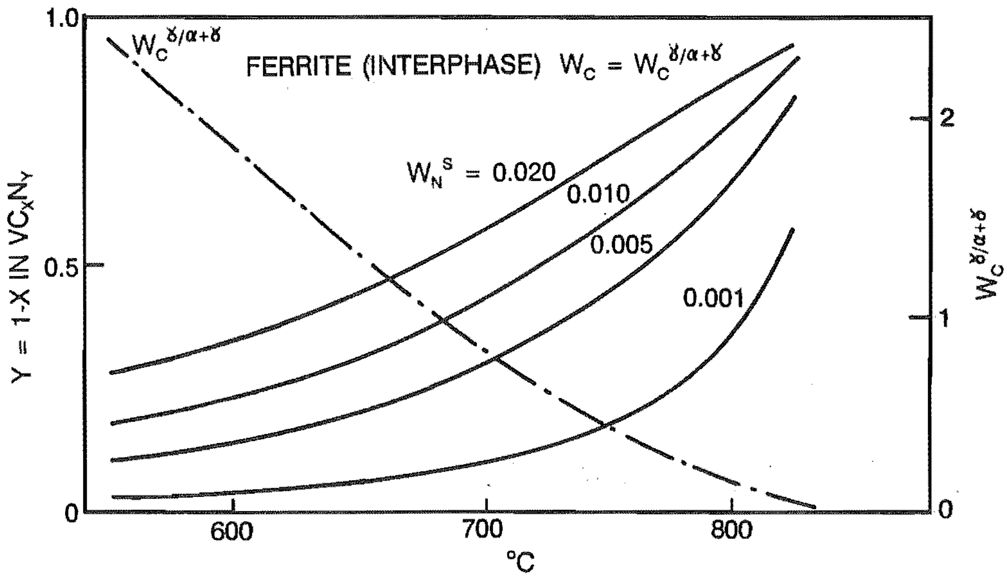

Figure 2.7 Composition of interphase vanadium carbo-nitride precipitates, with respect to temperature, when precipitation is dependent on austenite carbon concentration [19].

W_N^S = wt. % nitrogen in solution before start of precipitation.

$W_C^{\gamma/\alpha+\gamma}$ = wt. % carbon in solution, as determined by the austenite carbon concentration.

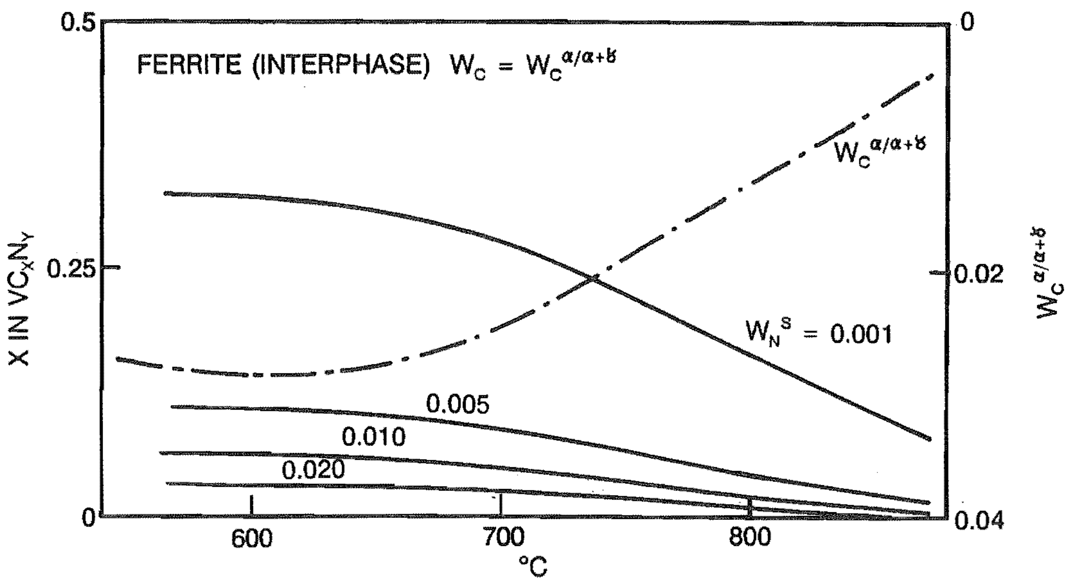

Figure 2.8 Composition of interphase vanadium carbo-nitride precipitates, with respect to temperature, when precipitation is dependent on ferrite carbon concentration [19].

W_N^S = wt. % nitrogen in solution before start of precipitation.

$W_C^{\alpha/\alpha+\gamma}$ = wt. % carbon in solution, as determined by the ferrite carbon concentration.

The volume of interphase precipitation in a vanadium micro-alloyed steel is likely to be small [18]. It is controlled by the bulk composition of the steel, with respect to vanadium, carbon and nitrogen. As interphase precipitation exists as closely spaced rows of fine precipitates, it plays an important part in determining the mechanical properties of the steel [24] (see section 2.5).

Other precipitation in the ferrite phase is general in nature (random), occurring at local high energy sites such as ferrite grain boundaries and dislocation structures within the ferrite grains [27]. Again considering the thermodynamic analysis done by Roberts and Sandberg, the results of which are shown in figure 2.9 [19], it can be said these precipitates are nitrogen rich carbo-nitrides. As mentioned previously, the maximum precipitation rate of these nitrogen rich carbo-nitrides in ferrite is at approximately 700 °C [5,29]. Figure 2.10 [5], relates to samples that were initially heated in an argon atmosphere for four hours at 1125 °C before being placed in a furnace at a "simulated coiling temperature" for 30 minutes, one hour, or two hours. They were not exposed to any mechanical treatments. Analysis of nitrogen combined as VN was carried out using a technique which involves dissolving a sample of the steel in dilute sulphuric acid. Micro-alloy precipitates in the sample (VN in this case) will not dissolve, and can therefore be separated and analysed. (Details of this analysis technique can be found in Appendix A). The peak at 700 °C indicates that precipitation rate of vanadium nitride in ferrite is greatest at this temperature, being the point where maximum volume fraction of ferrite is at its highest temperature.

The growth (coarsening) rate of micro-alloy precipitates is primarily a function of temperature [8]. High temperatures accelerate the diffusion rates of the atomic species, enhancing the growth rate of the precipitates. In the case of vanadium carbo-nitride precipitates however, their growth rate is also determined by their composition. Balliger and Honeycombe [31], using dark field electron optical images produced by transmission electron microscopy of thin film samples, found that carbon rich precipitates (close to VC) coarsen more rapidly than those having larger nitrogen concentrations. Figure 2.11 [31], considers the mean particle size of both vanadium carbide and carbo-nitride precipitates, as a function of time, while being aged at a temperature of 790 °C. The error bars represent the standard deviation of the mean. It can be seen that anywhere within the time period shown, the size of the carbide precipitates are between two and three times the size of the carbo-nitride precipitates, despite the fact that they were of a very similar size before ageing. The gradient of the carbide curve, representing the coarsening rate of the precipitates, is also significantly greater than that for the carbo-nitride curve. The coarsening rates of vanadium nitride and carbo-nitride were found to be very similar [31], indicating that the presence of nitrogen in the precipitate has a very significant effect on the coarsening rate. Balliger and Honeycombe [31] have suggested that the segregation of nitrogen to the perimeter of the carbo-nitride would cause its coarsening rate to decrease as its nitrogen concentration increased, the smaller size of the nitrogen atom, when compared with the carbon atom, producing a lower mismatch with the ferrite matrix. A nitrogen rich precipitate would, therefore, produce a lower coherency strain in the surrounding matrix, allowing the formation of "larger" coherent precipitates. Coherent precipitates have a lower interfacial energy associated with them, and therefore a lower rate of coarsening. A secondary result of this nitrogen segregation would be seen in the mechanical properties of the steel. For the same precipitate size, a coherent precipitate will produce a larger value of frictional stress in the steel (see section 2.5), and thus a higher yield stress value, all other parameters being equal [20]. It would therefore appear that a vanadium micro-addition to a low carbon steel could be optimised by having a proportionally larger nitrogen concentration in the steel, such that sufficient nitrogen exists in solution to allow the formation of high nitrogen carbo-nitride precipitates. It must be noted, however, that high values of

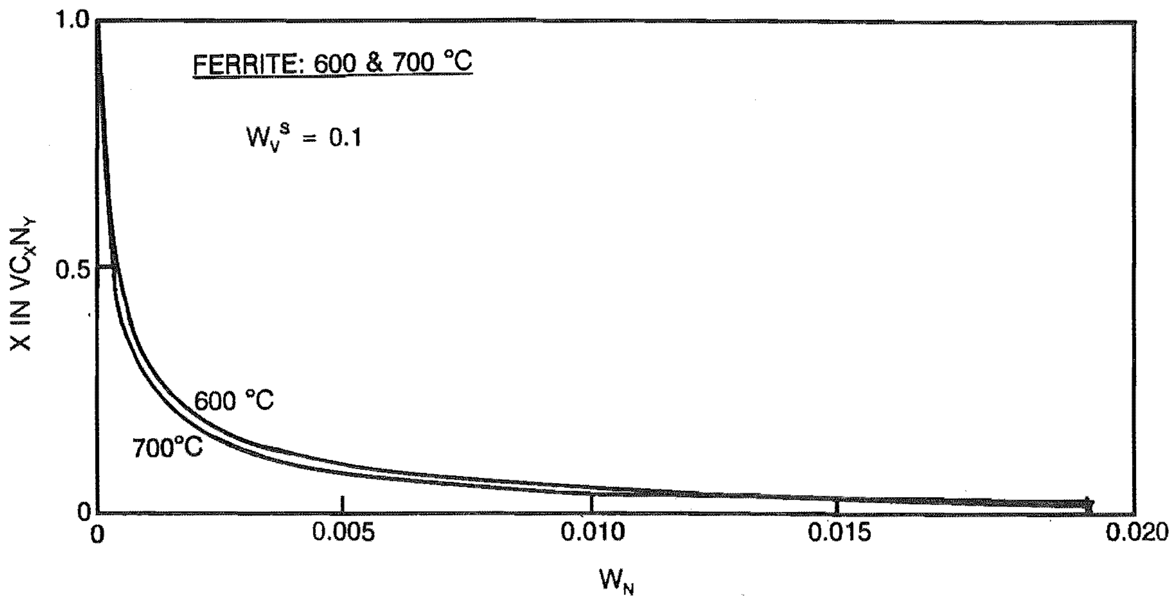

Figure 2.9 Composition of vanadium carbo-nitride precipitates, with respect to nitrogen content, in ferrite at 600 °C and 700 °C [19].

W_V^S = wt. % vanadium in solution before start of precipitation.
W_N = wt. % nitrogen in solution.

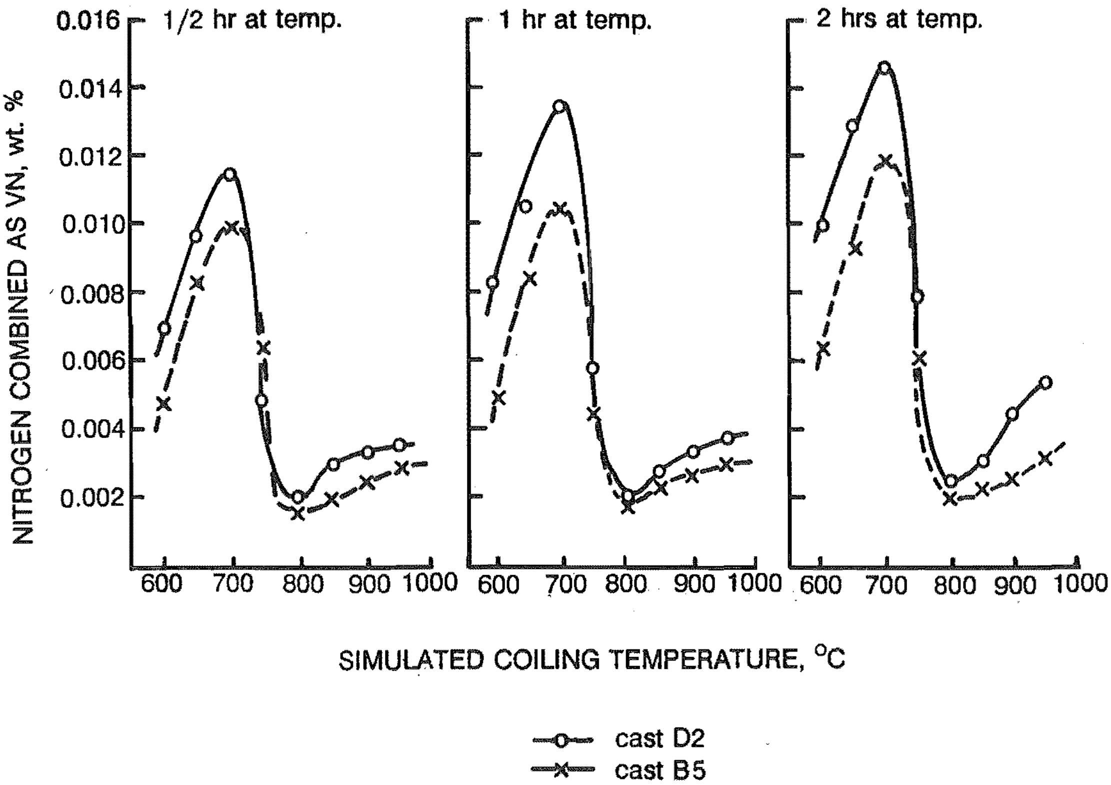

Figure 2.10 The effect of temperature on precipitation rate of vanadium nitride in ferrite [5].

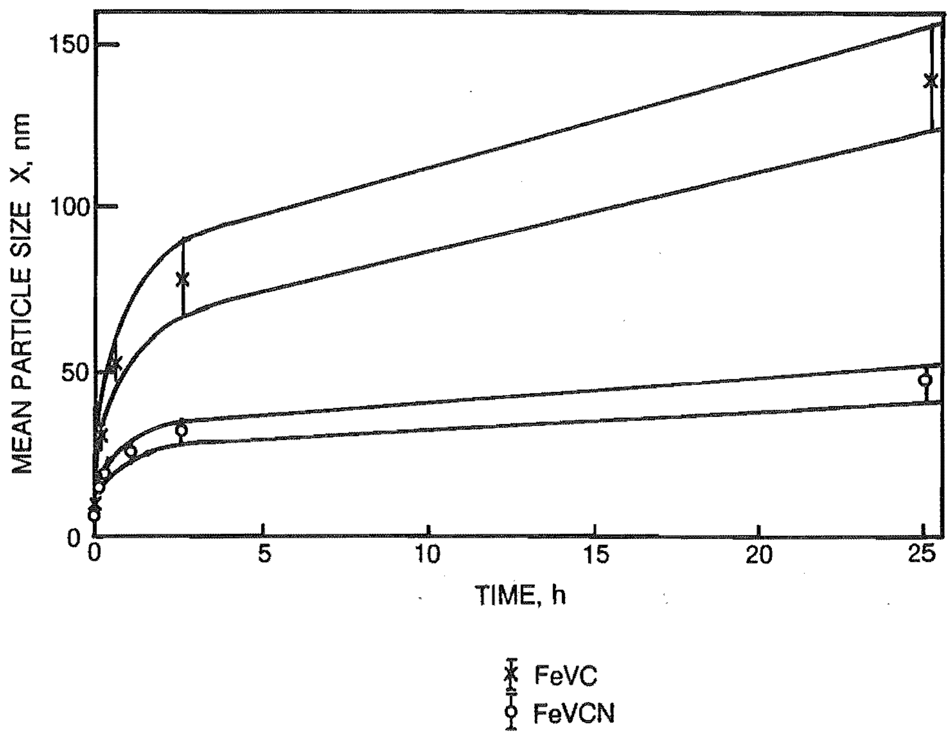

Figure 2.11 The effect of precipitate composition on the ageing characteristics of a vanadium micro-alloyed steel aged at 790 °C [31].

interstitial nitrogen increase the strain ageing propensity of the steel, this being detrimental (see section 2.5).

Precipitate coarsening has been shown to give a linear relationship between a logarithmic plot of mean particle size versus log time during ageing at elevated temperature. Figure 2.12 [31] shows such a plot for vanadium carbide and carbo-nitride precipitates in a vanadium micro-alloyed steel aged at 790 °C. The inverse gradient of the VCN line on this figure ("n") varies from 2, through 3, to 5, the coarsening rate of each portion of the curve being proportional to $(\text{time})^{0.5}$, $(\text{time})^{0.33}$, and $(\text{time})^{0.2}$ respectively. The VC line follows similar gradients. Balliger and Honeycombe [31] have suggested a possible explanation for this trend. For the vanadium carbo-nitride precipitates: the micro-structure of a vanadium micro-alloyed low carbon steel contains nitrogen rich carbo-nitride precipitates spread randomly throughout the ferrite matrix. The ferrite matrix will also have a minor dislocation network, formed during the austenite to ferrite transformation. During ageing, precipitates which have formed on dislocation networks will grow rapidly, diffusion being assisted by the presence of these dislocations (ie. coarsening rate is controlled by pipe diffusion $(\text{time})^{0.5}$). Initially, however, the majority of the precipitates do not form on dislocation, but rather in the ferrite matrix itself. Growth of these precipitates is controlled by the two directional transfer of vanadium, nitrogen and carbon across the interface between the precipitate and the ferrite matrix (ie. coarsening rate is controlled by the interface reaction $(\text{time})^{0.2}$). In the early stages of ageing, this is the dominant coarsening mechanism, there being only a comparatively small number of precipitates existing on dislocations. As ageing proceeds however, precipitates formed on dislocation grow faster then those in the ferrite matrix, some of the latter dissolving to "feed" the growth of larger, more stable precipitates. At this stage coarsening of the precipitates is equally controlled by both interface reaction and pipe diffusion (ie. coarsening rate is controlled by bulk diffusion $(\text{time})^{0.33}$). Finally, only a relatively "few" large precipitates exist, the majority of these existing on dislocations. Coarsening rate is dependent primarily on pipe diffusion after this point.

Considering now the vanadium carbide precipitates, it appears that pipe diffusion coarsening does not take place. Balliger and Honeycombe [31] suggest that the presence of nitrogen in the steel accelerates the austenite to ferrite transformation, thus increasing the dislocation density of the ferrite. This would cause the change from bulk diffusion controlled coarsening to coarsening by pipe diffusion to occur sooner in the VCN steel. This would also explain why coarsening primarily by pipe diffusion had not yet been observed for VC steel.

In the case of ageing a cold rolled steel, precipitate coarsening would evolve rapidly, due to the high dislocation density present after rolling. Coarsening by interface reaction would not, therefore, be significant [31].

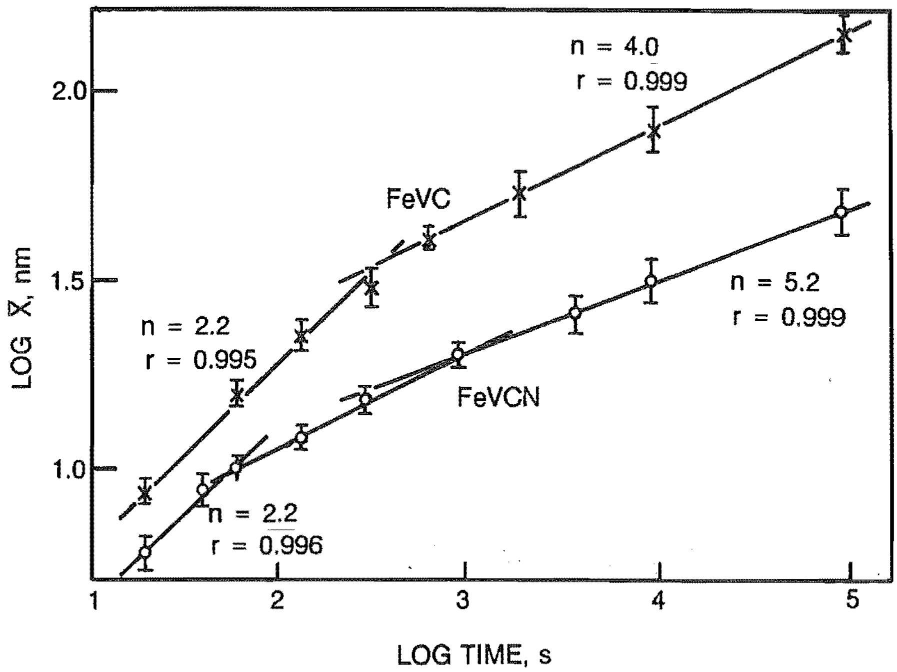

Figure 2.12 Logarithmic plot of mean precipitate size, as a log function of ageing time ($\bar{X}=Kt^{1/n}$), for vanadium carbide and vanadium carbo-nitride precipitates aged at 790 °C [31].

n = reciprocal of gradient.
r = correlation coefficient.

2.2 The Effect of Precipitation on Austenite Recrystallisation in a Vanadium Micro-alloyed Low Carbon Steel.

Micro-alloying elements, such as titanium, niobium, and vanadium are known to have a retarding effect on austenite recrystallisation during hot or controlled temperature rolling [11]. This effect becomes more pronounced as the rolling temperature is reduced, such that recrystallisation may be completely inhibited if rolling is carried out at temperatures close to the Ar_3 temperature. The temperature below which recrystallisation no longer occurs, is known as the Recrystallisation Stop temperature. The R-S temperature of a micro-alloyed steel increases with the micro-alloy addition, the rate of increase being dependent on the micro-alloy involved [32], as shown in figure 2.13 [32]. It should be noted from the figure that niobium has the greatest effect on the R-S temperature (as a function of atomic percent), vanadium having the least. Also, the result for aluminium should be considered sceptically, as it appears to be based on only one measurement.

The retardation of recrystallisation in deformed austenite is caused by the presence of micro-alloy solute atoms in the austenite lattice, or by strain induced precipitates on sub-boundaries in the austenite [33]. Micro-alloy solute atoms in the austenite phase prevent dislocations on slip bands "climbing" to form sub-grain boundaries within the existing deformed austenite grains. This prevents the nucleation of new austenite grains [33]. Strain induced precipitates form on the grain boundaries of new recrystallised grains, preventing their growth, and thus halting recrystallisation before it is completed [11]. Titanium, niobium, and vanadium retard the onset of recrystallisation by both these mechanisms. Vanadium, however, exerts only a limited retarding effect in the solute form [8,11], producing no delay in austenite recrystallisation at temperatures above 1100 °C [33]. Below 950 °C, however, recrystallisation has been observed to be retarded by the presence of strain induced precipitates of vanadium nitride [18,33,34,35]. Figure 2.14 [36] shows static recrystallisation and precipitation as functions of time and temperature. In the case of micro-alloying with vanadium and nitrogen, the recrystallisation and precipitation curves intersect at approximately 900 °C, indicating that recrystallisation cannot occur in the absence of precipitation at this temperature. This precipitation would be expected to retard recrystallisation.

Recrystallisation at high rolling temperatures is primarily dependent on the amount of rolling reduction. Large rolling reductions produce a high dislocation density in the austenite, overcoming the effects of micro-alloy solute atoms, and thus accelerating recrystallisation. At low rolling temperatures, recrystallisation is largely solute dependent [32]. Increasing the concentration of vanadium and/or nitrogen will decrease the solubility of vanadium nitride at that temperature, so enhancing the potential for strain induced precipitation, and thus the potential to retard recrystallisation [33].

In a multi-pass rolling sequence the initial austenite grain size has no effect on either the recrystallisation stop temperature [32], or the final austenite grain size [37,38,39], assuming recrystallisation of the austenite has occurred after one or more of these rolling passes. In this case the austenite grain size before transformation to ferrite is primarily dependent on the reduction of the last rolling pass and on the rolling temperature [38]. Engl and Kaup [38] found that when hot rolling a micro-alloyed steel, an increase in rolling reduction produced an increase in austenite grain refinement. This was true for austenite grain refinement by both grain elongation (ie. effective grain refinement) and recrystallisation. In the case of austenite grain refinement by recrystallisation, small rolling reductions produced a proportionally greater decrease in austenite grain size after recrystallisation than large reductions. This trend was not observed for grain refinement by grain elongation. Hence large rolling

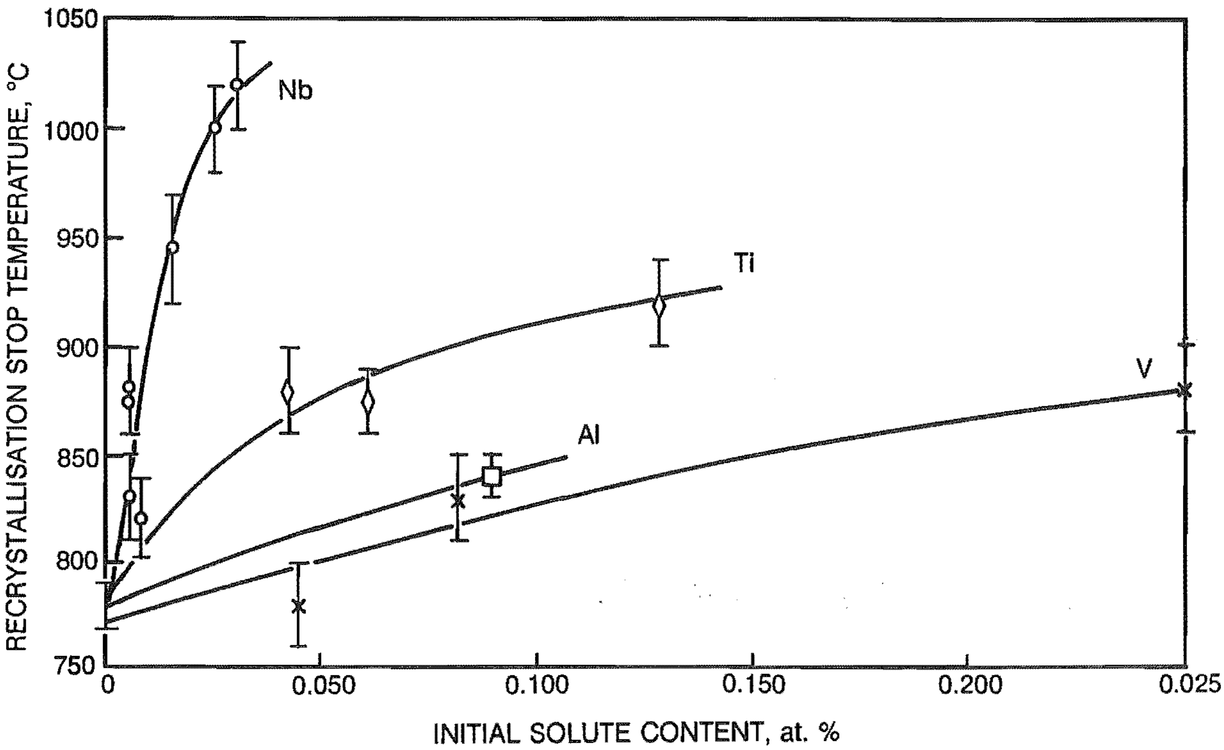

Figure 2.13 The effect of solute content on the recrystallisation stop temperature of a micro-alloyed steel [32].

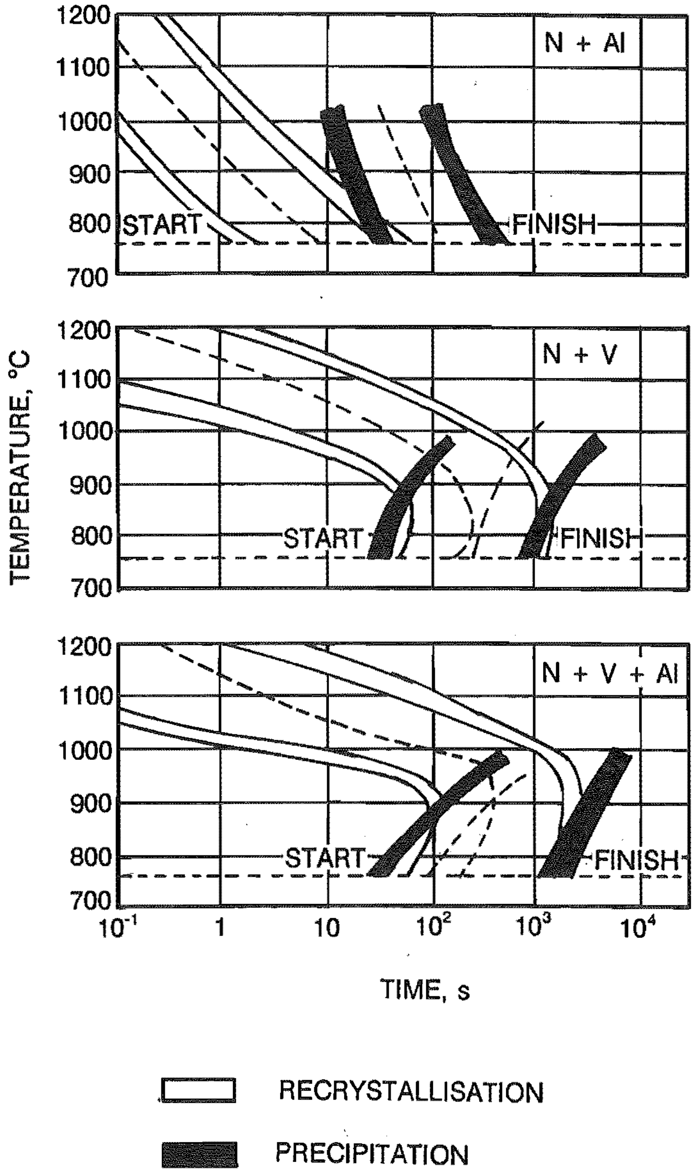

Figure 2.14 Static recrystallisation and static nitride precipitation time - temperature curves for steels micro-alloyed with aluminium, vanadium, and aluminium plus vanadium [36].

reductions are more efficient when austenite grain refinement is being achieved via grain elongation, than via recrystallisation. Processing of a steel micro-alloyed with vanadium should consequently include both high temperature passes to refine the austenite grain size, and lower temperature passes to deform the grains before the transformation to the ferrite phase [25]. Care must be taken, however, when rolling at "low" hot rolling temperatures. Though large rolling reductions assist in the formation of severely elongated austenite grains, they may also lead to unsatisfactory product tolerances, especially if a large deformation is carried out on the last rolling pass [39].

Precipitates present in the austenite phase of a micro-alloyed steel are primarily those which have formed during cooling of the steel, or those remaining undissolved after re-heating [40]. The size and distribution of these precipitates is dependent on the thermo-mechanical history of the steel, the steel composition and on solubility criteria. Micro-alloy precipitates prevent temperature induced austenite grain growth during the re-heating of a steel prior to rolling by "pinning" austenite grain boundaries [2,5,8,29,33]. A thermodynamic argument of the mechanisms involved in this pinning has been developed by Gladman and Delieu [8]. Austenite grain boundary pinning is most effectively achieved by a large volume fraction of very fine precipitates, as shown in figure 2.15 [40]. For each of the three models considered, it can be seen that minimum austenite grain size (D) will be achieved when the ratio of precipitate size (d) over volume fraction (f_v) is minimised. Beyond a certain temperature, however, these precipitates coarsen, and no longer effectively pin grain boundaries, resulting in austenite grain growth. This temperature is generally lower than the solution temperature of the precipitate [40] and is known as the Austenite Grain Coarsening Temperature. Figure 2.16 [40] shows how the grain coarsening temperature is affected by micro-alloy concentration, generally increasing proportionally to the solution temperature of the precipitates.

Precipitates which have not dissolved during re-heating are retained in the austenite during rolling. They assist in grain nucleation during recrystallisation [33,36], and are subsequently retained on the austenite grain boundaries after rolling is completed. These precipitates, if fine, may assist in pinning the newly formed equiaxed grains, preventing their growth as the steel cools to the Ar_3 temperature. Large precipitates (>100nm [33]), however, have little effect on the structure.

Precipitation in the austenite phase may also be strain induced by the rolling process [24,41]. In the deformed austenite, at low rolling temperatures, recovery of dislocation networks allows the formation of sub-grain boundaries within the austenite grains. These areas of local high energy within the structure form ideal sites for precipitate nucleation.

Strain induced precipitation on these sub-boundaries delays the formation of new austenite grains, thereby retarding recrystallisation [33]. This precipitation will only occur at low hot rolling temperatures, however (given solubility criteria are satisfied), as at high rolling temperatures the rapid recrystallisation of the austenite relieves strain in the lattice before precipitation can be nucleated [24]. This is true of any hot rolling temperature where recrystallisation precedes precipitation [42]. Strain induced precipitation may either be static or dynamic [41]. Dynamic precipitation, induced by the first rolling passes, forms while the austenite lattice is being strained. It is likely to be present in the austenite during the final rolling passes, retarding subsequent recrystallisation and preventing the growth of the new equiaxed grains once recrystallisation has occurred. Further static precipitation will then occur as the steel cools after leaving the final rolling stand. Dynamic precipitation has been shown to be less effective than static precipitation in retarding the recrystallisation of austenite in a vanadium micro-alloyed steel rolled at low temperatures [38,41].

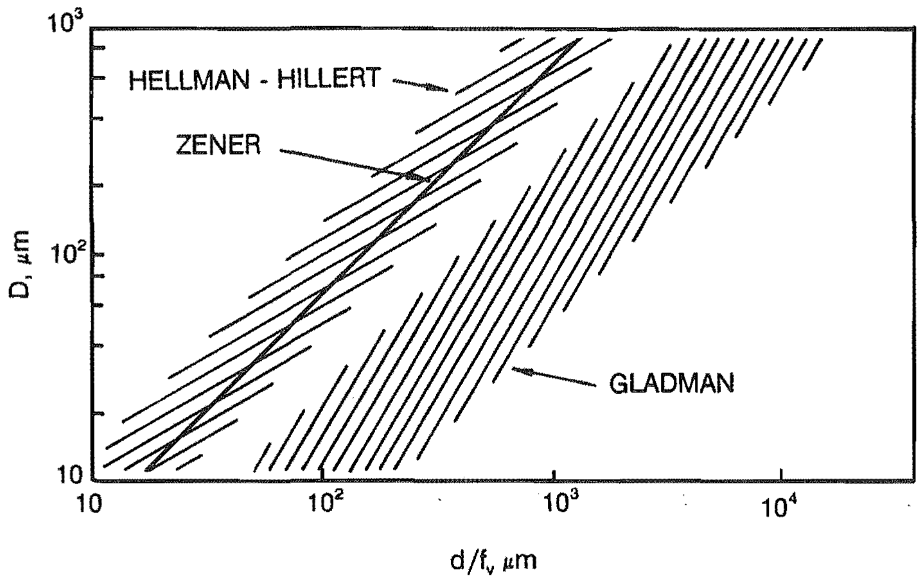

Figure 2.15 Relationship between grain size (D), precipitate size (d), and volume fraction (f_v), as described by three models [40].

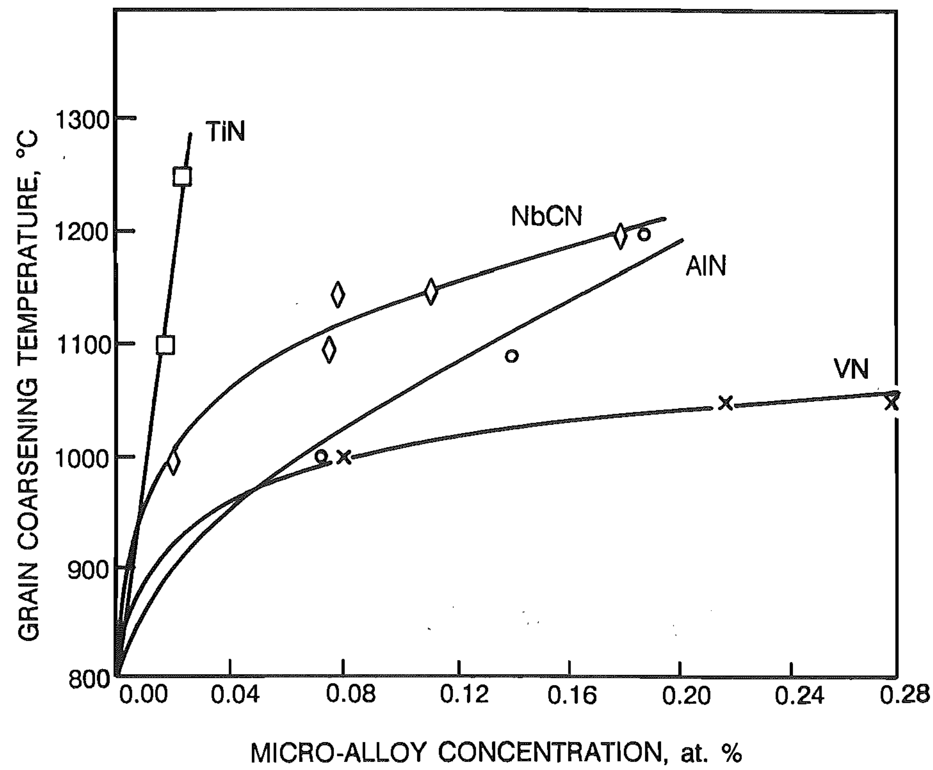

Figure 2.16 The effect of micro-alloy concentration on the austenite grain coarsening temperature for a series of common micro-alloying additions [40].

In a steel micro-alloyed with niobium, strain has been found to accelerate and enhance precipitation in deformed austenite, such that niobium carbo-nitride will precipitate at a higher temperature when under the influence of strain than it will when under equilibrium conditions [11]. This can be seen in figure 2.17 [11], where solubility curves, with and without strain, are plotted on the same graph for the precipitation of niobium carbo-nitride in austenite. It is considered likely that the high energy conditions found in deformed austenite would induce precipitation in a vanadium micro-alloyed steel at temperatures higher than those defined by equilibrium solubility [43]. Precipitates formed under conditions of strain are likely to be transitory in nature if they remain in an elevated temperature environment. Under equilibrium conditions these precipitates are unstable, such that over a period of time they will re-dissolve, allowing recrystallisation and rapid austenite grain growth. This can be prevented, however, if accelerated cooling is applied to the steel as it leaves the last rolling stand.

As an example of how long strain induced precipitation in a vanadium micro-alloyed steel may take, Akben and Jonas [9] found that maximum precipitation in a 0.115 V and 0.006 N steel, under dynamic conditions, occurred at 900 °C, and began after a time period of 26 seconds. See figure 2.18 [9]. (Maximum dynamic precipitation of VN at approximately 900 °C has also been noted by other authors [42,43].)

It should be noted from the figure that in the case of a vanadium micro-alloyed steel, the curves for dynamic recrystallisation start temperature (R_S - solid line) and dynamic precipitation start temperature (P_S -broken line) intersect at approximately 920 °C. Below this temperature strain induced precipitation precedes recrystallisation, such that a deformed austenite structure can be maintained as the steel is cooled to the Ar_3 temperature.

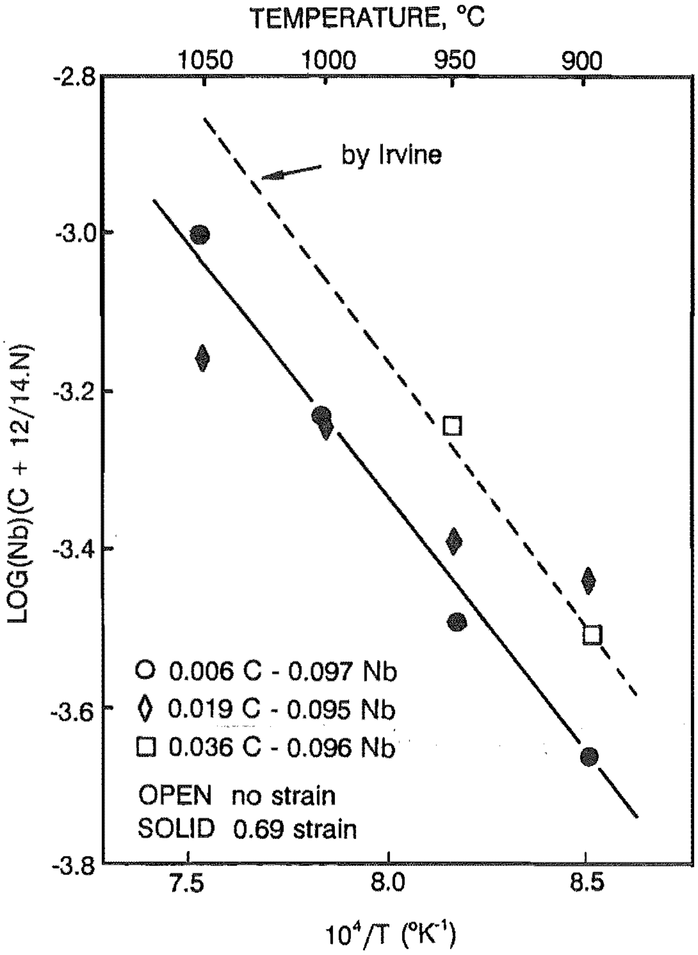

Figure 2.17 The effect of strain on the solubility of niobium carbo-nitride in austenite [11].

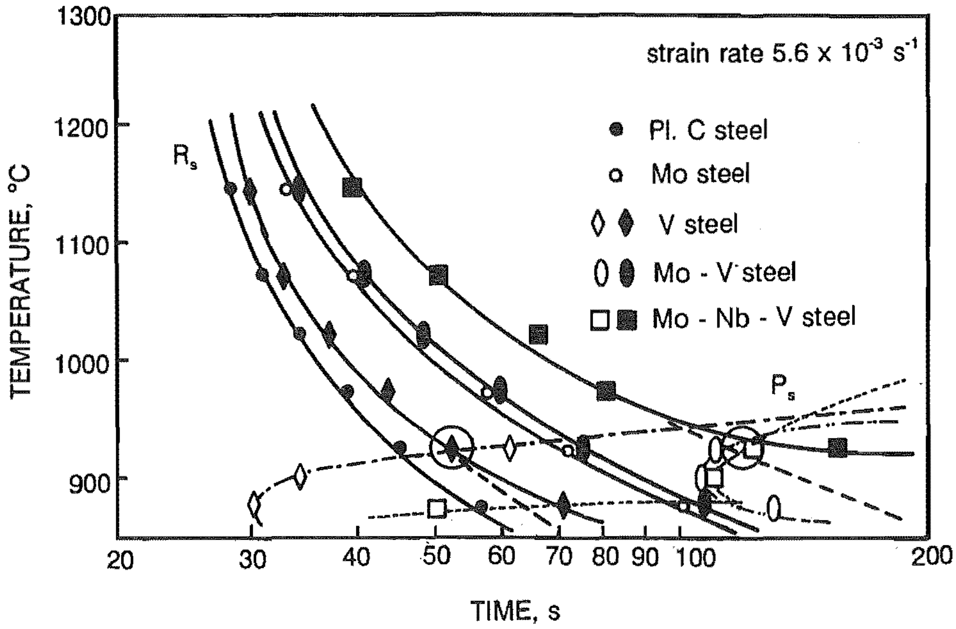

Figure 2.18 Time - temperature curves for dynamic recrystallisation and dynamic precipitation, in the austenite phase, for a series of micro-alloyed steels [9].

R_S = Recrystallisation start (solid curves)
P_S = Precipitation start (broken curves)

2.3 Ferrite Grain Size After the Austenite to Ferrite Transformation in a Vanadium Micro-alloyed Low Carbon Steel.

The size of the ferrite grains formed during the transformation from austenite is primarily dependent on the austenite grain size, the transformation temperature, and the cooling rate applied to the steel at the completion of deformation [18,25,34]. This can be seen in figures 2.19 [25] and 2.20 [18]. Figure 2.19 compares austenite and ferrite grain sizes at three cooling rates for a series of different steel compositions (compositions unknown, however). At a constant cooling rate, a decrease in austenite grain size will result in a proportional decrease in ferrite grain size after transformation. Alternatively, for a constant initial austenite grain size, a more rapid cooling rate will cause a reduction in the ferrite grain size after transformation from austenite. The lines on this figure, representing cooling rates, appear to follow similar curves, implying that ferrite grain size dependence on cooling rate is independent of austenite grain size [44]. Accelerated cooling can be used, therefore, to replace large deformation passes in a rolling schedule without loss of ferrite grain size refinement [34]. Accelerated cooling should not, however, be applied to a vanadium micro-alloyed low carbon steel during the transformation from austenite to ferrite if a large austenite grain structure exists prior to the transformation and the concentration of vanadium is close to 0.1 wt. %. This may lead the formation of regions of bainite/acicular ferrite within the ferrite/pearlite structure [12,34], the hardenability of the steel being increased by the presence of vanadium in solid solution [17]. A mixed acicular ferrite - ferrite/pearlite structure has been shown to produce low levels of ductility [45]. This is rare, however, as under most thermo-mechanical processing conditions, the presence of vanadium assists in the formation of a fine grained austenite structure prior to transformation (see section 2.2) [43].

Figure 2.20 shows the additional effect of the austenite to ferrite transformation temperature on ferrite grain size. The addition of carbon to a low carbon steel produces a decrease in its transformation temperature, resulting in a finer ferrite grain size after transformation (assuming a constant cooling rate). Increasing the carbon content of the steel to lower its transformation temperature, however, is not the best way of refining the ferrite grain structure. Higher carbon contents produce an increase in the pearlite volume fraction of the steel, this having a detrimental effect on low temperature impact properties [12] (see section 2.5(c)). Increasing the manganese concentration of the steel is also known to lower its austenite to ferrite transformation temperature [2,12,20], but unlike carbon, manganese additions have a generally favourable effect on low temperature impact properties [20]. Vanadium raises the austenite to ferrite transformation temperature, enlarging the pro-eutectoid ferrite phase field. As a result of this, a vanadium micro-alloyed steel contains about 10 percent more ferrite than a plain low carbon steel [46]. The lower range of ferrite grain sizes for the vanadium alloyed steel in the figure is therefore a result of grain boundary pinning by vanadium nitride precipitates in the austenite phase.

Umemoto et. al. [44] have defined a mathematical expression relating ferrite grain size after transformation to the austenite grain size prior to transformation, and the cooling rate applied to the steel during transformation. This expression is $d=5.7q^{-0.26}D^{0.46}$, where q is the cooling rate in Ks^{-1} and D and d are the austenite and ferrite grain sizes before and after transformation, respectively, measured in micrometers. The correlation of this expression with experimental results is shown in figure 2.21 [44], plotted as a log-log relationship. The larger exponent associated with austenite grain size implies that austenite grain refinement is a more efficient method of obtaining ferrite grain refinement than accelerating the cooling rate applied to the steel during transformation. Considering the production costs of these two options, however, any advantages associated with increasing rolling

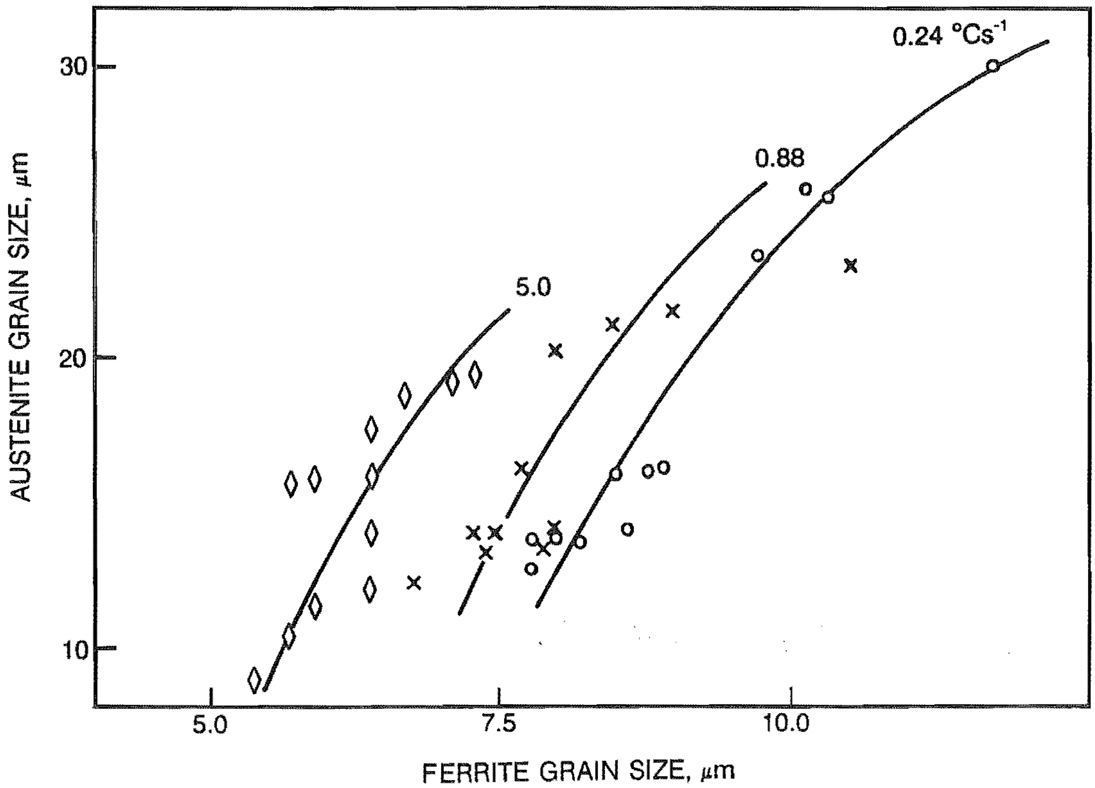

Figure 2.19 The effect of cooling rate during the austenite to ferrite transformation on ferrite grain size [25].

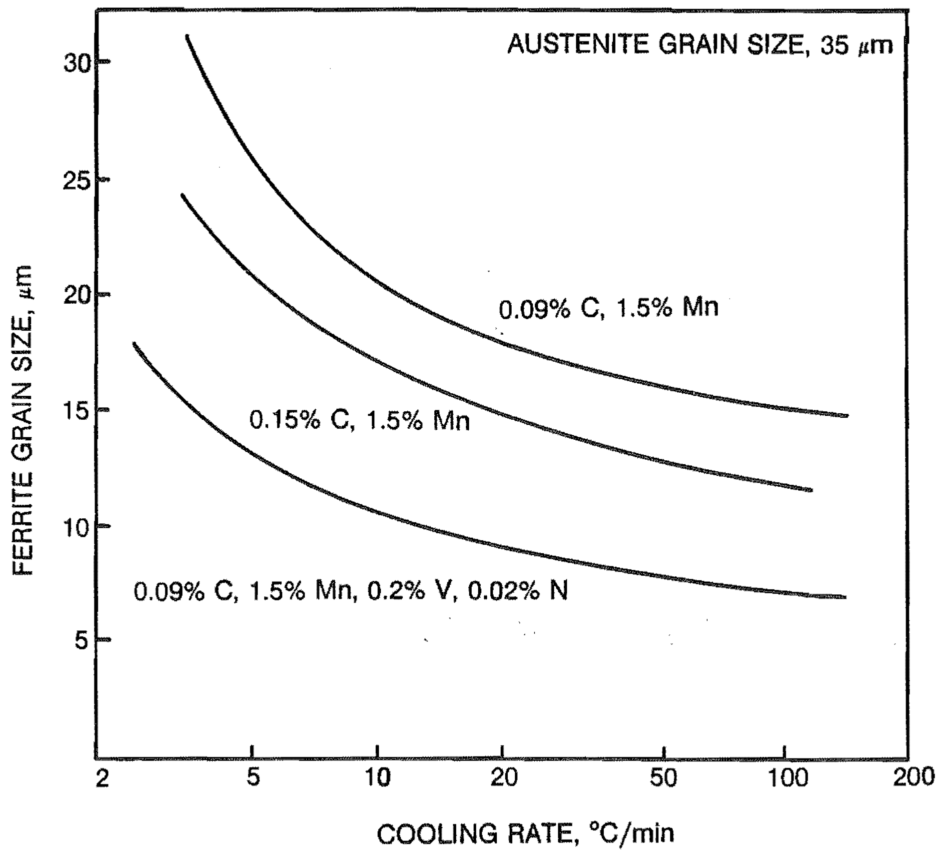

Figure 2.20 The effect of cooling rate during the austenite to ferrite transformation, and composition, on ferrite grain size [18].

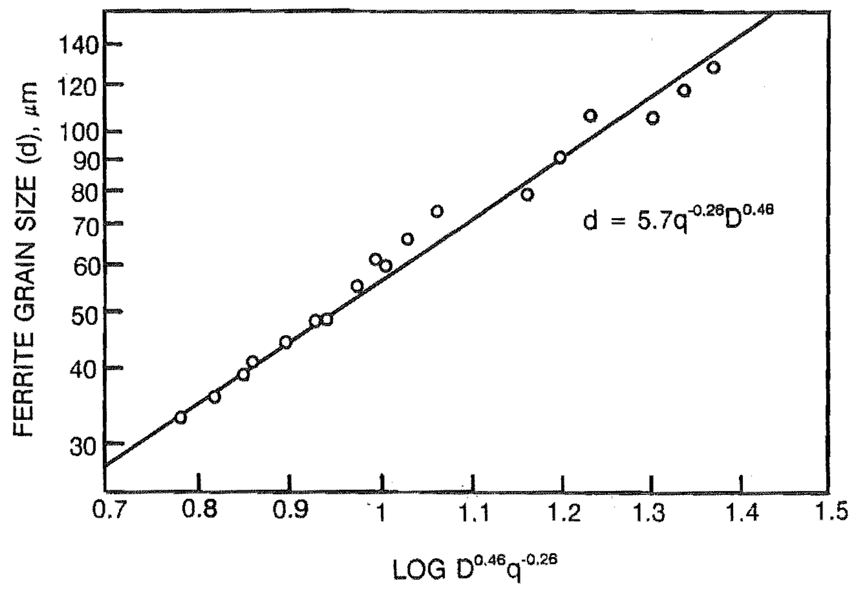

Figure 2.21 Correlation of the calculated relationship between cooling rate, austenite grain size, and ferrite grain size by Umemoto et. al. with experimental results [44].

D = austenite grain size (μm)
d = ferrite grain size (μm)
q = cooling rate (Ks^{-1})

reductions may only be theoretical.

The minimum austenite grain size obtained during hot rolling, with recrystallisation, is of the order of 15 - 20 micrometers [32,34], transforming to a ferrite grain size of 7 - 10 micrometers [32]. This can be seen from figure 2.22 [34], which relates ferrite grain size to the austenite grain size (equiaxed) prior to transformation under constant cooling conditions. Also considered in the figure is the transformation of a deformed austenite structure. It should be noted from figure 2.22 that when a fine austenite grain structure exists, no further advantage is gained (in terms of ferrite grain size reduction) by further deformation below the recrystallisation stop temperature.

Ferrite is nucleated in austenite on the austenite grain boundaries and on deformation bands within the austenite grains. Considering a deformed austenite structure transforming to ferrite, Smith et. al. [35] found that no nucleation occurred on deformation bands within the austenite grains until all the nucleation sites on the grain boundaries had been used up. Grain boundary nucleation can, therefore, be considered to be the dominant nucleation mechanism, independent of whether the austenite grains are elongated in the direction of rolling, or equiaxed. This is especially true when the austenite grain size is fine, as the length of deformation bands within the grains is small when compared with total grain boundary area [25].

Ferrite nucleation is dependent on the "geography" of the austenite grain boundary. Discontinuities on a grain boundary, such as corners and edges, produce areas of inhomogeneity along the boundary, and as a consequence a higher local energy level is required to overcome a proportionally larger mis-match with adjacent grains [47]. These discontinuities are prime sites for ferrite nucleation. This is also shown in results obtained by Umemoto et. al. [44] (figure 2.21). The logarithmic constant associated with the effect austenite grain size has on ferrite grain size after transformation is a function of nucleation site dominance along the austenite grain boundary, being a weighted average of grain surface nucleation ($D^{0.33}$), grain edge nucleation ($D^{0.67}$) and grain corner nucleation (D).

Ferrite nucleation on deformation bands within the ferrite grains is enhanced by an increasing level of deformation [48], and accelerated cooling [34,47]. Though deformation bands are secondary nucleation sites, increasing their associated energy level by further straining the austenite below the recrystallisation stop temperature will make these sites more "attractive" for ferrite nucleation, especially as more dominant nucleation sites along grain boundaries become used. Accelerated cooling lowers the transformation temperature of a vanadium micro-alloyed steel by under-cooling the austenite. This increases the driving force for ferrite nucleation, increasing the nucleation rate, and thereby activating more intra-granular nucleation sites as grain boundary nucleation sites are rapidly used.

Ferrite may also be nucleated by non-coherent precipitates present in the austenite phase [34]. The interface between these precipitates and the austenite grains is a local high energy site within the structure, and thus provides an excellent secondary nucleation site. Fine coherent precipitates, however, retard transformation from austenite to ferrite [27]. Although straining the lattice, these precipitates provide no ferrite nucleation sites, but rather, they pin the transformation interface and thus retard its movement.

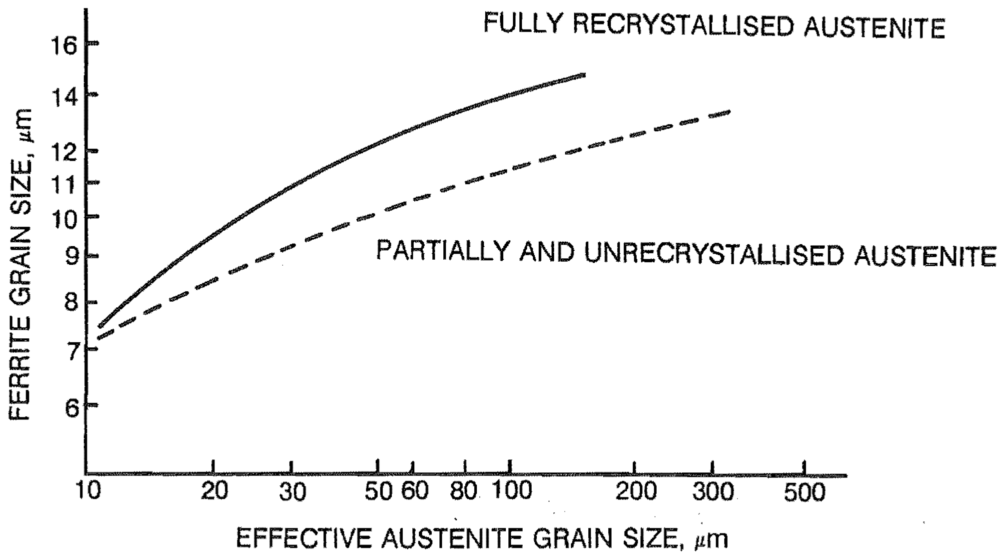

Figure 2.22 The effect of austenite recrystallisation on the relationship between austenite and ferrite grain size after transformation [34].

The austenite grain size of a steel prior to transformation is often difficult to define. For an equiaxed structure, each grain can be approximated as a sphere, the size of the grain thus defined with respect to the diameter of the sphere. This approximation, however, is not possible if the austenite grain structure has been elongated by rolling below the recrystallisation stop temperature. An ellipsoidal approximation is possible in this case, but measurement of axis lengths in a physical specimen would require two or more sections of any grain considered. This is not a practical solution. A more effective way of defining austenite grain size prior to transformation to ferrite is by measuring the grain boundary area per unit volume, S_v (mm^{-1}) [21]. As mentioned previously, nucleation of ferrite primarily occurs at austenite grain boundaries. A measurement of nucleation potential between two grain structures (ie. measuring S_v), therefore, is the most accurate method of distinguishing between them. In the case of two identical samples of steel, undergoing different thermo-mechanical treatments, the sample with a higher value of S_v at the start of the phase transformation to ferrite will transform to a structure with a finer ferrite grain size, assuming identical cooling rates during the transformation [25,49]. The effect of S_v on ferrite grain size can be seen in figure 2.23 [25]. For the hot rolling of both plate and bar, increasing the value of S_v produces an increasingly finer ferrite grain size after transformation, independent of austenite grain structure. It can be seen, therefore, that excellent ferrite grain refinement can be achieved from recrystallised austenite under air cooling if S_v is greater than 100 mm^{-1} [25].

Though measured as a ratio of area to volume, S_v has been approximated as a ratio of grain boundary length to grain area on a two dimensional plane [47]. In the case of a sphere, the ratio of surface area to volume area is proportional to the ratio of circumference to planar area for all values of grain diameter. This is not necessarily true for other grain shapes, however. For this reason S_v should not be regarded as anything more than an indication of equivalent equiaxed grain size for a deformed austenite grain.

DeArdo [47] argues that S_v should also take into account deformation bands within the deformed austenite. Intra-granular nucleation only occurs, however, when more favourable nucleation sites (such as along the grain boundary) are scarce, even if the austenite grains are heavily deformed. Also, the total length of deformation bands within a deformed austenite grain is not an easy parameter to measure. Considering these points, it can be seen that under most cases, taking deformation bands into account when measuring S_v will introduce more errors than will be eliminated.

Figure 2.24 [47] shows schematically how steel composition (alloy design), hot deformation, and accelerated cooling inter-relate to effect the austenite grain size (S_v) and transformation temperature (Ar_3) of a micro-alloyed steel, and therefore the resulting grain size after transformation to ferrite. Though not detailed, this schematic shows factors to be considered when designing a sequence of thermo-mechanical treatments to maximise the properties of a micro-alloyed steel.

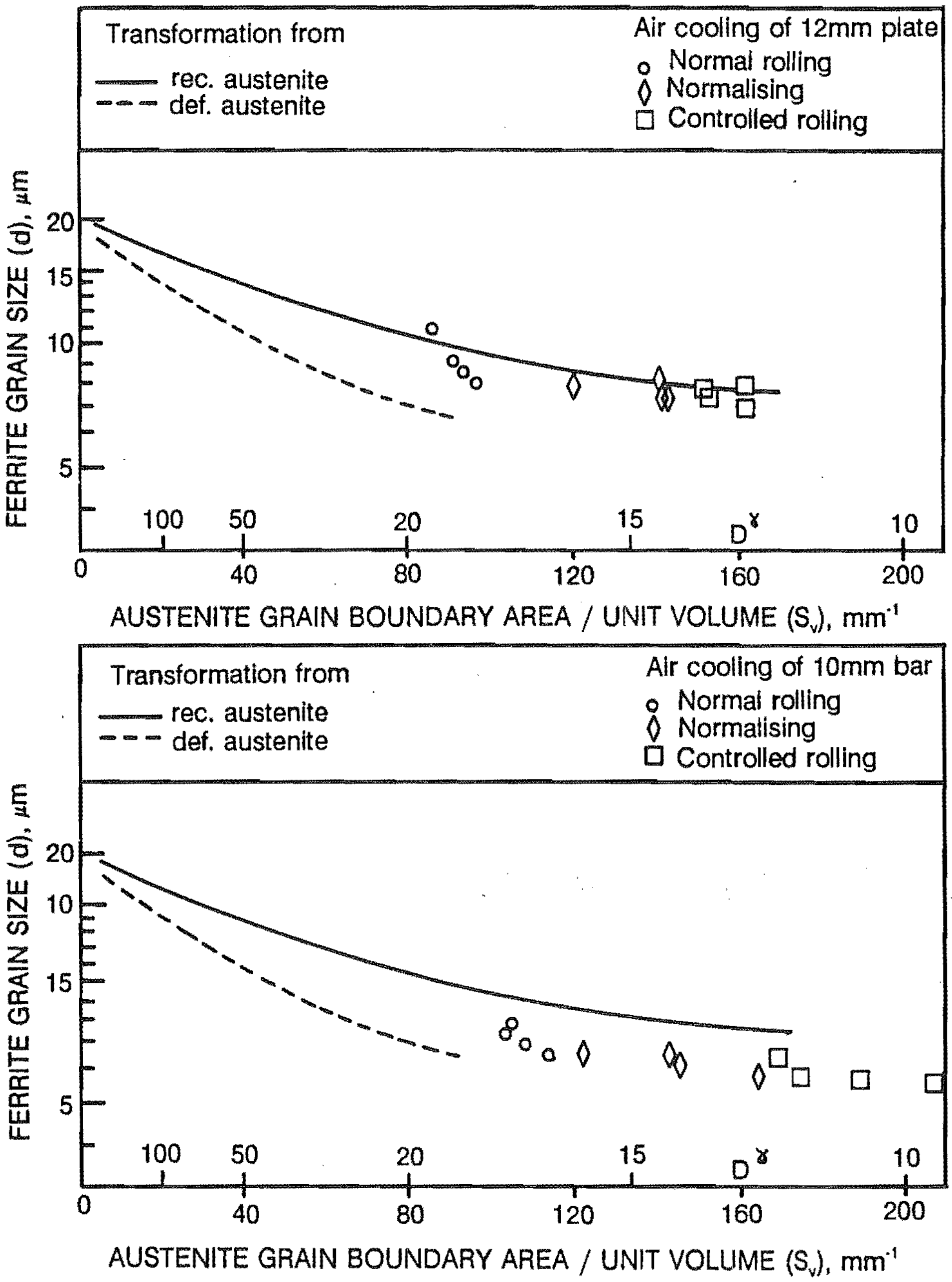

Figure 2.23 The effect of austenite grain boundary area per unit volume (S_v) on ferrite grain size after transformation from recrystallised and deformed austenite [25].

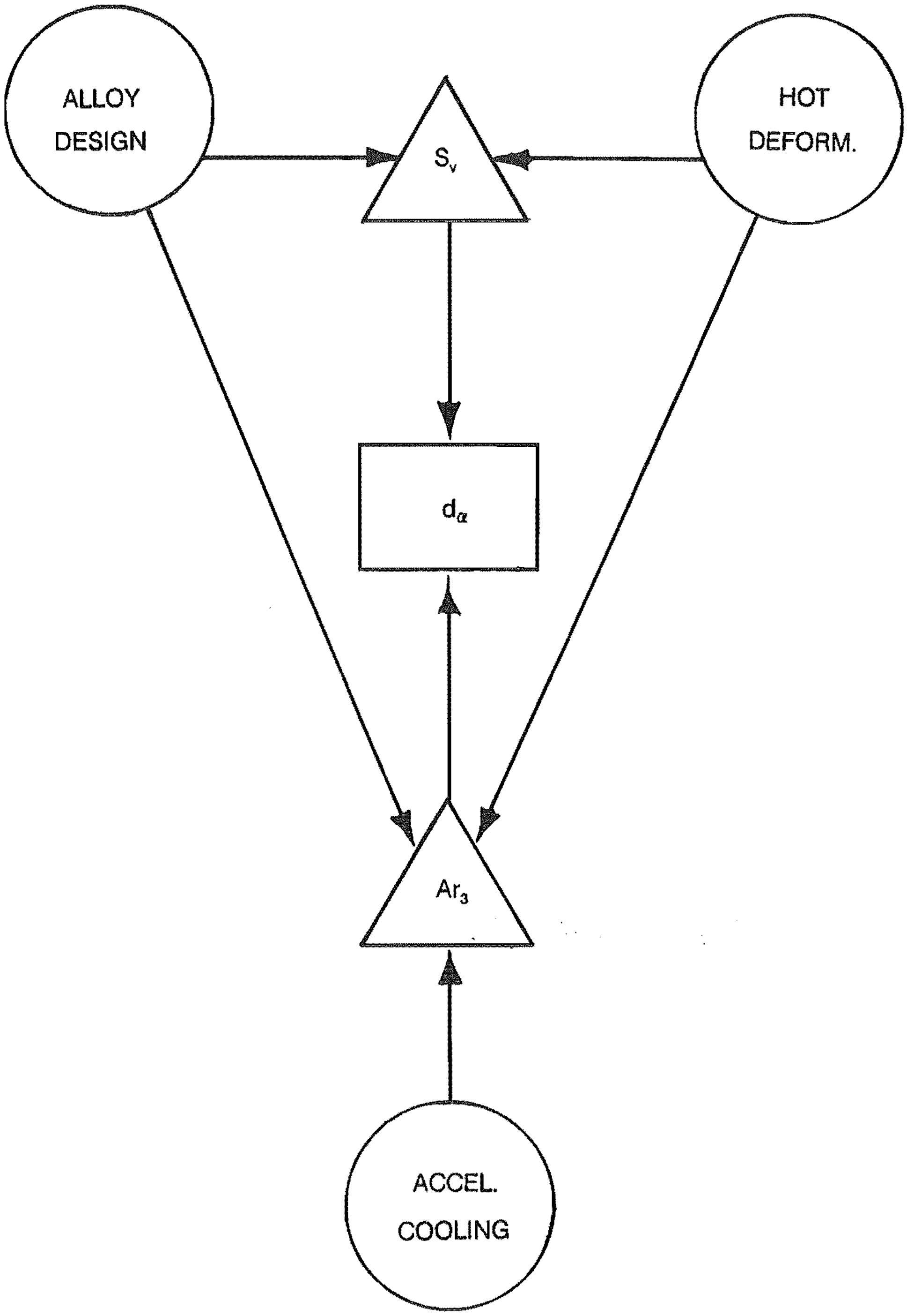

Figure 2.24 Schematic showing the inter-relationships between alloy design and processing parameters on ferrite grain size for a micro-alloyed steel [47].

2.4 Precipitation in the Ferrite Phase During and After the Austenite to Ferrite Transformation in a Vanadium Micro-alloyed Low Carbon Steel.

In a vanadium micro-alloyed steel, the growth of ferrite grains in austenite during the phase transformation is accompanied by the precipitation of fine particles along the phase transformation front [30]. The composition of these particles is essentially vanadium nitride, though there may be a varying carbon concentration, depending on the composition and thermo-mechanical history of the steel [19]. (A more complete argument as to the composition of these particles is contained in Section 2.1). These particles are known as interphase precipitates, and can be seen as small discrete needles aligned parallel, or at a low angle to the advancing austenite - ferrite interface [28]. They adopt the Baker - Nutting orientation ($(001)_{ppt}//(001)_{ferrite}$; $[110]_{ppt}//[010]_{ferrite}$) with respect to the ferrite phase [50]. A typical size of these precipitates is 17 nanometres, with a row spacing of about 20 nanometres [28].

Formation of interphase precipitates is associated with the planar/step growth mechanism of the ferrite phase as it moves into the austenite phase [2,27]. The non-migrating planar boundaries of these ferrite steps provide ideal nucleation sites for precipitation, being slow moving, and having low interfacial energy. The height of these migrating steps determines the row spacing of the precipitates, step height becoming smaller with decreasing transformation temperature [27]. A result of this is that the row spacing of interphase precipitates throughout the ferrite will vary, as under most conditions, hot or controlled rolled steels do not transform from austenite to ferrite isothermally. If the planar boundaries have a high interfacial energy condition (due, for example, to a large mis-match between the crystallographic orientation of the growing ferrite phase and the austenite phase), propagation of the ferrite phase does not follow a planar/step mechanism, but rather, the steps start to bulge locally, leaving a random [27] or a curved band formation [30,35,51] of precipitates. This local bulging of the ferrite planar interface increases its area, thereby lowering the average interfacial energy and slowing its movement. Figures 2.25 [27] and 2.26 [27] show schematically the growth of the ferrite - austenite interface, under conditions of low and high interfacial energy, respectively. It should be noted from these figures that the interphase precipitates form on the ferrite side of the interphase boundary. This is an important consideration when evaluating the composition of these precipitates (see section 2.1). Fibrous precipitates have also been observed to form during interphase precipitation [27]. It has been suggested that this precipitate morphology occurs when the ferrite - austenite interface is at its highest energy level (maximum mis-match in crystallographic orientation) [27], but a mechanism for their formation has not been outlined.

Interphase precipitation has also been observed in pearlitic ferrite, the size and row spacing of these precipitates being less than that of precipitates formed in pro-eutectoid ferrite, however, as pearlitic ferrite is formed at a lower temperature [3].

Interphase precipitation, however, is relatively rare in vanadium micro-alloyed steels [51], as under most cooling conditions there is insufficient time available for diffusion of vanadium and nitrogen over "large" distances along the transformation interface. The majority of precipitation occurs randomly on dislocations in the ferrite matrix [2], these dislocations being produced by the austenite to ferrite phase transformation [24,27]. Coherent strain fields associated with these precipitates (and interphase precipitates) produce a significant enhancement in the strength of a steel [52].

The size and distribution of the precipitates formed in the ferrite phase, after transformation from austenite, is dependent on the micro-alloy concentration of the steel, and the cooling rate applied

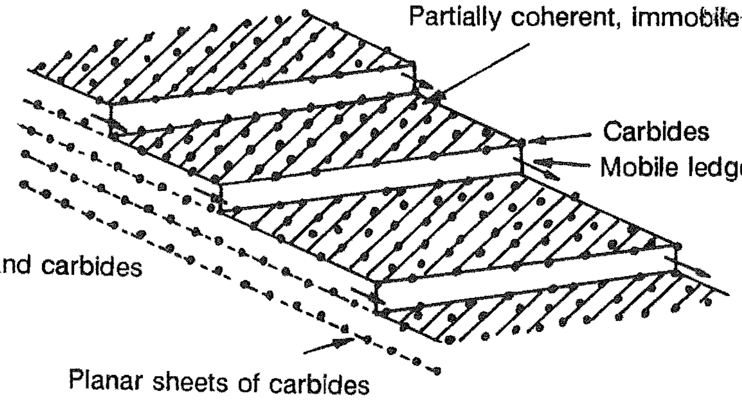

Figure 2.25 A diagrammatic representation of the growth of ferrite at the austenite to ferrite interface by a step mechanism [27].

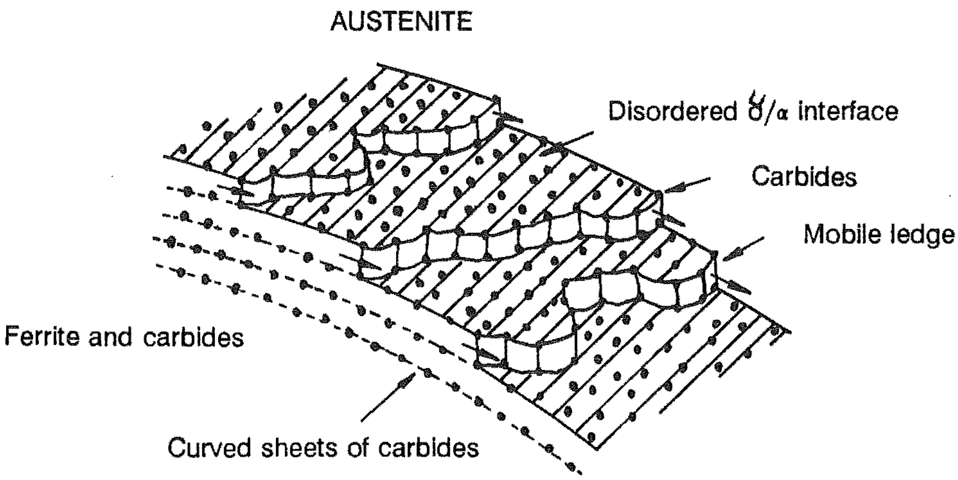

Figure 2.26 A diagrammatic representation of the growth of ferrite at the austenite to ferrite interface by a bulge mechanism [27].

after transformation [26,53].

Amin et al. [24], and others [54,55], have found that increasing the nitrogen content of a vanadium micro-alloyed steel results in an increase in precipitation strengthening. (Fine precipitates distributed throughout the ferrite lattice impede the strain induced motion of dislocations through the lattice, and thus raise the stress levels required to produce plastic deformation of the structure). They suggest that this strength increment is primarily the result of an increase in precipitate volume fraction [25], as vanadium is usually present in micro-alloy steels in concentrations greater than those required for stoichiometry with nitrogen. Figure 2.27 [25] shows the effect of increasing nitrogen content on the portion of the lower yield strength attributable to precipitation strengthening in a vanadium micro-alloyed steel (0.087 wt. % $<$ V $<$ 0.094 wt. %). The symbols on this figure represent experimental results for four different nitrogen concentrations. In the case of the controlled rolled and hot rolled samples, an increase in the nitrogen concentration produced a proportional increase in precipitation strengthening. The result for the normalised sample, however, indicates that massive precipitate coarsening has occurred at the normalising temperature of the higher nitrogen steels, the resulting loss in precipitation strengthening negating any advantage gained from an increased precipitate volume fraction. Honeycombe [31] has suggested that additional strengthening produced by increasing the nitrogen concentration of a vanadium micro-alloyed steel results from an increase in the coherency strain associated with vanadium carbo-nitride precipitates [7,56] as their nitrogen concentration increases. (The effect of nitrogen composition on the coherency and growth rate of vanadium carbo-nitride precipitates is given in section 2.1). Nitrogen rich vanadium carbo-nitrides have been observed to lose coherency at about 60 nanometres, whereas carbon rich vanadium carbo-nitrides were observed to lose coherency at about 20 nanometres [31]. Increasing the nitrogen concentration of the steel will, therefore, produce a structure containing a greater proportion of coherent precipitates, and consequently, a larger degree of precipitation strengthening.

Accelerated cooling of a vanadium micro-alloyed steel will enhance precipitation strengthening [44]. Applying accelerated cooling to the steel when it is in the austenite phase causes it to become under-cooled, producing an increased precipitate nucleation rate. This under-cooling will also decrease the rate of solute diffusion, thereby retarding the coarsening rate of the precipitates [25]. The combination of these two effects results in a larger (high volume fraction) distribution of finer precipitates, producing higher strength levels in the steel. In the case of interphase precipitation, accelerated cooling produces the additional effect of decreasing the row spacing of the precipitates [25]. Figure 2.28 [25] shows the effect of cooling rate on interphase precipitation. It should be noted that increasing the cooling rate applied to a vanadium micro-alloyed steel has more effect on the row spacing of interphase precipitates, than it does on their size. This implies that the growth of ferrite into austenite is more sensitive to cooling rate than is the nucleation and growth of the precipitates. Excessive cooling rates should be avoided, however, as this may lead to a decrease in the level of precipitate strengthening in the steel [12], insufficient time being available to nucleate precipitation. A bainitic or martensitic structure may instead result (see earlier in this section).

Vanadium carbo-nitride precipitation in the austenite phase (for example, strain induced precipitation) leads to a decrease in the precipitation possible in ferrite phase. This loss of solute results in a loss of precipitation hardening of the steel [18,24,26], as precipitates formed in the austenite phase are usually larger than those formed in the ferrite phase, having had more time to grow, and consequently have only a minor ferrite strengthening effect [5].

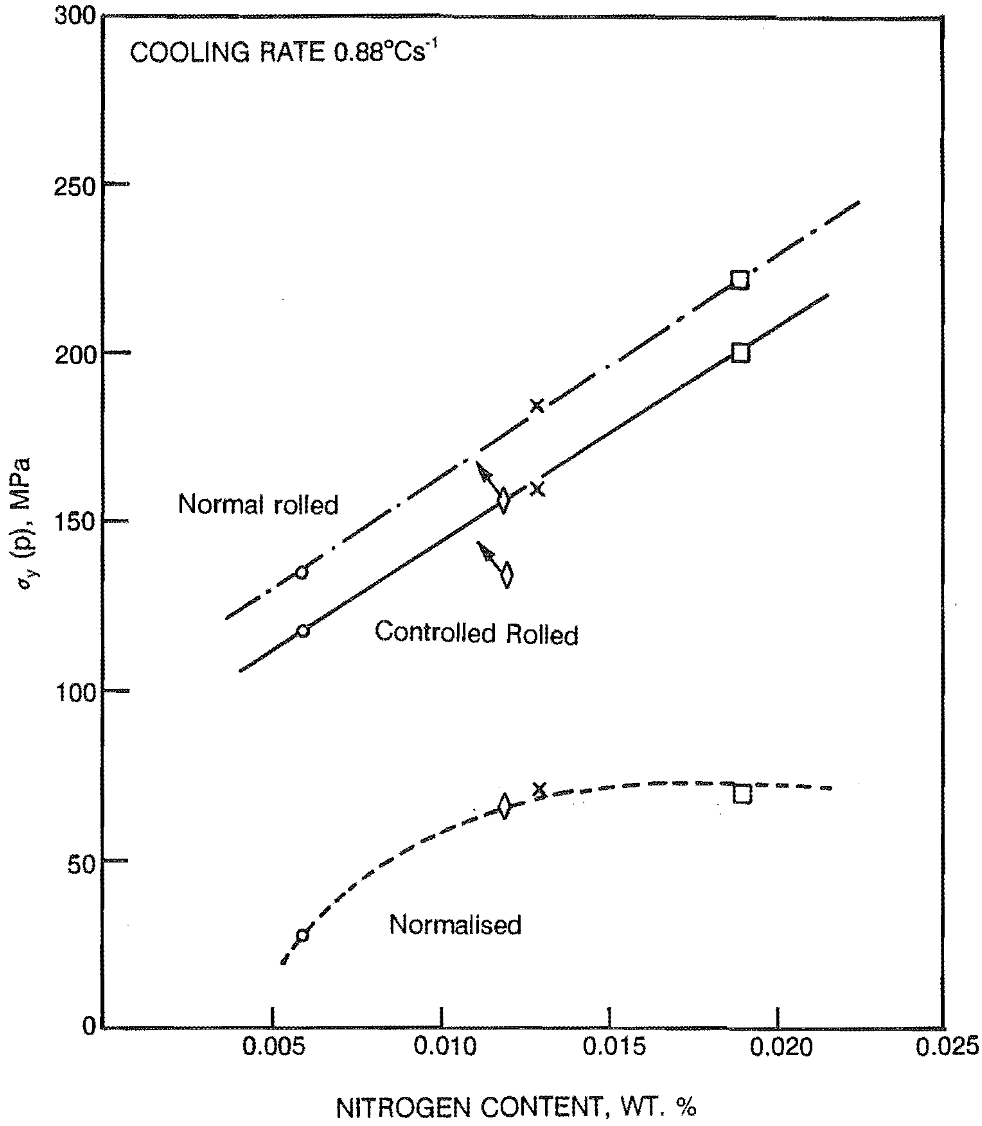

Figure 2.27 The effect of nitrogen content on precipitation strengthening in a vanadium micro-alloyed low carbon steel [25].

V 0.087 - 0.094 wt. %

C 0.12 wt. %

Mn 1.27 - 1.35 wt. %

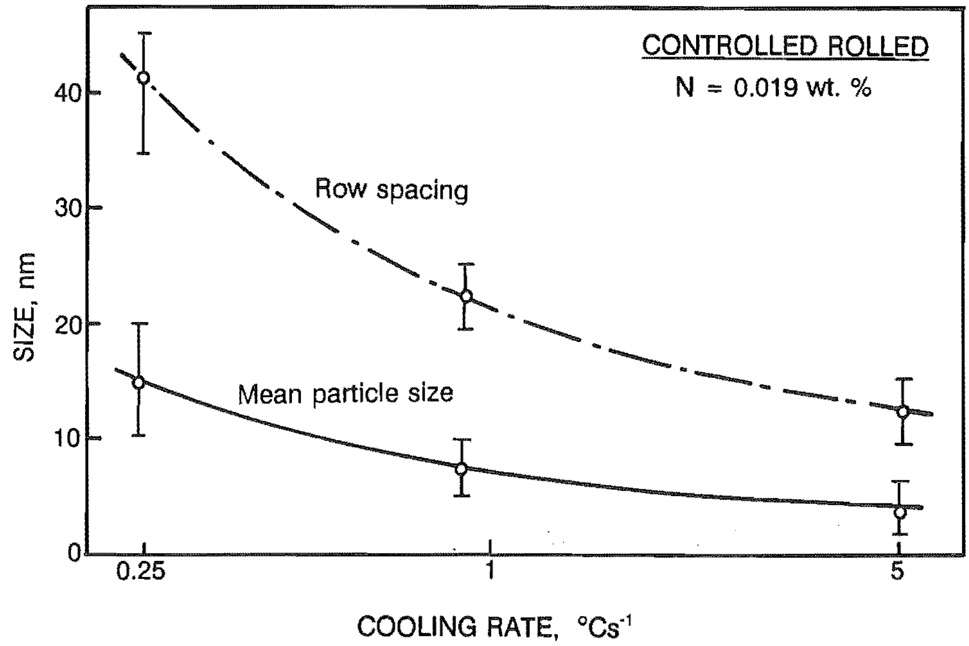

Figure 2.28 The effect of cooling rate on the size and spacing of interphase precipitates in a vanadium micro-alloyed low carbon steel [25].

V 0.09 wt. %

C 0.12 wt. %

Mn 1.28 wt. %

The size (and volume fraction) of precipitates formed in the ferrite phase has a significant influence on the precipitation strengthening of a vanadium micro-alloyed low carbon steel. For a constant volume fraction of precipitate, a decrease in their average size must be compensated by increasing the number of precipitates. This higher precipitate density produces a greater degree of strain in the ferrite lattice, and thus increases the strengthening attributable to precipitation. This is displayed in figure 2.29 [12]. For a precipitate with a volume fraction of 0.001 (ie. 0.1 %), changing precipitate size from 0.03 micrometers to 0.003 micrometers is predicted to increase the precipitation strengthening by approximately 50 MPa. The shaded areas on the figure represent typical experimental values for precipitate volume fraction and size, and the resulting strengthening of the steel due to these precipitates.

The size of carbo-nitride precipitates found in a vanadium micro-alloyed steel at room temperature has been reported to vary from 2 to 100 nanometres [29]. Mean precipitate sizes ranging from 15 to 50 nanometres [41] and 8 to 14 nanometres [57] have also been reported. Crooks et. al. [46] found sheets of precipitates of dimension 100 nanometres, which on closer inspection were revealed to be clusters of precipitates less than 3 nanometres in diameter. (These precipitate sizes are similar to those reported to halt recrystallisation in the austenite phase, ranging in size from 0.5 to 10 nanometres [32]). Typical particle size distributions for controlled rolled, hot rolled and normalised samples with varying vanadium and nitrogen contents are shown in figure 2.30 [25]. The form of these particle size distributions is essentially independent of time, as defined by the Lifshitz - Wagner theory [31,58].

Precipitation in the ferrite phase during cooling after transformation from austenite provides ferrite grain size control as well as precipitation strengthening [18,34]. Any mobile ferrite grain boundaries would be restrained by precipitates in the grains being "consumed", such that massive ferrite grain growth would be prevented during prolonged holding periods at elevated temperatures in the ferrite phase (for example, coiling of sheet after hot rolling, at 700 °C).

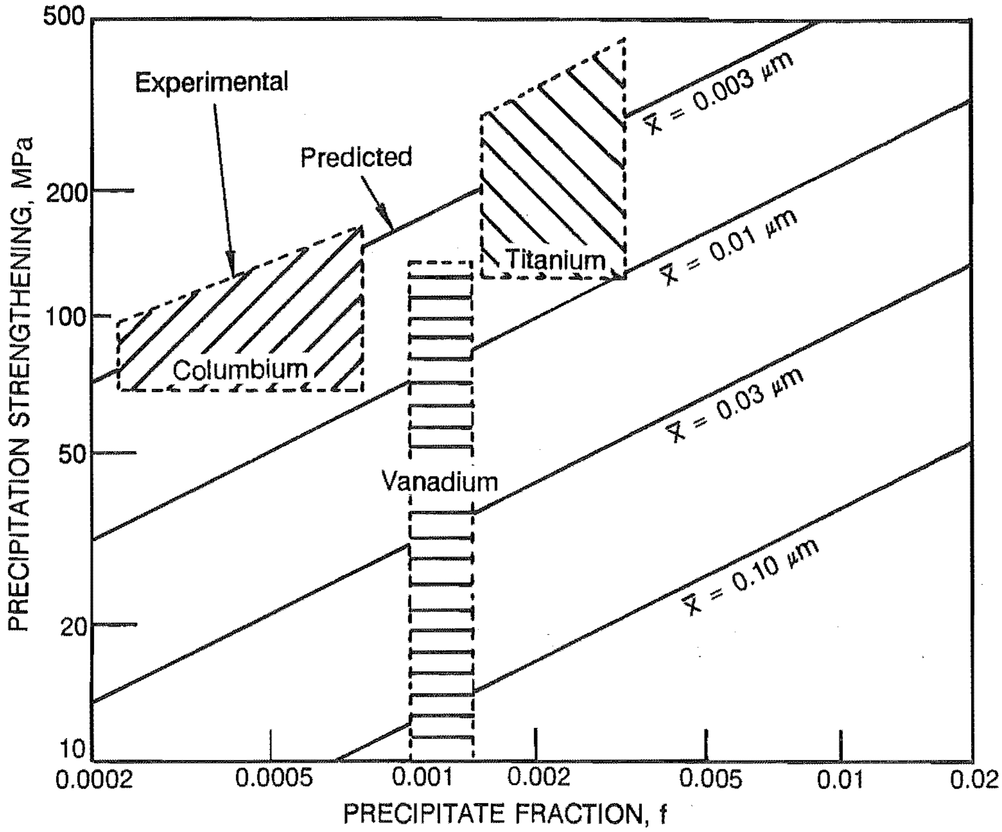

Figure 2.29 The combined effect of precipitate size ($\bar{x}$) and volume fraction on precipitation strengthening, as defined by the Ashby - Orowan model [12].

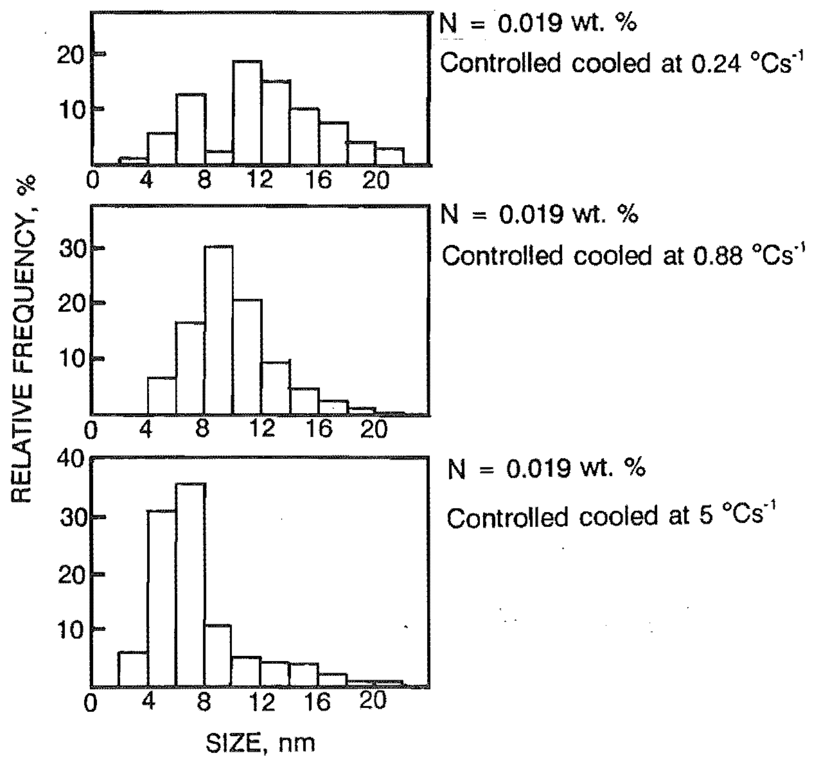

Figure 2.30 Typical particle size distributions for a vanadium micro-alloyed steel, illustrating also the effect of cooling rate on precipitate size [25].

V 0.09 wt. %

C 0.12 wt. %

Mn 1.28 wt. %

2.5 The Mechanical Properties of a Vanadium Micro-alloyed Low Carbon Steel.

a). Lower Yield Stress.

The Hall-Petch equation relating lower yield stress (σ_y) with the material parameters of a low carbon steel can be generalised as: [12]

$$\sigma_y = [\ \sigma_o + k_1(\text{Dispersion})\ ] + k_y.(d^{-1/2})$$

Frictional stress (σ_o) is a measure of the minimum level of stress required to move mobile dislocations along slip bands within a ferrite matrix, assuming these mobile dislocations exist, or can be generated. Strain fields in the ferrite, associated with interstitial (carbon and nitrogen) and substitutional (manganese, nickel, phosphorus) alloy systems increase frictional stress by impeding dislocation movement, such that higher stress levels must be applied to the steel in order for dislocations to have sufficient energy to either bypass or pass through these strain fields.

Dispersion strengthening (k_1(Dispersion)) is caused by additional strain fields associated with coherent and semi-coherent precipitation in the ferrite phase (carbides and nitrides of titanium, niobium, vanadium, chromium, molybdenum, tungsten, etc.). Dispersion strengthening is usually included as part of frictional stress.

The grain boundary factor (k_y) is a measure of the stress required to transmit yielding from one grain to the next [59]. This grain boundary factor has been found to be constant for normalised and annealed steels, where sufficient time exists during post heat treatment cooling to ensure all dislocations generated in the ferrite phase by the austenite to ferrite transformation are locked by carbon and/or nitrogen atoms. In this case k_y is purely a function of the stress required to generate new dislocations in poly-crystalline ferrite.

The inter-relationships between lower yield stress and material parameters in a low carbon steel can be seen in figures 2.31 [12] and 2.32 [12]. Figure 2.31 shows the combined effects of interstitial strengthening (N), solute strengthening (Si, Mn), and ferrite grain size on lower yield strength, plotted as the inverse square root of grain size. Figure 2.32 is similar, including also the effect precipitation strengthening (for example, precipitation of vanadium nitride in the ferrite phase), in this case being plotted as a function of manganese content. It can be seen from these figures that lower yield stress can be maximised in a vanadium micro-alloyed low carbon steel by refining ferrite grain size (d=7 micrometers, say, being equal to a value of 12 in the form $d^{-1/2}$), with additional strengthening produced by both elements in solid solution (Mn and Si, say), and a fine dispersion of vanadium nitride precipitates in the ferrite phase.

b). Tensile Strength.

A structure - property relationship similar to that for lower yield stress may also be defined for tensile strength. In this case, however, the movement of dislocations rather than their generation must be considered. The movement of mobile dislocations along slip planes within ferrite grains may be obstructed if these slip planes bisect strain fields associated with either alloying elements (interstitial or substitutional) or micro-alloy precipitates [60]. Once the movement of a dislocation has been halted, further movement is only possible if a higher level of stress is applied to the steel. This would allow

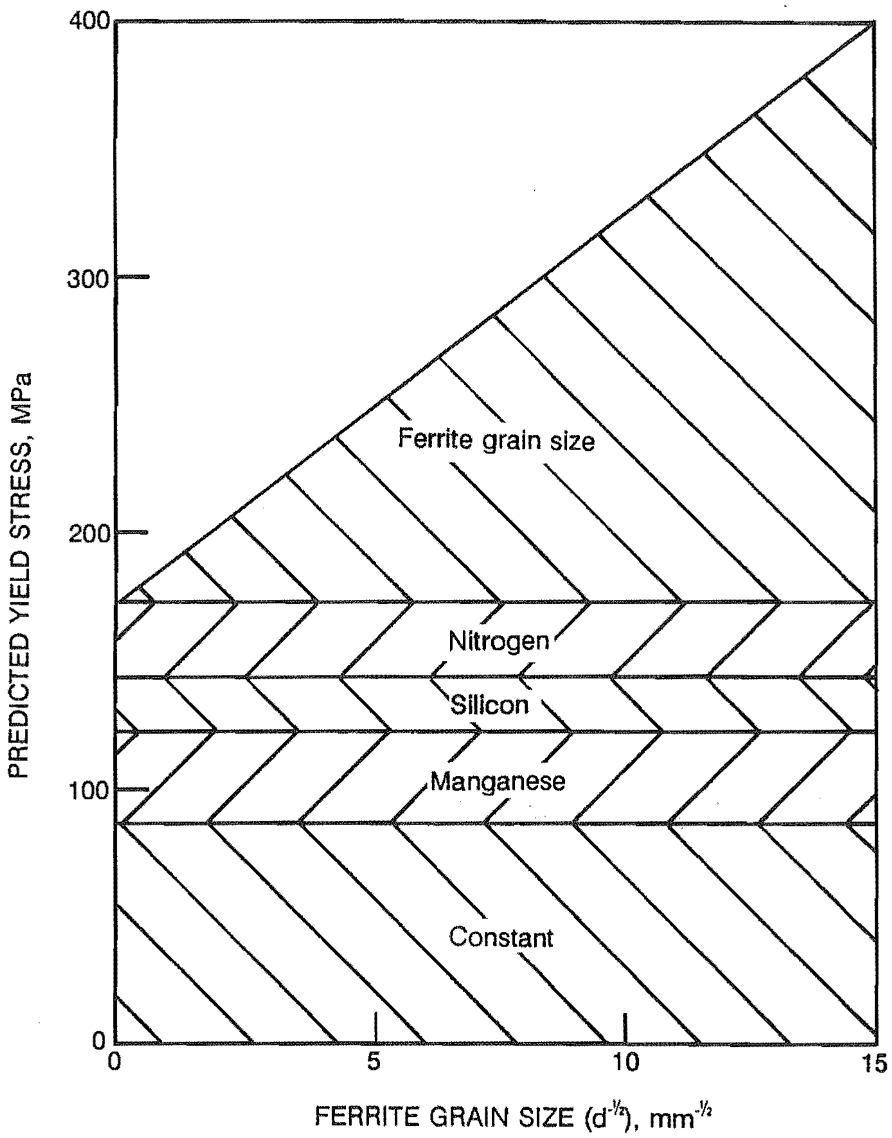

Figure 2.31 The effect of material parameters on lower yield stress, plotted as a function of grain size [12].

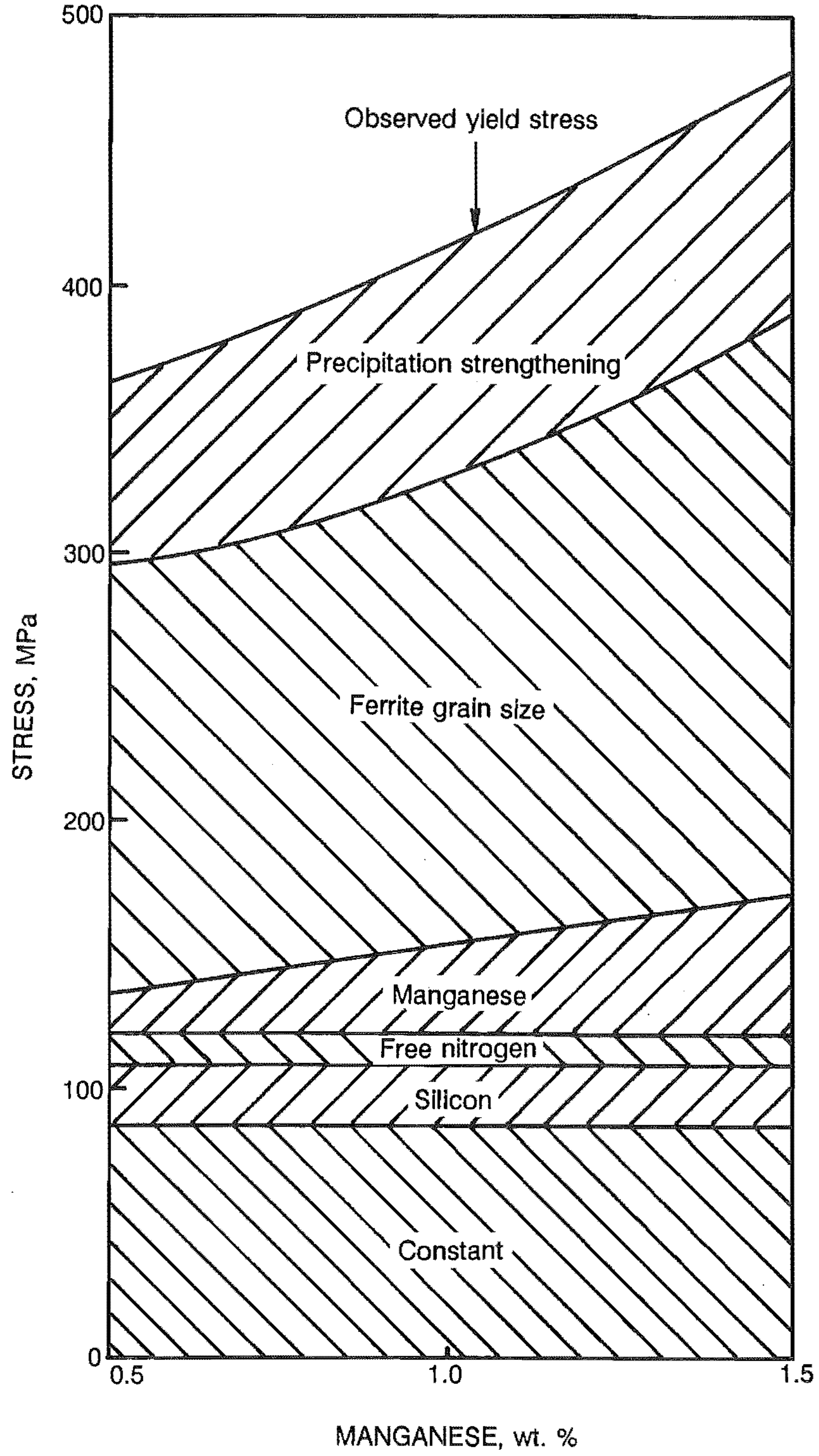

Figure 2.32 The effect of material parameters on lower yield stress, plotted as a function of manganese concentration [12].

the dislocation to proceed towards the obstruction, but not beyond it, the proximity of the dislocation to the obstruction being dependent on the level of applied stress. The interaction of dislocations with each other may also obstruct their movement, occurring when multiple dislocations are moving along the same slip plane, or when slip planes intersect [60]. As further stress is applied to the steel, the point will be reached where movement of dislocations along slip planes with a less favourable orientation to the applied stress is possible. Cross-slip may subsequently occur, allowing local stress to be relieved as dislocations accelerate past prior obstructions along unhindered slip planes. Under uni-directional strain in a tensile test, the stress measured across the cross-section of the sample reaches a maximum at this stage. Further strain produces localised necking and a drop in overall stress. This maximum stress is known as the tensile strength of the steel.

It can be seen that if the ferrite lattice is highly strained by the presence of interstitial (N) and substitutional (Mn, Si, P) alloy systems, and a large volume fraction of fine micro-alloy precipitates (vanadium nitride, say), slip becomes progressively more difficult, and as a result, the tensile strength of a steel increases. Ferrite grain boundaries (including the multiple grain boundary areas associated with pearlite lamellae) are additional permanent barriers to dislocation movement. For this reason both ferrite grain size and pearlite volume fraction (proportional to carbon content) are also important parameters in determining the tensile strength of a steel.

The effect of these multiple parameters can be seen in figure 2.33 [1]. Though not included in the figures, precipitation of vanadium nitride in the ferrite phase would produce a further increase in strength on both graphs (ie. independent of carbon or manganese content).

It should be noted that the grain boundary effect of lower yield stress, k_y, has a small influence on tensile strength, this being dependant on the motion of existing dislocations, rather than the generation of new ones.

c). Fracture Mode Transition Temperature.

The failure mode of low carbon steel under tensile stress is primarily dependent on the temperature at which this stress is applied, and the rate of loading [60]. A ductile mode of failure (micro-void coalescence) is usually the dominant mode of failure at temperatures above ambient, with strain rates which are not impulsive in nature. As the test temperature decreases, the failure mode changes with cleavage progressively becoming the dominant failure mechanism. The temperature range over which this change from the ductile to brittle mode of failure occurs is, in the case of a low carbon steel, quite narrow (usually less than 20 °C). High strain rates have an effect equivalent to decreasing temperature. Dislocation motion under these conditions requires higher stress levels in the steel. If these stress levels exceed the stress required to produce trans-granular cleavage, brittle failure of the steel will occur. A fracture mode transition temperature can thus be defined as the temperature at which the failure mode, under a standardised loading schedule on a standardised sample (For example, the Charpy impact test), changes from being mainly ductile to being mainly brittle in nature as the temperature is lowered.

For a steel to fail in a ductile manner, it must first yield. This generates an abundance of mobile dislocations within the ferrite lattice. As the temperature decreases, however, the effect of temperature

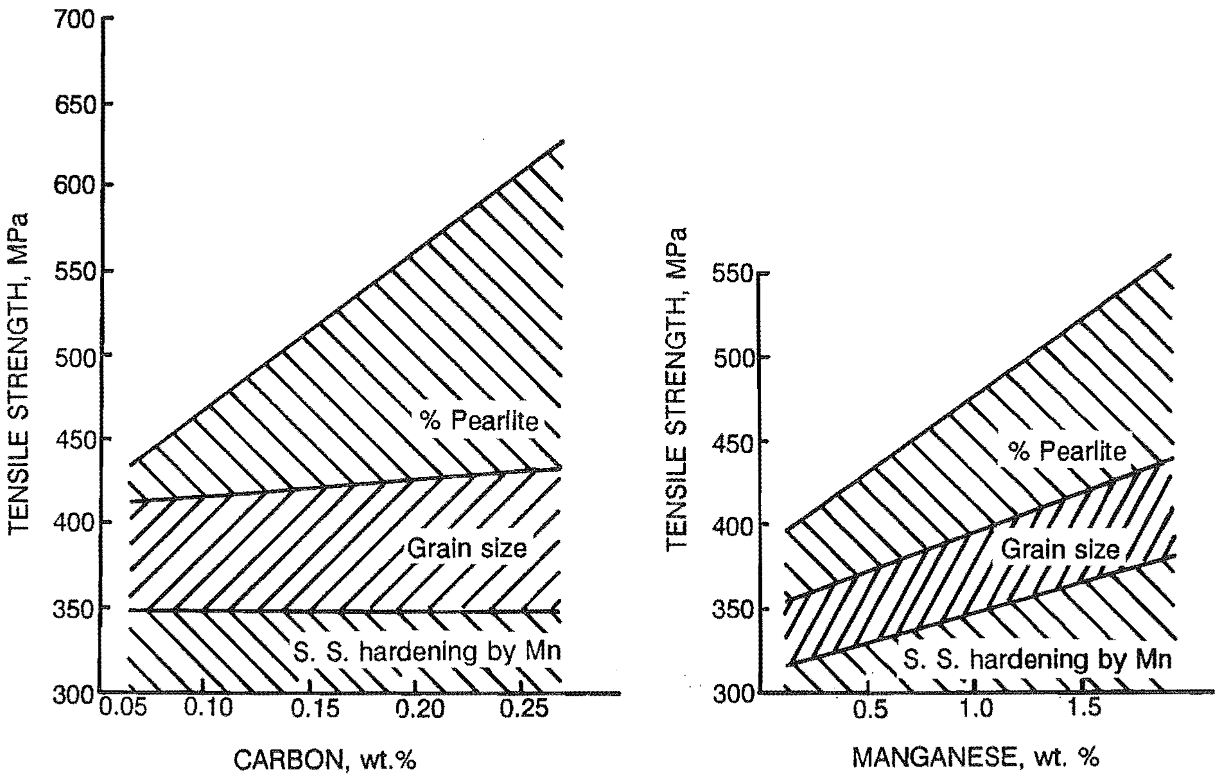

Figure 2.33 The effect of material parameters on tensile strength, plotted as functions of both grain size and manganese concentration [1].

on frictional stress (σ_o) must be considered (see section 2.5(a)). Frictional stress, as well as being increased by the presence of interstitial and substitutional alloy systems, and micro-alloy precipitation, is dependent on temperature. Any movement of atoms, in the ferrite lattice during dislocation motion is dependent on the energy level of the atoms. Unless sufficient energy exists locally, dislocations in the ferrite lattice will not be able to overcome restraining bond forces between atoms and move through the lattice. This minimum local energy level becomes progressively less likely to exist as the temperature of the steel decreases. The result of this is that the generation of dislocations in ferrite at sub-ambient temperatures requires progressively higher stress levels to be applied to the ferrite as its temperature is decreased, increasing the local energy level of the steel. Anything which exerts an effect on k_y must also be considered. In a vanadium micro-alloyed low carbon steel, say, the formation of vanadium nitride decreases the levels of free nitrogen in solution in the steel. This, in turn, decreases k_y, making the generation of dislocations in ferrite easier [59]. This change in k_y is independent of temperature, as is k_y itself and is generally regarded as a minor effect. The effect of temperature on the generation of a dislocation within the ferrite lattice is therefore adequately accounted for by considering its effects on frictional stress only.

As lower yield stress increases with decreasing temperature, it becomes increasingly likely that the steel will fail due to cleavage, initiated at micro-cracks within the structure. These are generated by the fracture of hard phases during initial yielding, or by coalescence of dislocations piled up at grain boundaries, or intersecting slip or twin bands [60]. This is because the energy levels associated with the length of these cracks are high enough to allow them to propagate through the structure. The energy required to stabilise the increasing surface area of the crack is supplied by the high energy level of the stressed ferrite lattice. Micro-cracks may be initiated by inclusions or iron carbide laminae in the steel. For this reason, increasing the carbon content of a steel increases its fracture mode transition temperature by increasing pearlite volume fraction, and therefore crack initiation sites, despite the fact that increasing the carbon content also produces grain refinement by lowering the transformation temperature from austenite to ferrite. This is shown schematically in figure 2.34 [12] for a carbon - manganese - aluminium steel.

Grain size also has a significant effect on the fracture mode transition temperature [12]. Apart from its effect on lower yield stress, a fine ferrite grain size limits the propagation of micro-cracks in the steel. The grain boundary, being an area of mis-match between two ferrite grains, provides a barrier against crack propagation from one grain to another. This crack blunting delays stable crack propagation, and therefore maximising ferrite grain boundary area will produce a decrease in the fracture mode transition temperature.

It can be seen from the optimum requirement of both a high lower yield stress and a low fracture mode transition temperature, that grain refinement is the preferable method of strengthening a low carbon steel. In the case of a vanadium micro-alloyed low carbon steel, with its associated strengthening resulting from precipitation in the ferrite phase, the maximum refinement of ferrite grain size must be achieved by thermo-mechanical processing if the harmful effects of ferrite precipitation on the fracture mode transition temperature are to be offset.

d). Strain Ageing Propensity.

Mobile dislocations, generated by the yielding of ferrite under an applied stress, may be pinned by diffusion of free nitrogen onto these dislocations at room temperature. This pinning causes a re-

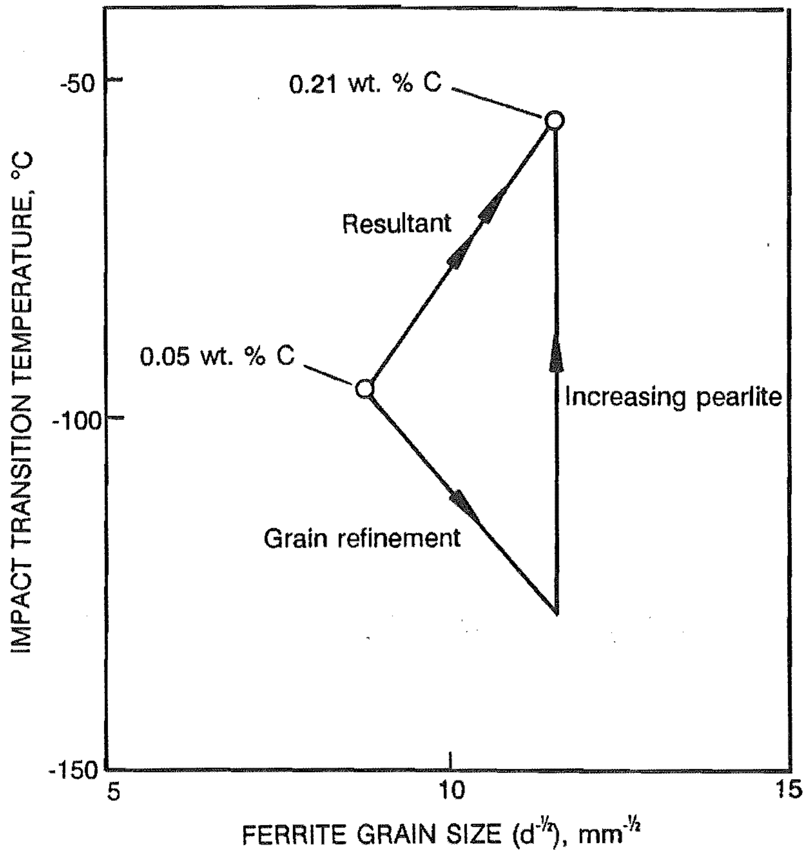

Figure 2.34 Schematic, showing the effects of increasing carbon concentration on the fracture mode transition temperature [12].

emergence of the yield point of the steel, as new mobile dislocations must be formed before further deformation of the structure can occur. Re-emergence of a yield point due to diffusion of nitrogen (strain ageing) carries with it a reduction in the ductility of the steel, such that the total strain at failure is reduced. The effect of strain ageing on a standard tensile stress - strain curve is shown in figure 2.35 [61]. Having been initially strained plastically to point A, the test piece is unloaded and allowed to age. (This ageing may be accelerated by a slight elevation of the ageing temperature (50 °C to 100 °C), thereby increasing the diffusion rate of nitrogen). The test piece is then re-loaded. As a result of strain ageing, a new yield point appears, being ΔY MN/m^2 higher than the stress level reached when the steel was unloaded. The tensile strength of the steel increases by ΔU MN/m^2, and the strain at failure decreases by Δ El. Strain ageing also increases the fracture mode transition temperature of the steel, this being associated with the accompanying rise in yield stress. This can lead to catastrophic failures if strain ageing raises the fracture mode transition temperature above ambient temperature. Lowering of the free nitrogen of the steel, either by the production of ultra low nitrogen steels by vacuum degassing techniques, or by "tying up" nitrogen in the formation of a micro-alloy precipitates, will further reduce strain ageing. This allows the re-straining of the steel during forming processes without any loss of ductility, as well as preventing strain age embrittlement.

The addition of 0.04 wt. % vanadium has been shown to effectively prevent the strain-ageing of a vanadium micro-alloyed steel with typical values of interstitial nitrogen [43,61]. Figure 2.36 [61] shows the effect of vanadium content on strain ageing parameters ΔY, ΔU and ΔEl for a vanadium micro-alloyed steel, pre-strained 5%, and aged at 100 °C for three hours. The total nitrogen content of these steels was 0.006 wt. %. It can be seen from the figure that for the steels considered, the addition of greater than 0.04 wt. % vanadium produces diminishing returns.

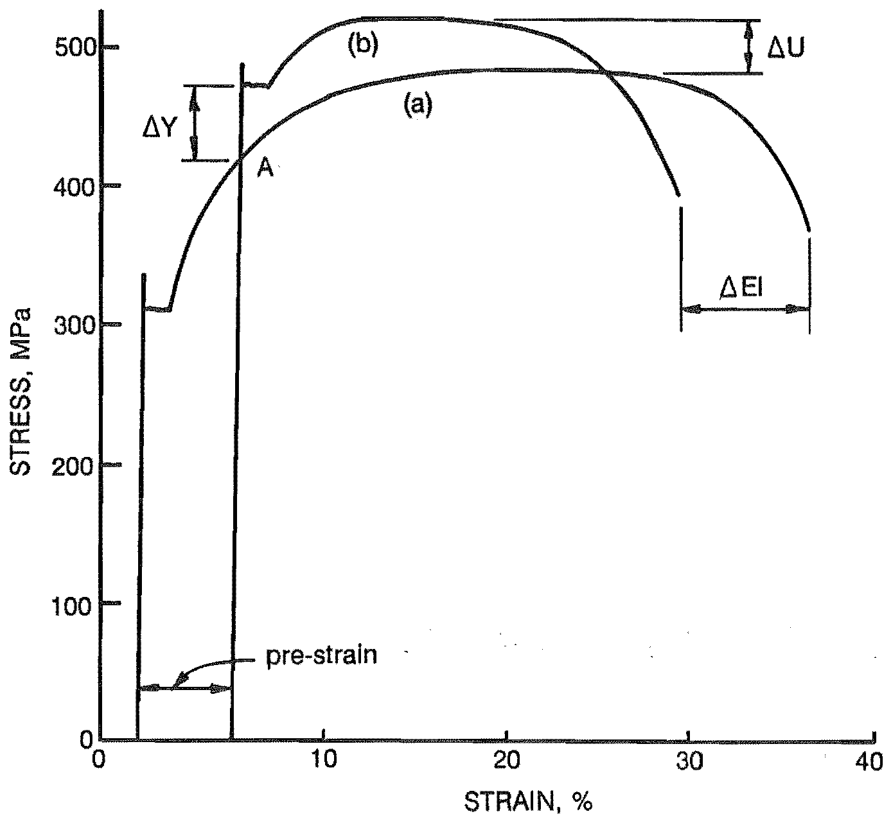

Figure 2.35 The effect of strain ageing on a low carbon steel, as described by its effect on the stress - strain curve for a tensile test specimen [61].

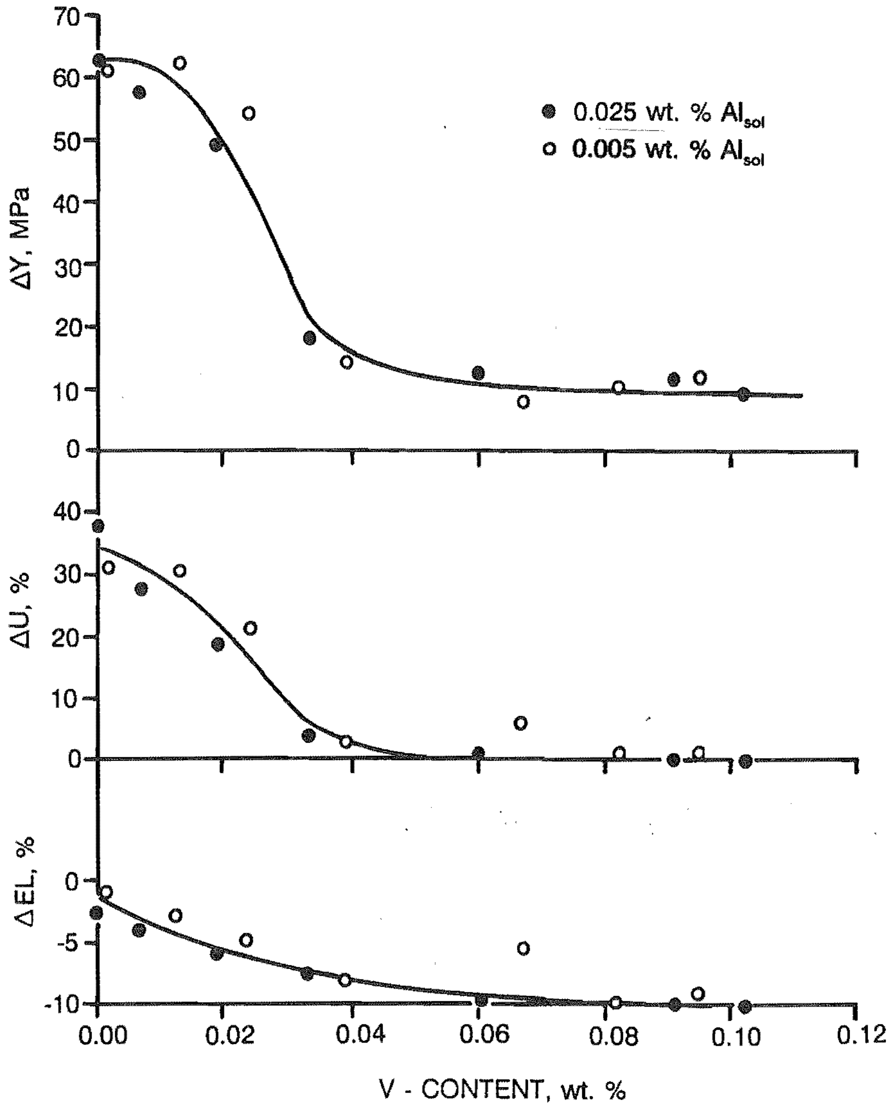

Figure 2.36 The effect of increasing vanadium concentration on strain ageing indicators in a vanadium micro-alloyed low carbon steel [61] (N = 0.006 wt. %).

2.6 Optimising the Mechanical Properties of a Vanadium Micro-alloyed Steel.

As can be seen from the previous discussion in this chapter, a variety of parameters can effect the final properties of the steel. The high cost of a micro-alloy addition, however, warrants the expenditure of effort to obtain the best possible properties.

In a multi-pass hot rolling schedule, a fine, and yet deformed austenite grain structure can be obtained through carefully controlled rolling and cooling. This would first require a slow, high temperature (1100 °C, say) roughing stage, during which time the austenite would under go multiple recrystallisations. A very fine austenite grain size will exist after this later stage of the rolling. It is unlikely that VN precipitates will be present in the austenite at this temperature (unless unnecessarily high micro-alloy additions have been made). It would therefore be required to begin the final rolling passes immediately, to avoid grain growth.

Cooling of the steel should be done by water spray techniques, between passes during the final rolling of the steel. This would allow the final two to five rolling passes to be completed in the temperature range 950 - 1000 °C. A small amount of strain induced VN will then be present during subsequent cooling to retard grain growth. The high strain rates used during the final rolling passes will assist in suppressing recrystallisation in the steel.

Once the steel has left the final rolling stand accelerated cooling should be applied, such that the steel cools as rapidly as possible without the formation of bainite/acicular ferrite. This accelerated cooling will both retard austenite grain growth (as well as recrystallisation) and lower the austenite/ferrite transformation temperature. The cooling rate required depends upon the austenite grain size of the steel as it leaves the final rolling stand, and the chemical composition of the steel. It should therefore be determined experimentally for each processing route and chemistry.

Under these processing conditions a vanadium micro-alloyed steel will have a fine deformed austenite grain structure before transformation to ferrite. The transformation temperature will be reduced due to the high cooling rate, producing a high ferrite nucleation rate, and thus a fine ferrite grain size. Any interphase precipitation will be small in size, with a small row spacing. Further precipitation, however will occur in the ferrite phase, this being enhanced by the fast cooling rate in the austenite phase suppressing VN precipitation.

Cooling in the ferrite phase should not be too rapid, as this may prevent maximum precipitation hardening being achieved. Still air cooling will probably be sufficiently slow, as ferrite grain growth will be inhibited by the presence of precipitates.

The final result of this thermo-mechanical treatment on a vanadium micro-alloyed steel will be a precipitate hardened, fine grained ferrite/pearlite steel. This will have a high yield stress, due to strengthening from both the fine ferrite grain size and the fine dispersion of vanadium carbo-nitride precipitates throughout the ferrite. This precipitation strengthening will result in the steel having a proportionally high tensile strength. The steel will also have low (sub-ambient) fracture mode transition temperature, the fine ferrite grain size offsetting the increase in the fracture mode transition temperature due to precipitation hardening. Strain ageing of the steel is unlikely, the precipitation of vanadium nitride removing most, if not all free nitrogen from solution.

Chapter 3.

Preparation of the Samples.

A set of samples ("sample set 1") was created using a single 40 t cast of steel. A single cast was used to make all of these samples to isolate the effect of vanadium and nitrogen on the mechanical properties of the steel. The composition of this cast is given in table 3.1. The cast contained nominally 0.04 wt. % vanadium and 0.009% wt. nitrogen in it's base composition.

It was decided to use full scale sampling (as opposed to preparing samples in a laboratory) to make the results obtained relevant to industrial production.

The steel was continuously cast into two 150mm square strands. Tundish additions of ferro-vanadium and "Nitrovan" were made during casting to produce a selection of micro-alloy compositions. These additions were made at five second intervals, and consisted of sachets of crushed alloy, of a size between 1.4mm grid and 4.0mm grid. The sizes were chosen to prevent the alloy forming a slag on the molten steel, yet allowing dissolution before casting. Of the blooms produced, five were selected to be rolled.

The micro-alloy concentrations (vanadium and nitrogen) of the five selected blooms are given in table 3.2. The solubility product for vanadium nitride ([V] x [N] = [VN]) and the corresponding temperature at which equilibrium precipitation will occur [7] is also given.

Each of the five blooms were heated separately in a furnace at 1250 °C for three hours. The blooms were spaced between 60 normal production blooms to prevent their rolling causing upset to production rolling schedules. Upon leaving the furnace, the blooms were rolled in a two high reversing mill into five billets 63mm x 63mm by 4.4m long, three being placed into a billet re-heat furnace for further rolling. The surface temperatures of the billets entering the billet re-heat furnace were between 1060 - 1080 °C. The core temperature of the billets, however, was probably closer to 1100 °C. Temperatures readings were made with an optical pyrometer.

The billets were left in the billet re-heat furnace for 30 minutes, at 1100 °C, after which time one of the three billets was rolled. Rolling of production billets continued during this time, as the design of the billet re-heat furnace allowed three billets to be held to one side of the furnace without interfering with furnace throughput. The set temperature of the re-heat furnace was then lowered until the production billet temperature reached 1000 °C. After a further 30 minutes the second billet was rolled. Each billet temperature was measured as it left the furnace with an optical pyrometer. The third billet was discarded if no mill cobble occurred.

The final rolling sequence consisted of eleven sequential rolling stands, the reduction of each stand being given in table 3.3. The final bar diameter was 12mm. Austenite grain size prior to final rolling was considered unimportant, and therefore not measured, as a multi-pass rolling schedule was used (see section 2.2).

Element	:	C	Mn	Si	S	P	Al	Ni
wt. %	:	0.22	1.16	0.31	0.032	0.018	0.004	0.09

Element	:	Cr	Cu	Mo	Sn	Ti	V	N
wt. %	:	0.12	0.24	0.013	0.036	0.003	0.04	0.009

Table 3.1 Composition of cast from which samples were prepared.

Sample	[V] wt. %	[N] wt. %	Sol. Prod. $x10^{-4}$	Ppt. Temp. °C
8	0.055	0.0091	5.0	954
19	0.096	0.0093	8.9	1004
27	0.069	0.0101	7.0	983
33	0.096	0.0135	13.0	1036
50	0.041	0.0094	3.9	933

Table 3.2 Micro-alloy concentrations after additions of ferro-vanadium and "Nitrovan".

Rolling Pass	1	2	3	4	5	6	7	8	9	10	11
Reduction (%)	36	34	30	31	27	31	29	24	12	19	17

Table 3.3 Roll pass reductions of final rolling passes after the billet re-heat furnace.

As the bars left the last rolling stand their temperature was again measured by optical pyrometer. Due to the deformation during rolling, it can be considered that there were no temperature variations through the bar, and thus the measured surface temperature is the same as the core temperature of the bar. Table 3.4 shows the temperatures of the billets as they emerge from the billet re-heat furnace, and of the bars as they leave the last rolling stand.

It can be seen from table 3.4 that the billets rolled at approximately 1100 °C (A) experienced a decrease in temperature as they passed through the rolling stands. The billets rolled at the approximately 1000 °C (B), however, experienced an increase in temperature. It is possible that the billet temperature measured as the billets left the billet re-heat furnace was not totally representative of their actual average through section temperature, this explaining the temperature changes. However, the effects of heating caused by he rolling deformation and cooling through contact with the rolls must also be considered, these effects being potentially more significant. Therefore, as the temperature of the bars as they leave the final rolling stand can not be regarded as the actual rolling temperature with any accuracy, the samples will be considered to have been rolled at their intended temperature.

The bars were allowed to air cool after leaving the final rolling stand. However, a ceramic blanket was placed over a two meter portion near one end of the bars, so as to retard the cooling of some of the material (symbol #). This slower cooling would be representative of the cooling rate of a larger diameter bar.

It should be noted that no sample was obtained for billet number 33, rolled at approximately 1100 °C and slow cooled (33A#).

This processing sequence provided samples which comprised five compositions, two rolling temperatures, and two cooling rates, ie. 20 variable combinations.

A second set of samples ("sample set 2") was obtained from standard production stock of vanadium micro-alloyed steel bars (typical vanadium content 0.04 wt. %). These bars had diameters ranging from 12mm to 40mm, the identification codes relating to these bars shown in table 3.5. The chemical analysis of these bars is given in tables 3.6 and 3.7. The bars were rolled through a multi-pass finishing sequence (11 rolling stands, with the exception of diameters 28, 32, and 40 mm where 10, 9, and 8 rolling stands were used respectively) at approximately 1100 °C (the exact temperature not recorded), and air cooled to room temperature.

These additional samples were included to provide a cross reference to the effects of composition and cooling rate (being dependant on bar diameter) on the mechanical properties of the steel (primarily the 27 joule Charpy impact transition temperature), and the ferrite grain size. Only limited test material was available from these bars, since they had been prepared for some earlier unpublished work.

Sample & Identification	Temperature at Furnace °C	Temperature after Final Stand °C
8A	1078	1040
8B	993	1021
19A	1156	1063
19B	971	998
27A	1096	1037
27B	971	1020
33A	1113	1050
33B	968	1011
50A	1095	1043
50B	1002	1026

Table 3.4 Material rolling temperatures.

Diameter mm	16	20	24	28	32	40
Bar Codes	B1	X1	C1	Z1	D1	E1
	B3	X2	C3	Z2	D2	E2
	B4	X4	C4	Z3	D3	E3
					D4	E4
					D5	E5

Table 3.5 Bar diameters for secondary samples.

Element		C	Mn	Si	S	P	Al	Ni
wt. %								
	B1 :	0.20	1.14	0.26	0.019	0.027	0.004	0.07
	B3 :	0.22	1.25	0.35	0.024	0.018	0.005	0.10
	B4 :	0.26	1.27	0.37	0.019	0.017	0.004	0.08
	X1 :	0.24	1.30	0.28	0.021	0.033	0.005	0.07
	X2 :	0.22	1.33	0.40	0.025	0.023	0.005	0.08
	X4 :	0.20	1.35	0.23	0.020	0.026	0.008	0.09
	C1 :	0.22	1.19	0.29	0.026	0.022	0.004	0.08
	C3 :	0.24	1.32	0.35	0.024	0.017	0.005	0.08
	C4 :	0.19	1.29	0.36	0.024	0.038	0.005	0.08
	Z1 :	0.22	1.34	0.40	0.026	0.014	0.004	0.08
	Z2 :	0.25	1.19	0.32	0.029	0.024	0.004	0.11
	Z3 :	0.21	1.28	0.38	0.018	0.014	0.004	0.09

Element		Cr	Cu	Mo	Sn	Ti	V	N
wt. %								
	B1 :	0.08	0.34	0.010	0.042	0.003	0.035	0.008
	B3 :	0.09	0.27	0.014	0.037	0.004	0.041	0.009
	B4 :	0.07	0.28	0.013	0.038	0.004	0.042	0.009
	X1 :	0.08	0.27	0.012	0.043	0.003	0.077	0.010
	X2 :	0.10	0.39	0.012	0.029	0.004	0.040	0.010
	X4 :	0.11	0.41	0.014	0.031	0.003	0.052	0.013
	C1 :	0.08	0.25	0.010	0.028	0.003	0.037	0.009
	C3 :	0.07	0.30	0.012	0.032	0.003	0.043	0.009
	C4 :	0.09	0.33	0.012	0.031	0.004	0.046	0.008
	Z1 :	0.06	0.29	0.012	0.035	0.004	0.042	0.009
	Z2 :	0.10	0.37	0.015	0.030	0.003	0.041	0.009
	Z3 :	0.09	0.28	0.010	0.029	0.003	0.043	0.010

Table 3.6 Steel composition, bar diameters 16, 20, 24 and 28mm.

Element		C	Mn	Si	S	P	Al	Ni
wt. %								
	D1 :	0.25	1.20	0.29	0.020	0.020	0.004	0.09
	D2 :	0.22	1.29	0.28	0.020	0.017	0.005	0.08
	D3 :	0.22	1.22	0.33	0.022	0.016	0.005	0.07
	D4 :	0.21	1.28	0.28	0.025	0.029	0.004	0.07
	D5 :	0.29	1.26	0.35	0.017	0.015	0.004	0.09
	E1 :	0.20	1.41	0.30	0.020	0.029	0.004	0.09
	E2 :	0.33	1.40	0.33	0.021	0.029	0.006	0.09
	E3 :	0.21	1.42	0.26	0.016	0.035	0.006	0.09
	E4 :	0.16	1.31	0.31	0.019	0.014	0.004	0.10
	E5 :	0.14	1.19	0.31	0.023	0.018	0.005	0.10

Element		Cr	Cu	Mo	Sn	Ti	V	N
wt. %								
	D1 :	0.09	0.26	0.013	0.033	0.003	0.040	0.010
	D2 :	0.08	0.32	0.014	0.039	0.003	0.044	0.009
	D3 :	0.06	0.20	0.009	0.026	0.003	0.040	0.009
	D4 :	0.08	0.29	0.010	0.049	0.003	0.039	0.007
	D5 :	0.07	0.32	0.013	0.040	0.004	0.040	0.009
	E1 :	0.11	0.35	0.013	0.028	0.004	0.047	0.010
	E2 :	0.13	0.28	0.015	0.028	0.004	0.044	0.008
	E3 :	0.10	0.34	0.018	0.033	0.004	0.044	0.012
	E4 :	0.09	0.26	0.013	0.028	0.003	0.039	0.009
	E5 :	0.14	0.32	0.014	0.026	0.003	0.040	0.009

<u>Table 3.7</u> Steel composition, bar diameters 32 and 40mm.

Chapter 4.

Method of Testing and Results.

4.1 Grain Size Measurement.

Estimates of effective ferrite grain size were carried out for both sample set 1 and sample set 2 using a linear intercept method in accordance with ASTM standard number (designation E112-74). Samples from each bar were cut and polished to a mirror finish (the final polishing grit being one micron diamond), then etched in 2% nital for 15 seconds. This allowed ferrite grain boundaries to become clearly visible when viewed under an optical microscope. Eight photo-micrographs were taken of each sample, and a micro-scale for size determination. Sets of parallel lines were then drawn across these photo-micrographs, extending from the center of a ferrite grain at one end of the photograph to the center of another ferrite grain at the opposite end, bisecting the ferrite grains between these two points. The combined length of these lines, when divided by the number of grain boundaries "cut" by them, and corrected for magnification, is the average ferrite grain diameter of the sample.

The lines on the micro-photographs were drawn both parallel and perpendicular to the direction of rolling. This was done to determine if any grain elongation had occurred in the direction of rolling. Equiaxed grains should show the same grain size when measured both parallel and perpendicular to the direction of rolling. No ferrite grain elongation was found in any of the samples.

Table 4.1 shows the mean values and standard deviations of the measured ferrite grain sizes of all the samples used in this project. The measurements are displayed in the form (diameter)$^{-1/2}$, which should give a linear relationship with lower yield stress (see section 2.4(a)).

	Sample	Grain Size $mm^{-1/2}$	Standard Deviation
Sample Set 1	8A	13.1	0.4
	8B	13.4	0.5
	8A#	12.5	0.4
	8B#	12.8	0.3
	19A	13.6	0.9
	19B	13.6	0.5
	19A#	12.5	0.6
	19B#	13.3	0.2
	27A	13.7	0.8
	27B	13.5	0.5
	27A#	12.6	0.2
	27B#	13.1	0.5
	33A	13.6	0.6
	33B	13.7	0.7
	33B#	13.3	0.5
	50A	13.2	0.7
	50B	13.7	0.7
	50A#	12.0	0.4
	50B#	12.6	1.1
Sample Set 2	B1	11.2	1.0
	B3	11.3	0.2
	B4	12.1	0.7
	X1	12.4	0.3
	X2	12.0	1.1
	X4	12.0	1.5
	C1	11.1	0.2
	C3	11.9	1.0
	C4	10.6	0.2
	Z1	10.4	0.6
	Z2	11.2	1.3
	Z3	11.8	1.2
	D1	9.8	0.2
	D2	11.2	1.1
	D3	10.8	0.4
	D4	11.0	0.3
	D5	11.0	0.2
	E1	10.0	0.2
	E2	10.2	0.2
	E3	10.7	0.8
	E4	9.3	0.8
	E5	8.3	0.1

KEY

"A" : Rolling Temp. 1100 °C
"B" : Rolling Temp. 1000 °C
"#" : Retarded Cooling Rate.

Table 4.1 Ferrite grain size, including standard deviations of the results.

4.2 Tensile Testing.

Tensile test pieces were machined out of the sample bars for all of the samples in sample set 1, and the two largest bar diameters in sample set 2 (32mm and 40mm diameter). Limited sample material prevented tensile test pieces being machined out of the smaller sample bars in set 2. The test pieces had a reduced section of diameter 5.0 mm.

The test pieces were strained until failure, at a crosshead speed of 0.02 cm/minute on an Instron 1126 testing machine. A plot of load against extension was taken from each test. From these plots the yield stress and tensile strength of the sample were calculated, the values being displayed in table 4.2. Elongation at fracture was also measured for a 25mm gauge length.

The tensile test results shown in table 4.2 are an average of two tensile tests, with the exception of sample D2. The result for this sample is based on one sample only, due to limited sample material.

Where possible, multiple tensile test pieces were machined adjacent to each other and parallel to the center of the sample bar. This allowed economy of sample material, and prevented the inclusion of any center-line defect in the test pieces.

The effect of strain ageing on samples was also measured. Two further tensile test pieces were machined from each sample, pre-strained five percent, and aged at 100 °C for three hours. According to Hundy [62], this will give an equivalent ageing to that which would be obtained after 68 days at a room temperature of 15 °C.

The change in the flow stress of the samples due to strain ageing (ΔY = LYS aged - 5% strained flow stress), is also shown in table 4.2.

	Sample	LYS MPa	TS MPa	El %	ΔY MPa
Sample Set 1	8A	511	661	33	22
	8B	504	651	33	18
	8A#	498	650	34	4
	8B#	501	642	32	2
	19A	553	705	28	16
	19B	550	683	30	9
	19A#	542	698	30	7
	19B#	526	669	31	11
	27A	542	681	29	2
	27B	545	676	33	5
	27A#	524	676	30	12
	27B#	538	679	31	12
	33A	585	736	26	11
	33B	580	716	29	5
	33B#	559	713	30	10
	50A	491	636	32	48
	50B	497	640	32	37
	50A#	474	628	33	38
	50B#	468	619	33	33

KEY "A" : Rolling Temp. 1100 °C
"B" : Rolling Temp. 1000 °C
"#" : Retarded Cooling Rate.

	Sample	LYS MPa	TS MPa	El %	ΔY MPa
Sample Set 2	D1	440	637	31	36
	D2	431	624	30	27
	D3	420	610	31	29
	D4	445	634	31	17
	D5	476	690	28	15
	E1	463	656	29	10
	E2	493	678	27	8
	E3	485	684	28	27
	E4	398	571	28	48
	E5	384	537	34	42

Table 4.2 Tensile results.

LYS = Lower Yield Stress.
TS = Tensile Strength.
El = Elongation at Fracture on a 25mm Gauge Length.
ΔY = Change in Flow Stress due to Strain Ageing.

4.3 Measurement of the Fracture Mode Transition Temperature using Charpy V Notch Test Pieces.

Charpy V notch testing was done in accordance with BS 131.

Test pieces were machined from all the samples. These included both 10mm x 10mm standard cross-section test pieces and 10mm x 7.5mm sub-standard test pieces.

The test pieces produced from sample set 1 were all machined as 7.5mm sub-standard test pieces since insufficient material was available in the cross-section of the 12mm bars to produce a 10mm square standard test pieces. The test pieces in sample set 2 were all machined as 10mm square standard test pieces.

Additional 7.5mm sub-stand test pieces were also machined from the 32mm and 40mm diameter bars from sample set 2. This additional testing was done to allow correlation between 7.5mm sub-standard and 10mm standard Charpy test pieces, when used to define the fracture mode transition temperature.

Where possible, test pieces were machined so as not to include material along the center-line of the bars.

Charpy transition curves were plotted for the samples, emphasis being placed on the lower portion of the curve. An energy level of 27 joules was used to define the transition temperature for both the 10mm standard and the 7.5mm substandard test pieces. A lower energy level was not used for the 7.5mm sub standard test pieces to compensate for their smaller cross-sectional area, as not all transition curves for the substandard test pieces passed below an energy level of 20 joules (the equivalent energy level in terms of j/mm^2).

The fracture mode transition temperatures of all the samples are shown in table 4.3 with the Charpy transition curves for sample set 1 being shown in appendix C.

	Sample	Charpy T_{27} 10mm (°C)	Charpy T_{27} 7.5mm (°C)
Sample Set 1	8A	..	- 36
	8B	..	- 55
	8A#	..	- 35
	8B#	..	- 58
	19A	..	- 13
	19B	..	- 60
	19A#	..	- 11
	19B#	..	- 58
	27A	..	- 23
	27B	..	- 57
	27A#	..	- 39
	27B#	..	- 59
	33A	..	- 20
	33B	..	- 44
	33B#	..	- 35
	50A	..	- 35
	50B	..	- 58
	50A#	..	- 34
	50B#	..	- 51
Sample Set 2	B1	- 10	..
	B3	- 31	..
	B4	2	..
	X1	- 36	..
	X2	- 15	..
	X4	- 8	..
	C1	2	..
	C3	- 30	..
	C4	- 12	..
	Z1	4	..
	Z2	- 18	..
	Z3	- 11	..
	D1	3	- 1
	D2	- 35	- 32
	D3	- 4	2
	D4	- 29	- 22
	D5	20	11
	E1	13	10
	E2	18	24
	E3	18	29
	E4	- 5	- 18
	E5	3	- 4

KEY

"A" : Rolling Temp. 1100 °C
"B" : Rolling Temp. 1000 °C
"#" : Retarded Cooling Rate.

Table 4.3 Charpy transition temperatures.

T27 = Temperature at the 27 Joule Level of Energy Absorbed in the Charpy Impact Test.

4.4 Analysis of nitrogen content in the steel.

Vanadium, when present in a low carbon steel, is known to combine with interstitial nitrogen to form stable micro-precipitates (see Chapter 2). When a sample of vanadium micro-alloyed steel is dissolved in dilute sulphuric acid, these precipitates remain undissolved, allowing the nitrogen in the sample which is "free" to be distinguished from that which is "tied up" in stable precipitates.

$$N_{total} = N_{acid\ soluble} + N_{acid\ insoluble}$$

Analysis of the nitrogen concentration of all the samples, and their soluble and insoluble components, are shown in tables 4.4 and 4.5. The "standard" method of analysis [63] used to determine these totals is shown in appendix A.

When comparing the results for the soluble nitrogen concentration of the samples, as defined by the "standard" analysis technique, with the results obtained for the change in flow stress due to strain ageing (table 4.2), a discrepancy becomes obvious. The change in flow stress due to strain ageing at room temperature is caused by the presence of "free" nitrogen. This is the equivalent of soluble nitrogen, as defined by the analysis. The results from the analysis show that greater than 50% of the total nitrogen content in the steel samples is in the form of soluble nitrogen, indicating a high strain ageing propensity, yet there are very small changes in flow stress due to strain ageing. It was, therefore, suspected that the nitrogen analysis technique was dissolving some of the fine VN precipitates.

An alteration to the analysis technique was made to try and overcome this problem. Instead of dissolving drillings in 20% v/v H_2SO_4 over boiling water (see appendix A), an anode was machined out of the sample material, a part of which was dissolved in 5% v/v H_2SO_4 under the influence of a current of 1.3 amps/cm^2 at room temperature. This "Alternate" analysis method is discussed in Chapter 5.5 and detailed in appendix B. The results of this analysis are also shown in tables 4.4 and 4.5.

Sample	Standard Method			Alternate Method		
	N_{sol}	N_{insol}	N_{total}	N_{sol}	N_{insol}	N_{total}
	wt. %	wt. %	wt. %	wt. %	wt. %	wt. %
8A	0.0068	0.0023	0.0091	0.0031	0.0051	0.0082
8B	0.0065	0.0026	0.0091	0.0031	0.0048	0.0079
8A#	0.0059	0.0029	0.0088	0.0008	0.0061	0.0069
8B#	0.0053	0.0033	0.0086	0.0008	0.0066	0.0074
19A	0.0059	0.0034	0.0093	0.0030	0.0049	0.0079
19B	0.0049	0.0044	0.0093	0.0020	0.0066	0.0086
19A#	0.0052	0.0042	0.0094	0.0008	0.0056	0.0064
19B#	0.0041	0.0054	0.0095	0.0006	0.0064	0.0070
27A	0.0077	0.0027	0.0104	0.0029	0.0077	0.0106
27B	0.0069	0.0029	0.0098	0.0029	0.0074	0.0103
27A#	0.0070	0.0038	0.0108	0.0015	0.0069	0.0084
27B#	0.0072	0.0038	0.0110	0.0024	0.0084	0.0108
33A	0.0095	0.0043	0.0138	0.0030	0.0089	0.0119
33B	0.0076	0.0059	0.0135	0.0021	0.0096	0.0117
33B#	0.0072	0.0062	0.0134	0.0015	0.0095	0.0110
50A	0.0072	0.0022	0.0094	0.0040	0.0041	0.0081
50B	0.0072	0.0022	0.0094	0.0042	0.0042	0.0084
50A#	0.0065	0.0025	0.0090	0.0033	0.0050	0.0083
50B#	0.0064	0.0027	0.0091	0.0017	0.0055	0.0072

KEY "A" : Rolling Temp. 1100 °C
"B" : Rolling Temp. 1000 °C
"#" : Retarded Cooling Rate.

Table 4.4 Nitrogen analysis - Sample Set 1.

Standard Method - see appendix A
Alternate Method - see appendix B

Sample	Standard Method			Alternate Method		
	N_{sol}	N_{insol}	N_{total}	N_{sol}	N_{insol}	N_{total}
	wt. %	wt. %	wt. %	wt. %	wt. %	wt. %
B1	0.0074	0.0007	0.0081	0.0046	0.0035	0.0081
B3	0.0069	0.0020	0.0089	0.0034	0.0044	0.0078
B4	0.0070	0.0018	0.0088	0.0042	0.0034	0.0076
X1	0.0047	0.0051	0.0098	0.0014	0.0083	0.0097
X2	0.0078	0.0021	0.0099	0.0054	0.0044	0.0098
X4	0.0100	0.0030	0.0130	0.0058	0.0069	0.0127
C1	0.0069	0.0021	0.0090	0.0035	0.0048	0.0083
C3	0.0064	0.0028	0.0092	0.0029	0.0056	0.0085
C4	0.0053	0.0027	0.0080	0.0019	0.0059	0.0078
Z1	0.0068	0.0021	0.0089	0.0042	0.0047	0.0089
Z2	0.0059	0.0029	0.0088	0.0024	0.0062	0.0086
Z3	0.0071	0.0027	0.0098	0.0032	0.0061	0.0093
D1	0.0076	0.0023	0.0099	0.0039	0.0054	0.0093
D2	0.0061	0.0031	0.0092	0.0028	0.0060	0.0088
D3	0.0063	0.0028	0.0091	0.0034	0.0057	0.0091
D4	0.0048	0.0025	0.0073	0.0031	0.0042	0.0073
D5	0.0062	0.0024	0.0086	0.0037	0.0049	0.0086
E1	0.0069	0.0027	0.0096	0.0019	0.0061	0.0080
E2	0.0037	0.0040	0.0077	0.0008	0.0069	0.0077
E3	0.0094	0.0023	0.0117	0.0059	0.0058	0.0117
E4	0.0067	0.0022	0.0089	0.0042	0.0047	0.0089
E5	0.0061	0.0025	0.0086	0.0021	0.0063	0.0084

Table 4.5 Nitrogen analysis - Sample Set 2.

Standard Method - see appendix A

Alternate Method - see appendix B

Chapter 5.

Discussion of Results.

5.1 Ferrite Grain Size.

Grain size, represented by grain diameter in the form $d^{-1/2}$, is plotted as a function of vanadium content in figure 5.1 for sample set 1. It can be seen from this figure and table 4.1 that all the samples considered have a fine ferrite grain size, the diameter of the equiaxed grains ranging from 6.9 micrometers ($d^{-1/2}$ = 12.0) to 5.3 micrometers ($d^{-1/2}$ = 13.7). If only the "fast cooled" samples are considered, the range of grain size decreases further, ranging from 5.8 micrometers ($d^{-1/2}$ = 13.1) to 5.3 micrometers ($d^{-1/2}$ = 13.7). It would appear that the high degree of ferrite grain refinement associated with these "fast cooled" samples is primarily the result of their rapid cooling rate, as ferrite grain size is independent of both vanadium concentration and rolling temperature. This is not true, however, for the slow cooled samples, which show a significant dependence on both vanadium concentration and rolling temperature. A few assumptions can, therefore, be made as to the micro-structural history of the austenite for the samples in sample set 1.

Firstly it can be assumed that both the samples rolled at 1100 °C and 1000 °C had very similar austenite grain sizes at the completion of rolling. This is based on the facts that:

a). the ferrite grain size of the fast cooled samples lay within a narrow range.

b). the cooling rates of the fast cooled samples rolled at both 1100 °C and 1000 °C were very similar.

c). cooling rate appears to be dominant over vanadium concentration in determining the ferrite grain size of the fast cooled samples, which showed only minor variation. (ie. the high cooling rate of the fast cooled samples has produced two near horizontal lines essentially independent of composition and rolling temperature, which is not the case for the slow cooled samples).

These facts imply that variations in rolling temperature experienced by the samples (rolling at 1100 °C and 1000 °C) did not produce any additional ferrite grain refinement. As rolling was carried out above the recrystallisation stop temperature of the steel [32] it can be said that the maximum possible austenite grain size reduction through recrystallisation has been achieved. The austenite grain size of the samples at the completion of rolling was therefore constant, independent of whether the samples were rolled at 1100 °C or 1000 °C.

It should also be noted that if the rolling temperature of a micro-alloyed steel was lowered, the rolling loads would increase, due to the larger forces required to deform the steel as its temperature decreases. This reduction in rolling temperature may not produce any improvement in the mechanical properties of the steel, as significant ferrite grain refinement can be achieved by rolling at higher temperatures, achieving multiple recrystallisations, followed by accelerated cooling. It would therefore be more desirable to roll the steel at higher temperatures, and, therefore, increase the life of the rolling mill.

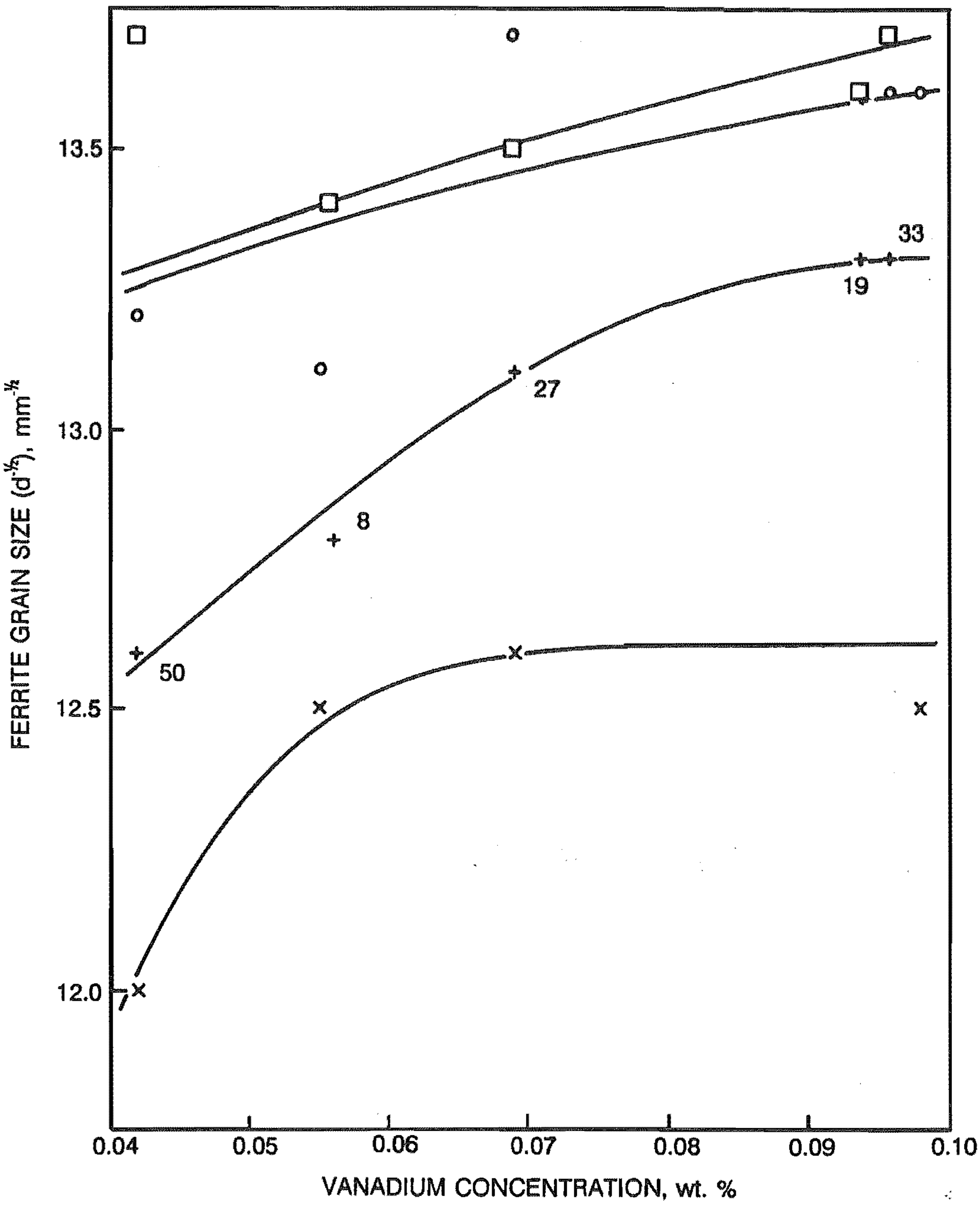

Figure 5.1 The effect of vanadium concentration on ferrite grain size - Sample Set 1.

(o) Approximate rolling temperature of 1100 °C, fast cooling rate applied.
(×) Approximate rolling temperature of 1100 °C, slow cooling rate applied.
(□) Approximate rolling temperature of 1000 °C, fast cooling rate applied.
(+) Approximate rolling temperature of 1000 °C, slow cooling rate applied.

A further assumption that can be made about the micro-structural history of the austenite is that there was significant strain induced precipitation of vanadium nitride in the austenite phase when rolling was carried out at both 1100 °C and 1000 °C, the effect of this precipitation only being significant, however, when the cooling rate of the samples was retarded. Considering solubility criteria, vanadium nitride precipitates were present in the two samples with the highest vanadium concentrations (19,33) prior to rolling at 1000 °C (see Chapter 3, table 3.2). Though these precipitates are probably too coarse to have a significant retarding effect on austenite grain growth, there presence indicates that conditions exist under which strain induced precipitation is most likely to occur during rolling (ie. maximum solubility in austenite, of vanadium in the presence of nitrogen). This strain induced precipitation is expected to retard temperature induced austenite grain growth. (This is discussed in more detail in Chapter 2.2).

Strain induced vanadium nitride precipitated as expected in samples 19 and 33 when rolled at 1000 °C. It also precipitated in samples 50, 8 and 27 at that temperature. Further, strain induced precipitation of vanadium nitride has also occurred in some of the samples rolled at 1100 °C, though in which of these samples this has occurred can not be stated accurately. This can be discerned from the effect that this precipitation has on ferrite grain size in figure 5.1. For the slow cooled samples, it can be seen that the ferrite grain size decreases ($d^{-1/2}$ increases) as the vanadium concentration of the samples increases. This is true for both the samples rolled at 1100 °C and 1000 °C. Further it can be seen that the samples which were slow cooled have experienced grain growth, the degree of this growth being reduced by either increasing the vanadium concentration of the samples, or decreasing the rolling temperature. Both of these methods increase the degree of strain induced precipitation experienced by the samples.

If it is assumed, as previously argued, that the austenite grain size of the samples was very similar at the completion of rolling, independent of rolling temperature, then it can be stated that sample 50 experienced strain induced precipitation of vanadium nitride when rolled at 1000 °C. This is because the ferrite grain size of sample 50, rolled at 1000 °C and slow cooled is smaller than the ferrite grain size of the same sample when rolled at 1100 °C and slow cooled. Both have a similar initial austenite grain size and cooling rate. They also had the same chemical composition. Therefore, difference in ferrite grain size must be solely the result of grain growth retardation by the presence of vanadium nitride precipitates on the austenite grain boundaries.

If the vanadium concentration of sample 50 is assumed to be the minimum vanadium concentration required to achieve strain induced precipitation of vanadium nitride when rolled at 1000 °C, then the degree of solubility reduction caused by the strain can be calculated. (Strain induced precipitation of vanadium nitride can be achieved at lower vanadium concentrations than this, as the ferrite grain size of sample 50, under slow cooling, differs depending on whether the sample was rolled at 1100 °C or 1000 °C. If no strain induced precipitation was present, then both samples would have very similar grain sizes). Assuming a nitrogen level of 0.009 wt. % (that of sample 50), the solubility product of vanadium nitride at this point is 3.6×10^{-4}. This relates to a solubility temperature under equilibrium conditions of 934 °C [7]. It can therefore be said that the effect of strain has decreased the solubility limit of vanadium nitride by 66 °C when the strain is carried out at 1000 °C.

The effect of cooling rate on grain size can also be seen in figure 5.2, plotted in the form of average ferrite grain diameter, ($d^{-1/2}$) against bar diameter. (In the case of the 12mm bar, the average value of ferrite grain size used considers only the samples rolled at 1100 °C and fast cooled, these being the normal production variables of these bars). Despite inaccuracies associated with varying unknown rolling temperatures, and different chemical compositions, it can be seen that a generally linear relationship exists between inverse square root of ferrite grain diameter and bar diameter. Figure 5.2 shows that the retarded cooling applied to the 12mm diameter bars is equivalent, in the worst case ($d^{-1/2} = 12$), to increasing the diameter of the bar to 16mm. Further observation of the figure reveals the difficulty of the task of maximising the mechanical properties of the larger diameter bars, these having a significantly larger ferrite grain structure than the 12mm diameter bars used in sample set 1. While further grain refinement is possible via accelerated cooling for these larger diameter bars, (for example, by using a water spray to cool the steel) this is limited by the formation of bainite/acicular ferrite, the presence of which has a detrimental effect on the mechanical properties of the steel [45]. (This will not occur if the acceleration of the cooling rate of the larger bars does not produce cooling rates faster than those experienced by the 12mm bars under air cooling). Beyond this limit the use of steels with larger vanadium concentrations is required to ensure that vanadium nitride precipitates are present during rolling to pin the grain boundaries of the austenite, and thereby refine the ferrite grain structure. It is recommended, therefore, that separate chemistries be prepared for each bar diameter in the production schedule, so as to maximise the ferrite grain refinement that can be achieved by thermo-mechanical treatment, and thus minimise the cost of expensive micro-alloy additions. In the case of smaller diameter bars, vanadium micro-alloy additions may not be necessary to meet strength requirements.

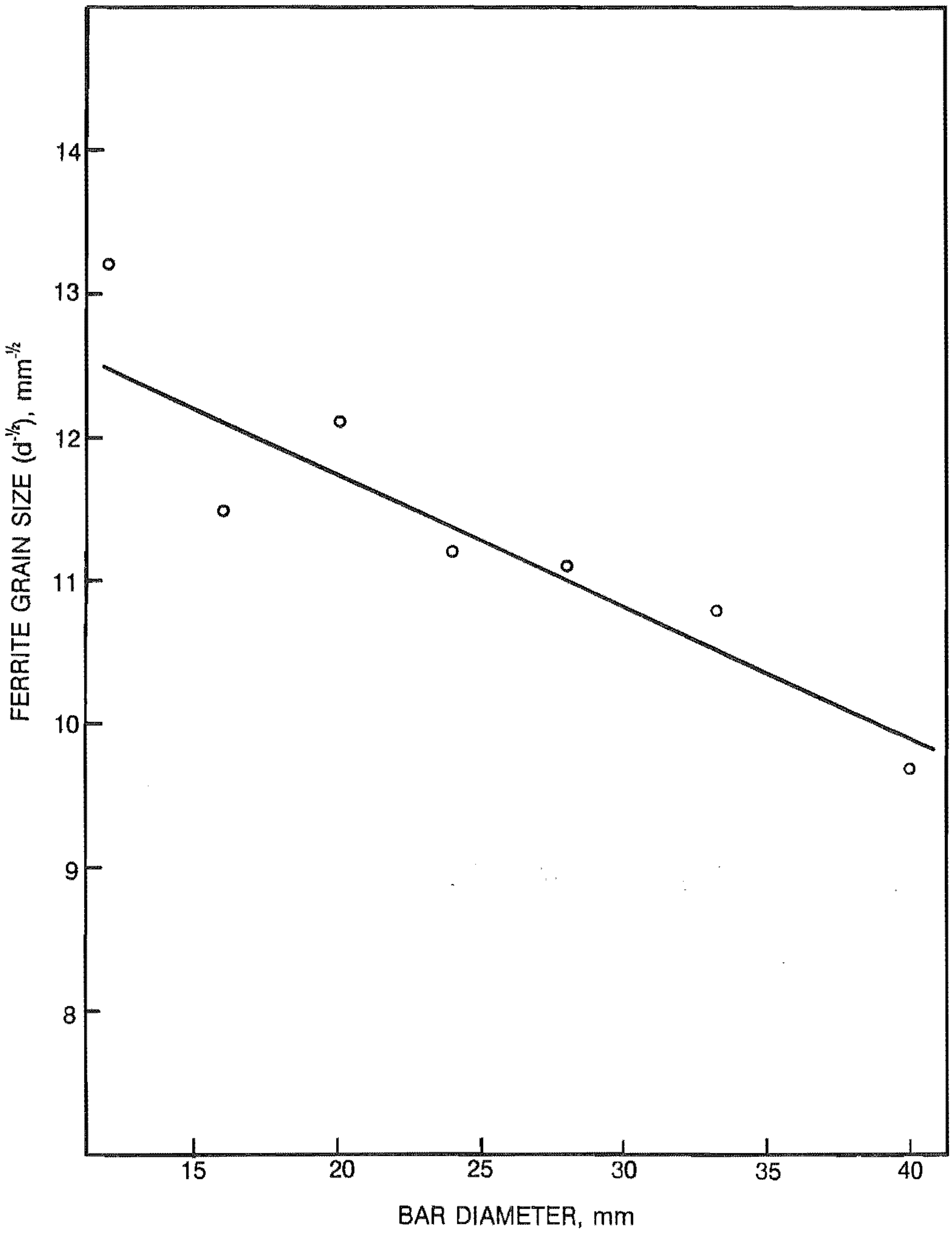

Figure 5.2 The effect of bar diameter on ferrite grain size.

5.2 Tensile Properties.

The addition of vanadium as a micro-alloying element to a low carbon steel is primarily to strengthen the steel through the production of a fine distribution of micro-precipitates in the ferrite phase. It would, therefore, be expected that the lower yield strength and tensile strength of the steel would increase as the vanadium concentration of the steel increased. This trend can be seen for sample set 1 in figure 5.3 (lower yield stress) and figure 5.4 (tensile strength), where an approximately linear relationship exists for both parameters, as a function of vanadium concentration. This linear relationship, with respect to vanadium concentration, for both lower yield strength and tensile strength, and the fact that the ferrite grain size of the samples fall within a narrow band implies that the primary factor contributing to both strength changes is vanadium carbo-nitride precipitation in the ferrite phase. Also, it would be probable that lower yield strength and tensile strength show a linear relationship when correlated with each other, both being a linear function of the same variable. This is shown to be true in figure 5.5.

Further evaluation of the relationship between both lower yield strength and tensile strength, and vanadium concentration, requires that the effects of precipitation in the ferrite phase be isolated from the effects of free (interstitial) nitrogen and ferrite grain size. Other factors such as carbon, silicon or phosphorus concentration can be ignored in this instance, since all the samples in set 1 were made from the same base steel. Vanadium lost from solution through precipitation of vanadium nitride in the austenite phase before rolling must also be deducted from the vanadium concentration of the samples, as the size of this precipitate is likely to be too large to have any significant effect on the strength of the steel. The resulting figures are then effectively plots of the frictional stress in the steel, as a function of ferrite phase micro-precipitation of vanadium carbo-nitride.

Irvine [64], by using multi-linear regression techniques to evaluate structure - property relationships for a set of normalised steels, produced a set of equations relating both lower yield strength and tensile strength to the chemical composition and micro-structure of the steels tested. Using these equations, the lower yield strength and the tensile strength of the samples in set 1 can be corrected for the effects of free nitrogen (N_f, as defined by the alternative nitrogen analysis technique - see section 5 of this chapter) and ferrite grain size (d). This correction has also been used by other authors [25]. Though Irvine's equations were generated from samples which were normalised, and are being applied to samples in the "as rolled" condition, the fact that the rolling of sample set 1 was carried out above the recrystallisation stop temperature means that an equilibrium, or near equilibrium structure existed upon cooling. Any residual strains in the austenite structure would not be carried through to the ferrite phase due to the strain free growth of the new structure. The resulting structure can be approximated by that of a normalised steel. Lower yield strength and tensile strength were, therefore, corrected by the following equations:

$$LYS' = LYS - 355.2(\%N_f^{1/2}) - 17.5(d^{-1/2}) \text{ N/mm}$$

$$TS' = TS - 7.7(d^{-1/2}) \text{ N/mm}$$

The vanadium lost from solution in the form of vanadium nitride precipitated under equilibrium in austenite can be calculated from solubility equations [7] at the respective rolling temperatures of the

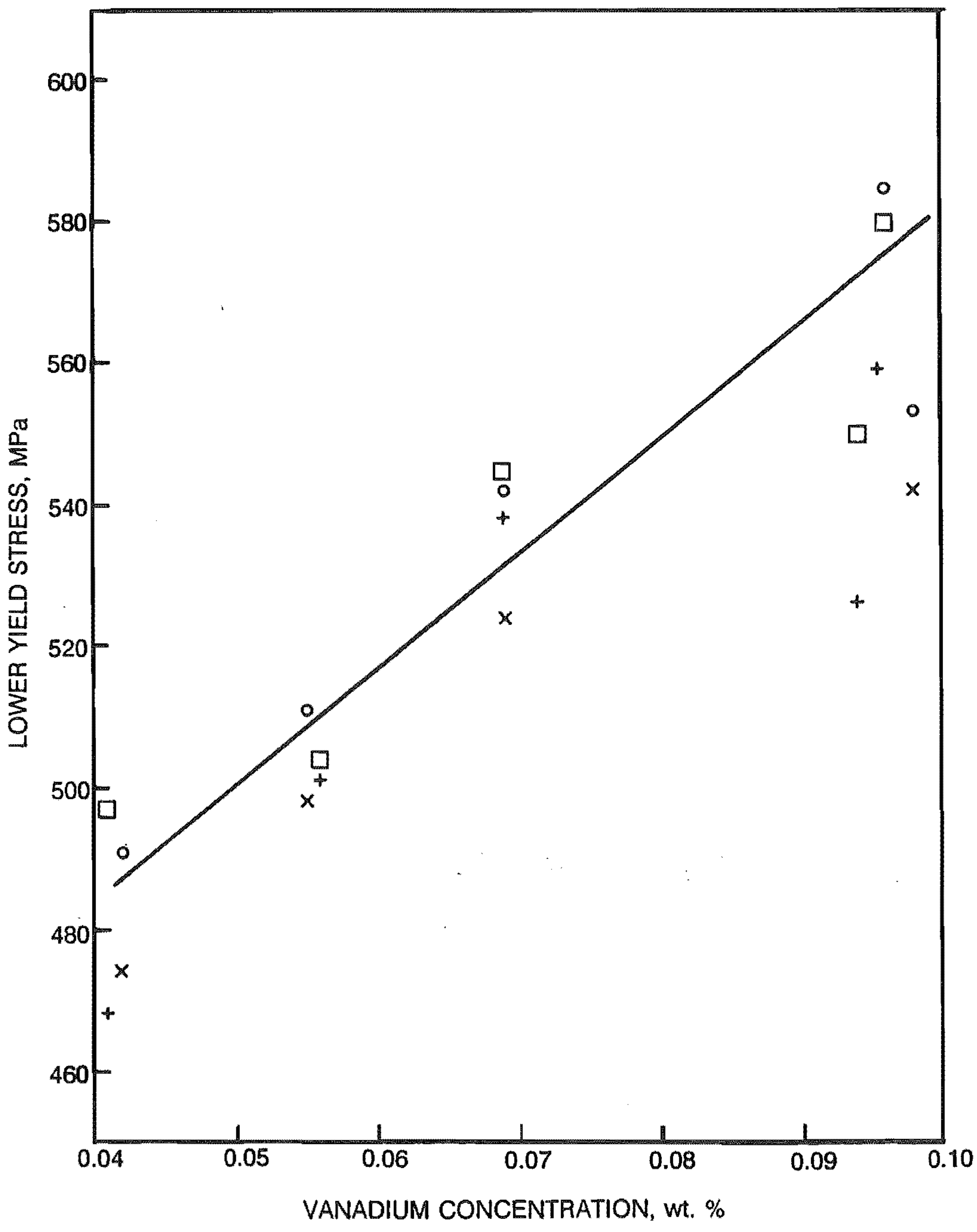

Figure 5.3 Lower yield stress as a function of total vanadium concentration - Sample Set 1.

(o) Approximate rolling temperature of 1100 °C, fast cooling rate applied.
(x) Approximate rolling temperature of 1100 °C, slow cooling rate applied.
(□) Approximate rolling temperature of 1000 °C, fast cooling rate applied.
(+) Approximate rolling temperature of 1000 °C, slow cooling rate applied.

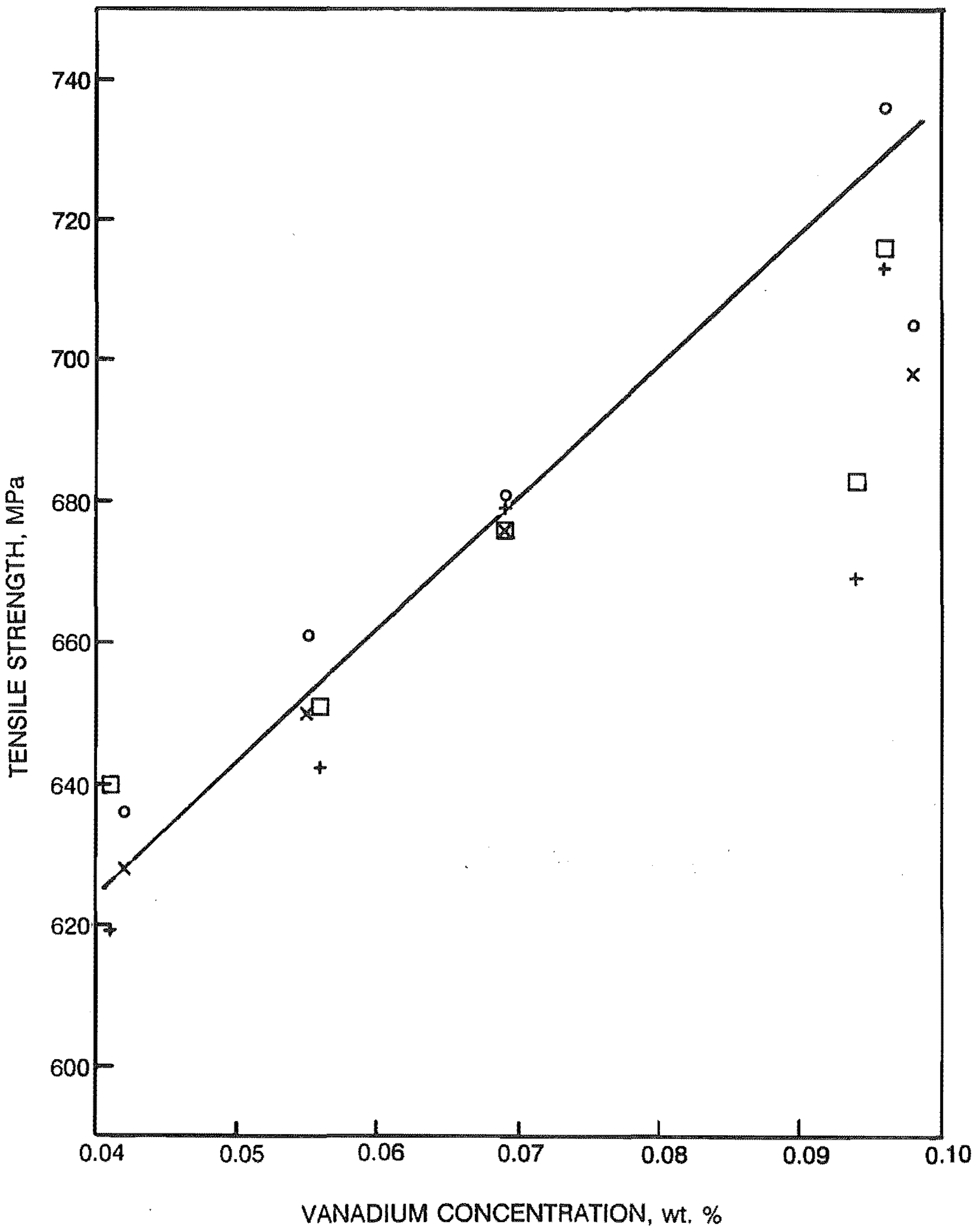

Figure 5.4 Tensile strength as a function of total vanadium concentration - Sample Set 1.

(o) Approximate rolling temperature of 1100 °C, fast cooling rate applied.
(x) Approximate rolling temperature of 1100 °C, slow cooling rate applied.
(□) Approximate rolling temperature of 1000 °C, fast cooling rate applied.
(+) Approximate rolling temperature of 1000 °C, slow cooling rate applied.

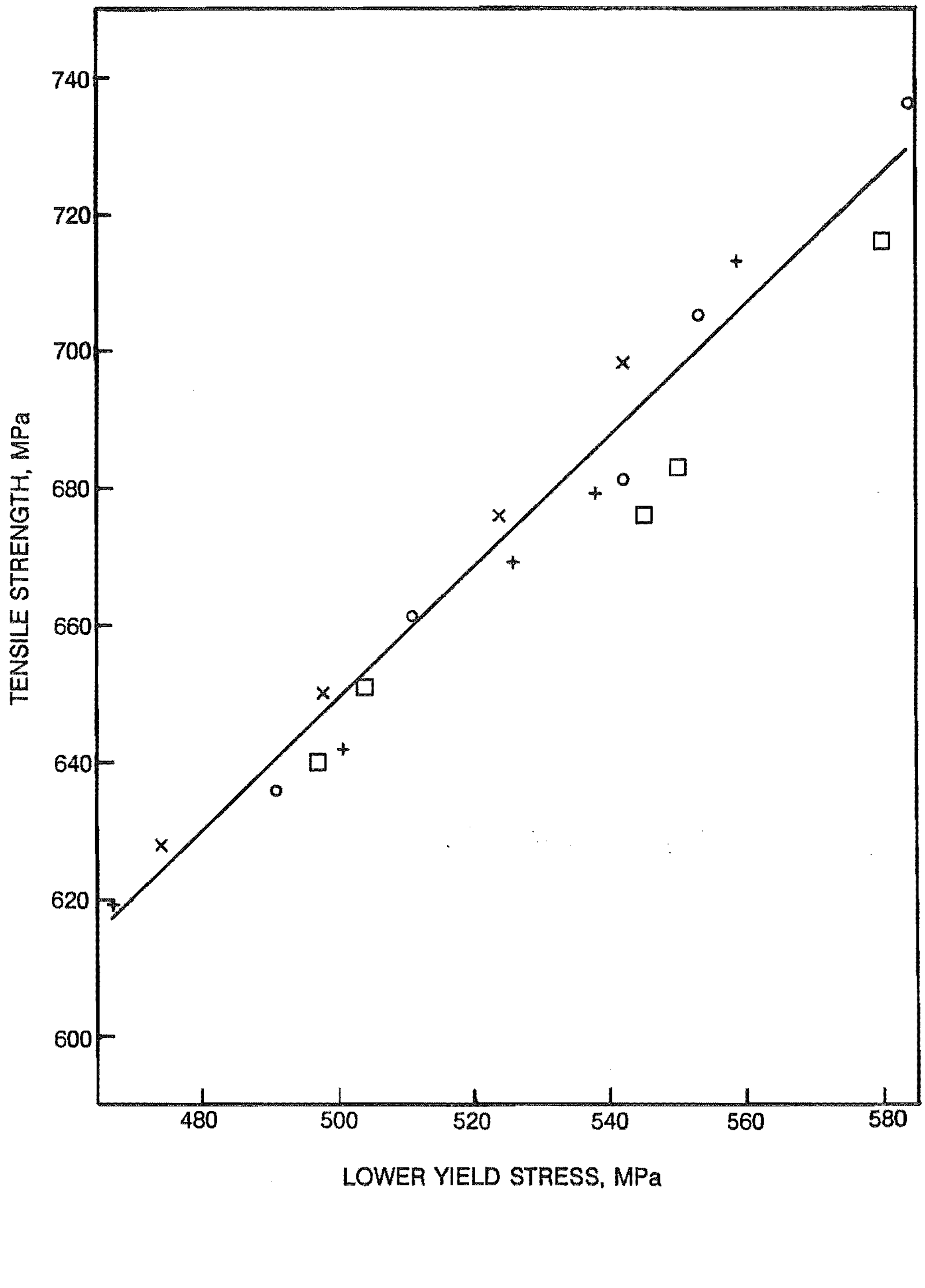

Figure 5.5 Correlation between lower yield stress and tensile strength - Sample Set 1.

(o) Approximate rolling temperature of 1100 °C, fast cooling rate applied.
(x) Approximate rolling temperature of 1100 °C, slow cooling rate applied.
(□) Approximate rolling temperature of 1000 °C, fast cooling rate applied.
(+) Approximate rolling temperature of 1000 °C, slow cooling rate applied.

samples ($\log_{10}[V][N] = -8330/T + 3.46$). Strain induced precipitation of vanadium nitride during the rolling of samples at 1000 °C cannot, however, be compensated for, as there is no easy way of measuring the volume fraction of this precipitation. It is possible, however, that these strain induced precipitates did not grow significantly during the cooling of the samples, such that they may not provide significant strengthening to the ferrite. Alternatively, these precipitates were not of sufficient volume fraction to remove large amounts of vanadium from solution during rolling. In either case, comparison with the results for the samples rolled at 1100 °C should show up any anomalies that this strain induced precipitation has caused.

Figures 5.6 and 5.7 show corrected lower yield strength (LYS') and tensile strength (TS') respectively, plotted against vanadium available for precipitation at the rolling temperature of the samples. It can be seen from both figures that results for the samples rolled at 1000 °C follow the results for the samples rolled at 1100 °C very closely. It would appear, therefore, that loss of vanadium from solution due to the strain induced precipitation of vanadium nitride during rolling has not adversely lessened precipitation strengthening in these samples. The concentration of vanadium available for precipitation during cooling in the ferrite phase can, therefore, be approximated for the samples considered by the concentration of vanadium available in solution at the start of rolling. Despite the obvious conflict in this assumption, all precipitation occurring after the start of rolling appears to play a significant part in the precipitation strengthening of ferrite phase, independent of the history of the steel, and can, therefore, be considered as a whole.

The above result suggests that statements by Pickering [24], that strain induced precipitation of vanadium nitride in austenite causes a reduction in the precipitation strengthening of a vanadium micro-alloyed steel, are not necessarily true. This loss of strengthening may only apply when large volume fractions of strain induced precipitates are formed during rolling, or when the cooling rate of the steel is such that strain induced precipitates coarsen excessively, and no longer enhance the precipitation strengthening of the steel.

The similarity of the curves in figures 5.6 and 5.7 indicates that there is a correlation between the effect of precipitation strengthening on lower yield strength and the effect of precipitation strengthening on tensile strength. This is understandable, as precipitation which would increase the frictional stress of the ferrite would also enhance the rate of work hardening of the steel. The correlation between these two curves is shown in figure 5.8.

The linear portions of the curves in figures 5.6 and 5.7 (ie. excluding the results for sample 19), indicate that the strengthening of the ferrite phase by micro-precipitation is directly proportional to the level of vanadium in solution during the rolling of the samples. It can be argued that this trend is primarily a result of the increase in the volume fraction of the precipitates that accompanies an increase in the vanadium in solution during the rolling of the steel, if it is assumed that the size of these precipitates is constant, and independent of the composition of the steel. (Variations in nitrogen concentration will only change the composition of the precipitates and not their size unless coherency with the matrix has been lost - see section 2.1). Increasing the concentration of vanadium available in solution for precipitation in the ferrite phase would, therefore, be expected to produce a proportional strengthening of the ferrite by progressively impeding the stress induced motion of dislocations through the ferrite lattice. The above assumptions, however, may not necessarily be true for all the steel samples under all the thermo-mechanical schedules. Certainly, under the "fast cooling" conditions experienced by some of the samples, it is likely that the precipitates formed would all be

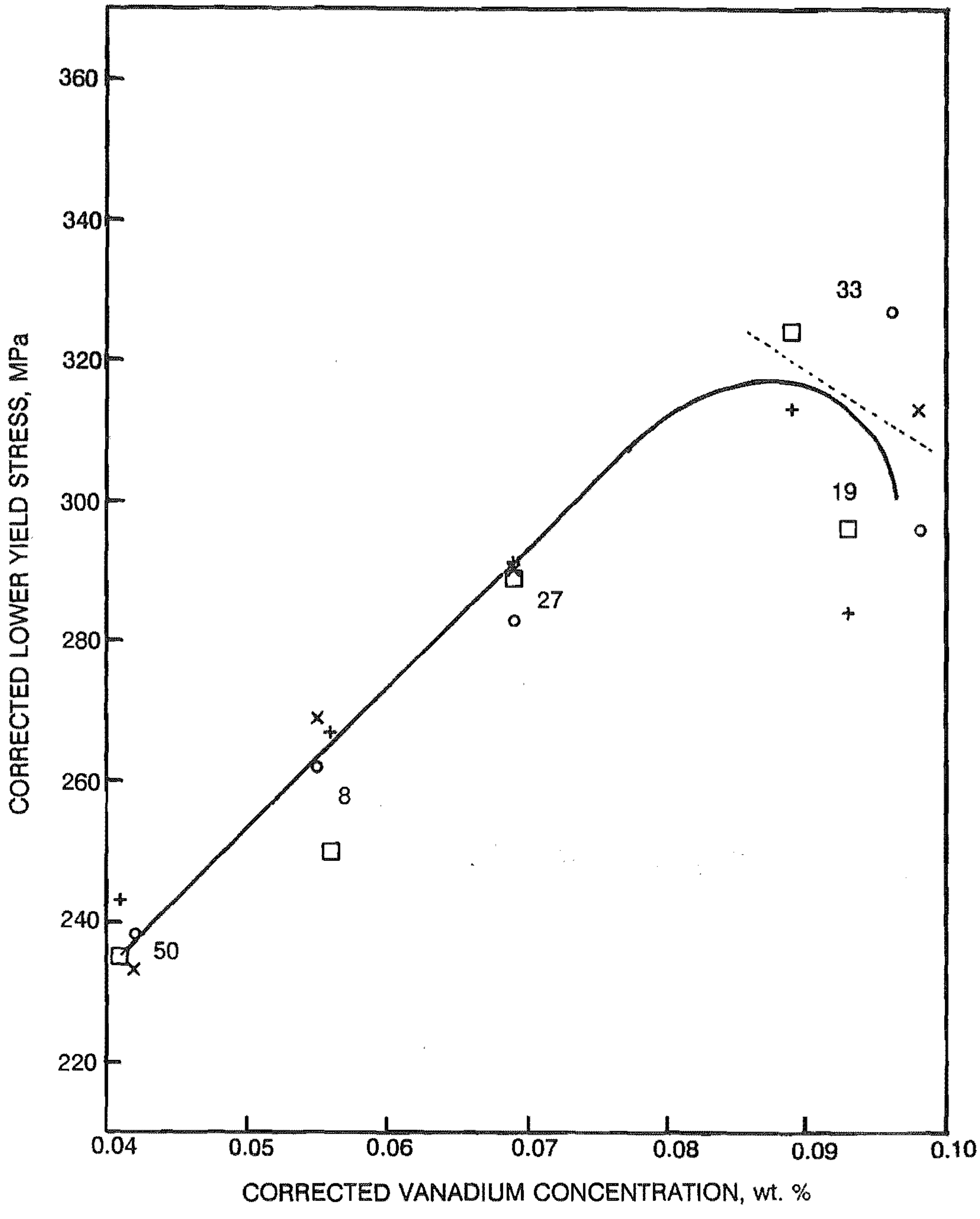

Figure 5.6 Corrected lower yield stress as a function of vanadium available in solution at the rolling temperature of the samples - Sample Set 1.

(o) Approximate rolling temperature of 1100 °C, fast cooling rate applied.
(×) Approximate rolling temperature of 1100 °C, slow cooling rate applied.
(□) Approximate rolling temperature of 1000 °C, fast cooling rate applied.
(+) Approximate rolling temperature of 1000 °C, slow cooling rate applied.

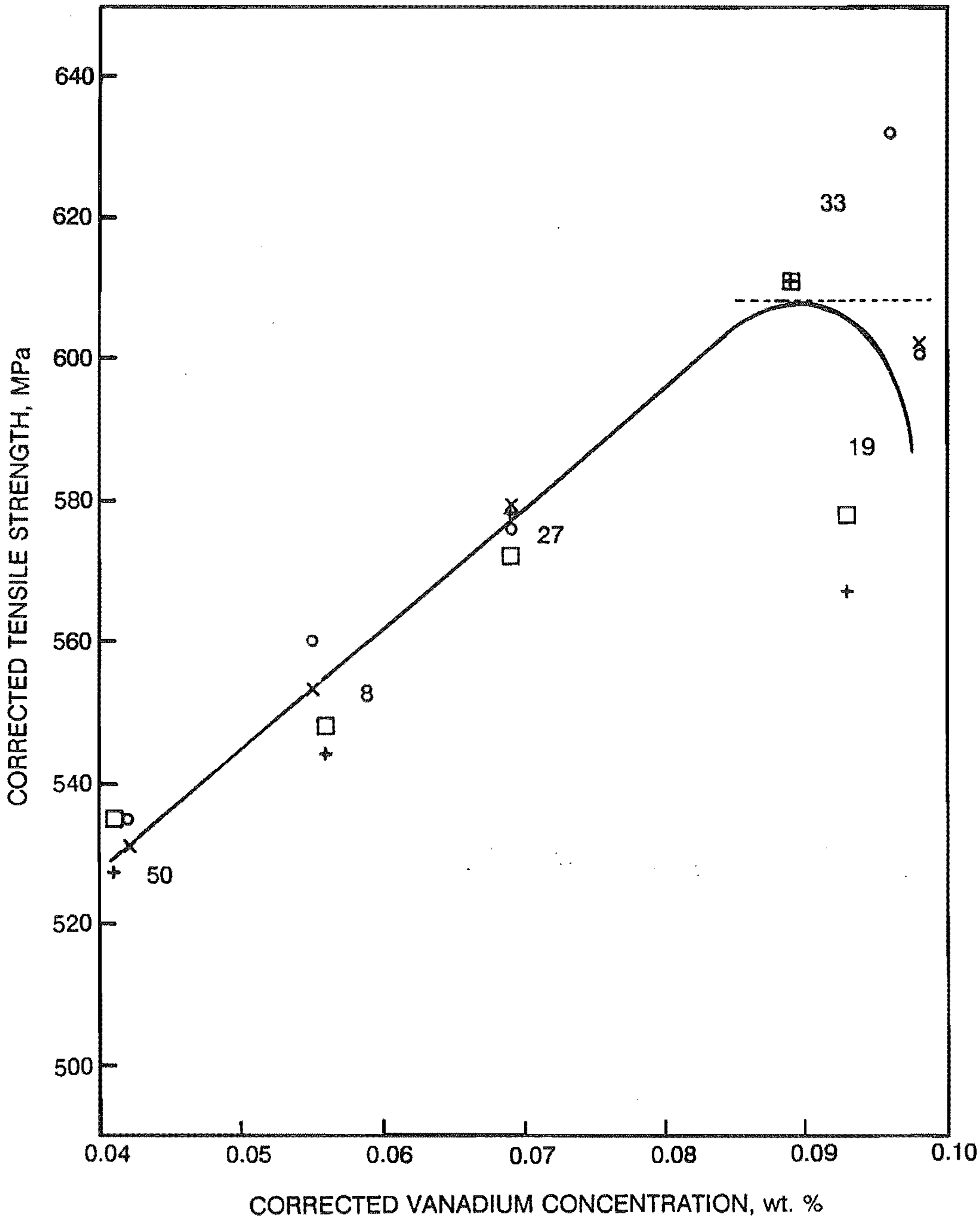

Figure 5.7 Corrected tensile strength as a function of vanadium available in solution at the rolling temperature of the samples - Sample Set 1.

(o) Approximate rolling temperature of 1100 °C, fast cooling rate applied.

(×) Approximate rolling temperature of 1100 °C, slow cooling rate applied.

(□) Approximate rolling temperature of 1000 °C, fast cooling rate applied.

(+) Approximate rolling temperature of 1000 °C, slow cooling rate applied.

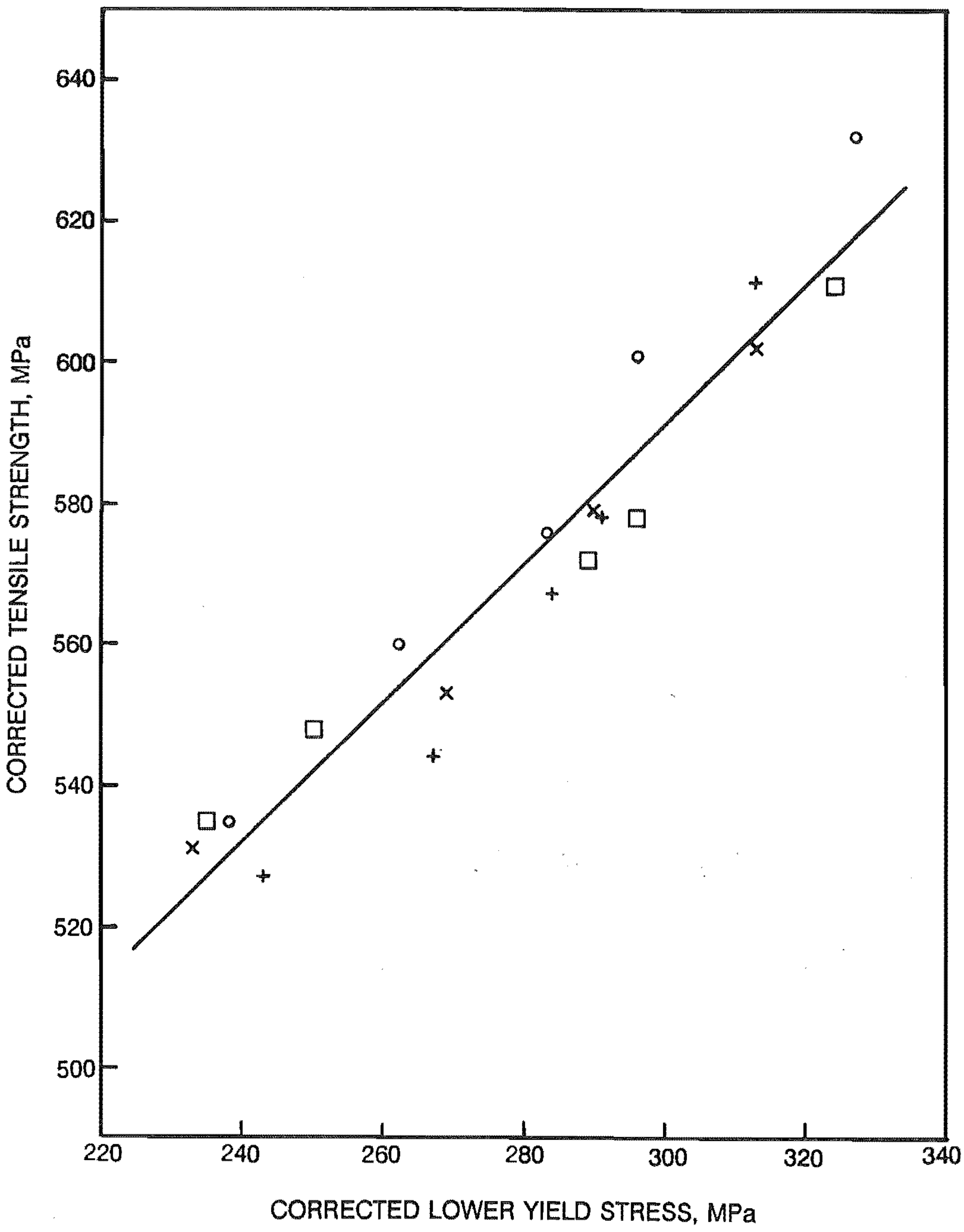

Figure 5.8 Correlation between corrected tensile strength and corrected lower yield stress - Sample Set 1.

(o) Approximate rolling temperature of 1100 °C, fast cooling rate applied.
(×) Approximate rolling temperature of 1100 °C, slow cooling rate applied.
(□) Approximate rolling temperature of 1000 °C, fast cooling rate applied.
(+) Approximate rolling temperature of 1000 °C, slow cooling rate applied.

of a similar size, independent of rolling temperature or chemistry. If the effect of cooling rate on ferrite grain size is considered, it can be seen from figure 5.1 that when the samples were under the "fast cooling" conditions, the ferrite grain size of the samples had only a minor dependence on their chemical composition (with respect to vanadium and nitrogen). This effect of cooling rate on grain size would be equivalent in magnitude to the similar effect of cooling rate on precipitate coarsening. This is because both grain growth and precipitate coarsening are essentially diffusion driven reactions. Cooling lowers the energy level of the migratory atoms, and thus slows their motion, retarding the growth of a ferrite grain or vanadium carbo-nitride precipitate in the same manner and to the same degree. It would, therefore, be expected that the size of the precipitates in the "fast cooled" samples was independent on the concentration of vanadium in solution. Thus, for sample set 1, all the precipitates formed under the "fast cooling" conditions would be unable to grow at the expense of other neighbouring precipitates, and would remain as a distribution of fine precipitates in the ferrite lattice, their spacing, and thus the volume fraction of the precipitates, dependent on the local concentration of vanadium. As the concentration of vanadium in solution increased, the separation of these precipitates would decrease. For the "slow cooled" samples, however, precipitate coarsening may occur, such that it would no longer be true that precipitation strengthening was proportional to the concentration of vanadium in solution. Under these conditions the growth of the precipitates would result in their associated strain fields decreasing, and, consequently, a reduction in the precipitation strengthening of the steel. This does not appear to have happened for the samples under consideration, however. The curve in figures 5.6 and 5.7 for the slow cooled samples follows the curve for the fast cooled samples, indicating that the slow cooling of the samples has not adversely affected the growth rate of the precipitates. It has been shown that the loss of coherency of vanadium carbo-nitride precipitates in a ferrite lattice is associated with a decrease in the strengthening that the precipitation produces in the lattice [31]. This is caused by the rapid growth rate experienced by the precipitates once they lose coherency with the surrounding ferrite lattice. For the samples considered, it is likely that there has been some growth of the precipitates in the "slow cooled" samples over and above that experienced by the "fast cooled" samples, but that the precipitates in the "slow cooled" samples have maintained coherency with the ferrite lattice, and thus no significant loss of strengthening has occurred.

A more significant point to note from figures 5.6 and 5.7 is the loss in strengthening as the maximum levels of vanadium in solution at the rolling temperature of the samples are reached. This loss of ferrite strengthening, despite an increase in the concentration of vanadium in solution, is at variance with the expected trend, described earlier. A possible explanation for this may be obtained, however, if it is realised that some of the samples had enhanced nitrogen levels (samples 27 and 33). The effect of these enhanced nitrogen levels being that a larger volume fraction of the vanadium carbo-nitride precipitates formed during the cooling of the steel will be nitrogen rich, as compared to carbon rich precipitates. (The higher solubility of vanadium carbide, with respect to vanadium nitride, results in the first carbo-nitride precipitates formed during the cooling of the steel having a composition close to that of vanadium nitride (ie. nitrogen rich), the carbon concentration of the precipitates increasing only as the levels of free nitrogen in the steel decrease. This is discussed in detail in Chapter 2.1). It has been suggested that these nitrogen rich vanadium carbo-nitride precipitates have a lower temperature induced growth rate than carbon rich vanadium carbo-nitride precipitates [31], such that a hyper-stoichiometric vanadium micro-alloyed steel containing an enhanced nitrogen level, and strengthened primarily by ferrite precipitation of vanadium carbo-nitride, would have a greater lower yield stress than the same steel without the enhanced nitrogen level, all other things being equal. The mechanism of this strengthening is attached in Chapter 2.4.

Considering figure 5.6 and 5.7, the two sets of samples shown to have a concentration of vanadium in solution during rolling of approximately 0.1 wt. % have differing nitrogen concentrations, the samples showing the higher strength values (33) having the higher total nitrogen concentration. This result, though predicted, does not apply, however, unless certain stoichiometry criteria are true. All the samples considered are hyper-stoichiometric with respect to nitrogen, yet only one of them shows signs of precipitate over-aging, (the other four samples producing a linear relationship with vanadium in solution at the rolling temperature). It can be assumed, therefore, that a threshold free nitrogen concentration exists, below which insufficient nitrogen is available in solution during the forming of these precipitates. Below this threshold the composition of the precipitates no longer gives them resistance to temperature induced growth. For the samples in sample set 1 this ratio appears to be an atomic ratio of 2:1.

Honeycombe [31] suggests that segregation of nitrogen to the surface of the nitrogen rich precipitates lowers their mismatch with the surrounding ferrite (when compared with carbon rich precipitates). This allows the nitrogen rich carbo-nitride precipitates to remain coherent with the ferrite lattice to larger "sizes" (ie. larger numbers of atoms forming the precipitates) than would be the case for the same precipitates if they were carbon rich. It can be seen, therefore, that during the growth of vanadium carbo-nitride precipitates, carbon rich precipitates would lose coherency with the ferrite lattice before nitrogen rich precipitates under the same growth rate. Having lost coherency with the surrounding ferrite lattice, these precipitates grow rapidly, the region of mismatch between the precipitate and the ferrite lattice being a high energy region, allowing high rates of solute diffusion to the precipitate. The precipitates subsequently "over-age", decreasing their resulting strengthening effect on the ferrite lattice. Relating this to figures 5.6 and 5.7, it would appear that sample 19, having a high vanadium concentration, but not having an enhanced nitrogen level, has a significant proportion of its strengthening produced by carbon rich vanadium carbo-nitride precipitates. These precipitates, being more susceptible to temperature induced growth than nitrogen rich carbo-nitride precipitates, have experienced some degree of over-aging. The result of this is that the lower yield strength and tensile strength of sample 19 is lower than its vanadium concentration would suggest, as can be seen by the lower yield strength and tensile strength of sample 33, which has an enhanced nitrogen concentration. This is true for all the four thermo-mechanical processing schedules considered. It would appear that the loss in strength due to "over-aging" is more significant than that due to retarding the cooling rate of the samples. This appears to be a reasonable observation, as the loss of coherency of a precipitate would be expected to cause a major drop in the strength of the ferrite. The diffusion rate at low temperatures in the ferrite, however, would only allow slight growth of precipitates during a retarded cooling schedule, the resulting loss in strengthening of the ferrite due to this growth being minor by comparison.

This result indicates the importance of enhancing the nitrogen content of a vanadium micro-alloyed steel when high levels of micro-alloy are added. If this not done, maximum strengthening of the ferrite will not be achieved, thus reducing the economics of the micro-addition.

Roberts and Sandberg [25], and other authors [24,54,55], found that for vanadium micro-alloyed steels, increasing the nitrogen level in the steel produced a commensurate increase in the proportion of the lower yield strength attributable to precipitation in the ferrite phase. It is possible that what they actually observed was the effect of increasing the volume fraction of nitrogen rich vanadium carbo-nitride precipitates in the ferrite phase, these precipitates resisting a loss in ferrite strength due to the over-aging of carbon rich precipitates. Their suggestion that precipitation strengthening of the ferrite phase in a vanadium micro-alloyed steel is purely dependant on the concentration of nitrogen in the steel implies that all the precipitates formed in the ferrite phase during cooling are vanadium nitride, or that the volume fraction of vanadium carbide (or carbon rich vanadium carbo-nitride) formed in the ferrite phase during cooling is independent of nitrogen concentration. This, however, in the case of Roberts and Sandberg, is in disagreement with their own work [19]. They argue that precipitates formed in the ferrite phase during the cooling of a vanadium micro-alloyed steel are nitrogen rich carbo-nitrides, the composition of these precipitates being dependent on the relative concentrations of vanadium, nitrogen, and carbon in solution in the ferrite as it cools. It can be assumed from the above argument that increases in the lower yield strength of a vanadium micro-alloyed low carbon steel, resulting from precipitation in the ferrite phase during cooling and attributable to increasing the nitrogen concentration of the steel, are in fact the result of increasing the proportion of nitrogen rich carbo-nitride precipitates in the ferrite phase. These precipitates reduce the loss of precipitation strengthening resulting from over-aging of carbon rich carbo-nitride precipitates in the ferrite phase.

The effect of nitrogen on k_y can be suggested as a factor influencing the lower yield strength, with respect to the concentration of vanadium and nitrogen in the steel. This effect has been discussed in detail in Chapter 2.5(a). The similarity of the results plotted in figure 5.6, relating to lower yield stress, with those plotted in figure 5.7, relating to tensile strength, however, removes the possibility that k_y is an important factor, as the tensile strength of a steel is totally independent of this parameter.

The effect of bar diameter on the lower yield strength and tensile strength of a vanadium micro-alloyed steel could not be accurately determined, and thus has not been included in this discussion. Though tensile results are available for the 32mm and 40mm bars, the variations in the chemistry of these bars prevented any meaningful correlations being obtained with respect to these bars and the 12mm samples. It can, however, be seen from figure 5.9 that there is a strong correlation between lower yield strength and tensile strength, similar to that shown by the 12mm bar samples. Though the effects of chemistry and micro-structure cannot be removed from this correlation, it can be reasonably assumed that the volume fraction and morphology of vanadium carbo-nitride precipitation has a significant effect on the mechanical properties of a vanadium micro-alloyed low carbon steel, even when the cooling rate of the steel is greatly retarded, as is the case for 32mm and 40mm bar diameters.

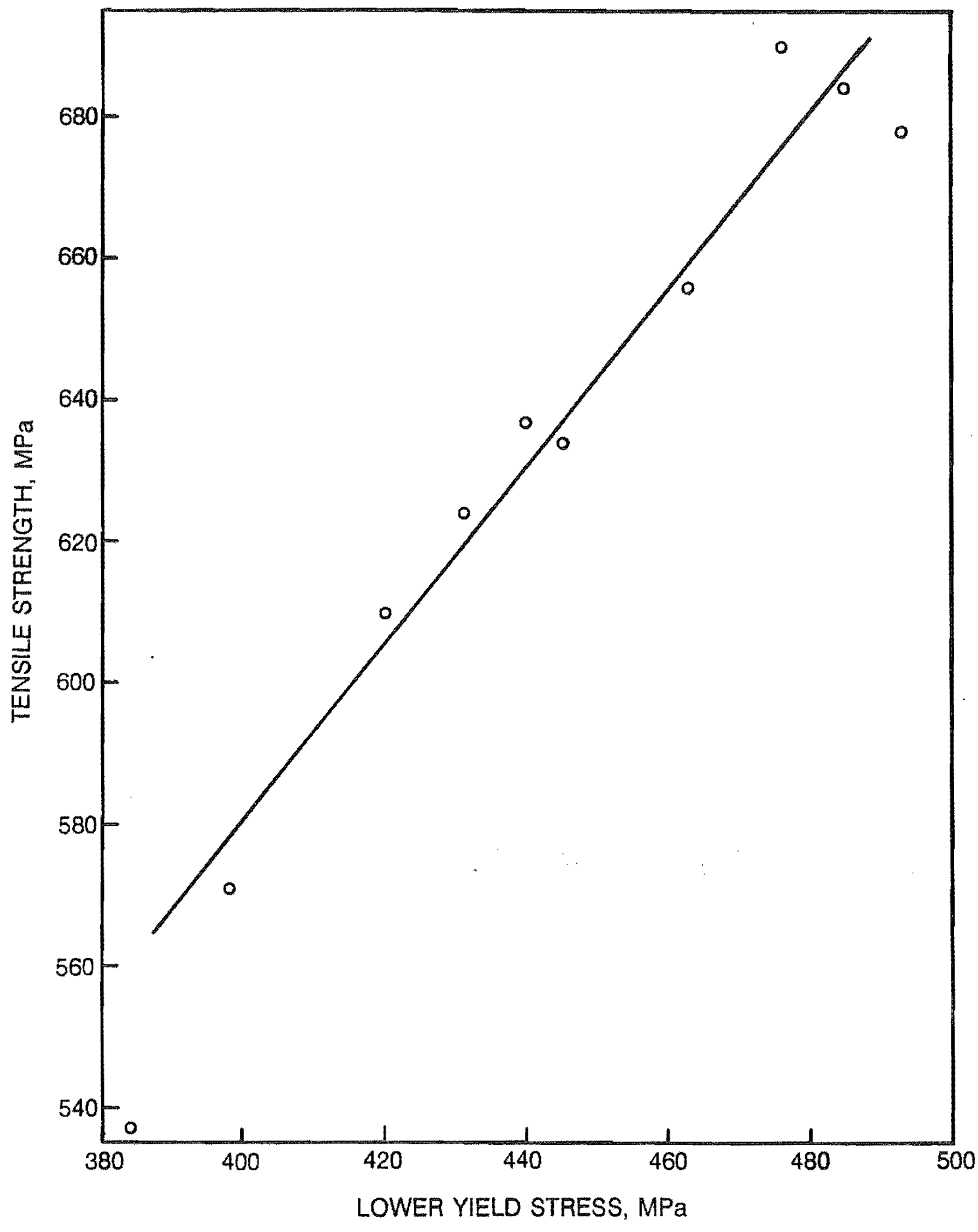

Figure 5.9 Correlation between tensile strength and lower yield stress - Sample Set 2 (Bar sizes 32mm and 40mm).

5.3 Fracture Mode Transition Temperature.

The fracture mode transition temperature, as measured by the Charpy impact test (T_{27}), is plotted in figure 5.10 for sample set 1 as a function of vanadium available in solution during rolling. The plotted values of Charpy transition temperature have been corrected for the effects of free nitrogen (N_f (wt. %), as defined by the alternative nitrogen analysis technique - see section 5 of this chapter) and ferrite grain size in the form of $d^{-1/2}$ ($mm^{-1/2}$), using a multi-linear equation suggested by Gladman [12], where corrected Charpy transition temperature is defined by the equation:

$$T_{27}' = T_{27} - 700(\%N_f^{1/2}) + 11.5(d^{-1/2}) \ ^\circ C$$

Gladman does not indicate whether his data was derived from as rolled or normalised samples, but it is assumed normalised steels were used. This would overcome grain orientation effects on the fracture mode transition temperature.

The concentration of vanadium available in solution during rolling is plotted against T_{27}', as the dependent variable, rather than total vanadium concentration, as the fore-mentioned variable does not include vanadium lost from solution by equilibrium precipitation of vanadium nitride in austenite prior to rolling. As stated earlier in this chapter, this precipitation is likely to be too coarse to play a significant role in the mechanical properties of steel. This correction, however, does not take into account the loss of strengthening produced by strain induced precipitation of vanadium nitride during rolling in the austenite phase. As this effect cannot be easily compensated for, it will not be isolated from the results, but rather, compensated for should any anomalies arise during the analysis of the results.

The resulting figure, therefore, is effectively a plot of frictional stress as a function of ferrite phase micro-precipitation of vanadium carbo-nitride and vanadium in solution in the ferrite lattice. This being the case, figure 5.10 can be compared with figure 5.6, as both show the same parameter (friction stress), though both are derived from different mechanical properties. Like figure 5.6, figure 5.10 shows a linear correlation between T_{27}' and vanadium available in solution during rolling, with the linear relationship being a function of the volume fraction of precipitate and the vanadium in solution in the ferrite lattice. Also, figure 5.10 shows a loss of strengthening when high concentrations of vanadium are added to the steel without enhancing the nitrogen level. The reasons for this are fully explained in section 2 of this chapter and will not be repeated here.

It may be further observed from figure 5.10 that the corrected values of Charpy transition temperature (T_{27}) for all the samples rolled at 1000 °C are lower than those for the samples rolled at 1100 °C, the difference between the two curves being approximately 16 °C. This difference may be very significant, especially if the failure mode of the steel near ambient temperature is by cleavage failure (brittle). In such cases it would be desirable to have the rolling temperature of the steel as low as possible, despite the increase in rolling loads, as from these results it can be argued that lowering the rolling temperature of the steel will result in a change to a ductile failure mode (micro-void coalescence) at ambient temperature. This difference in Charpy transition temperature is further highlighted by figure 5.11, which is a plot of corrected lower yield stress (LYS') against corrected Charpy transition temperature (T_{27}') ie. frictional stress derived from lower yield stress against frictional stress derived from Charpy transition temperature. The resulting figure shows two linear, near parallel, curves, indicating a direct one to one relationship between the variables (corrected Charpy transition

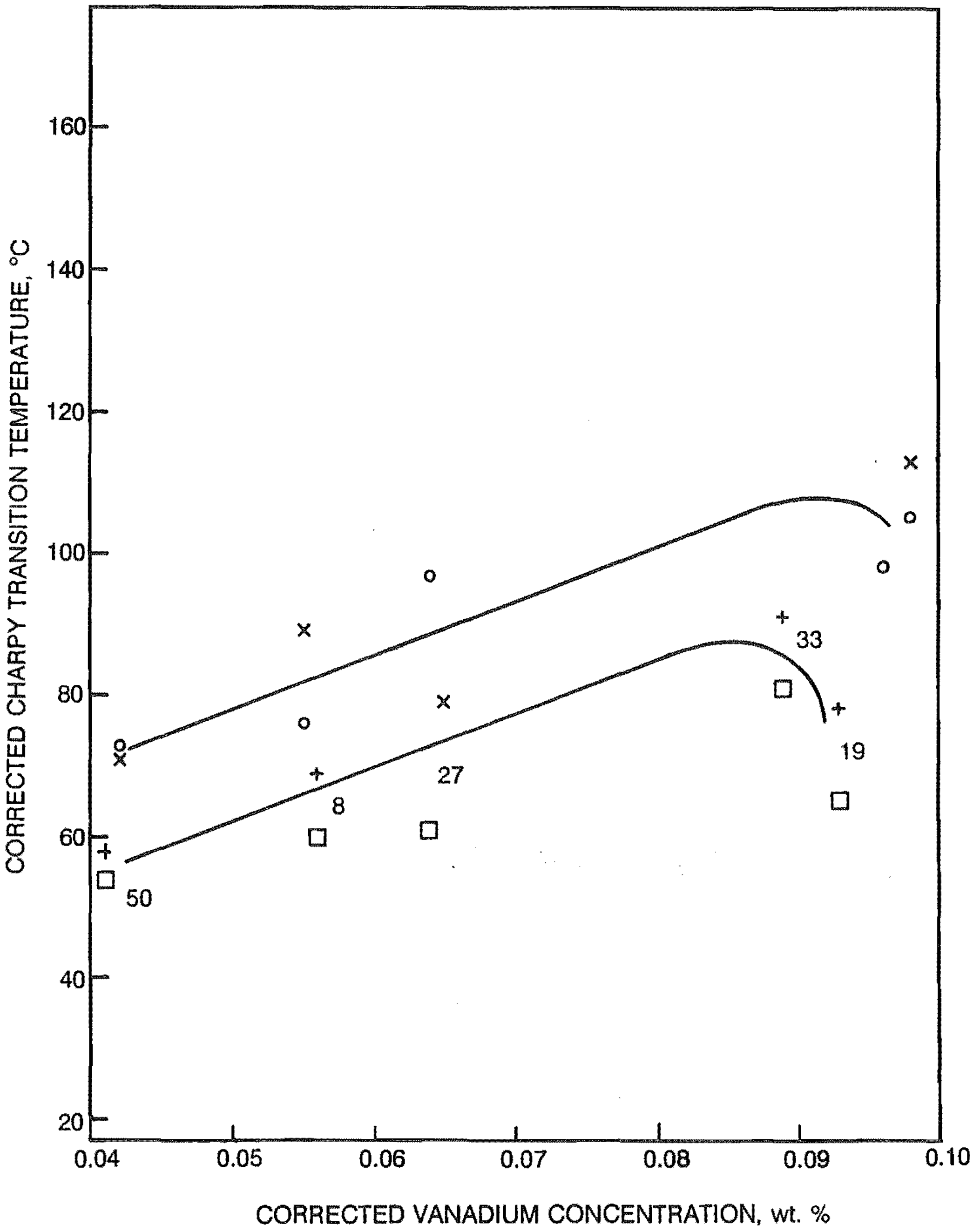

Figure 5.10 Corrected Charpy transition temperature as a function of vanadium available in solution at the rolling temperature of the samples - Sample Set 1.

(o) Approximate rolling temperature of 1100 °C, fast cooling rate applied.
(x) Approximate rolling temperature of 1100 °C, slow cooling rate applied.
(□) Approximate rolling temperature of 1000 °C, fast cooling rate applied.
(+) Approximate rolling temperature of 1000 °C, slow cooling rate applied.

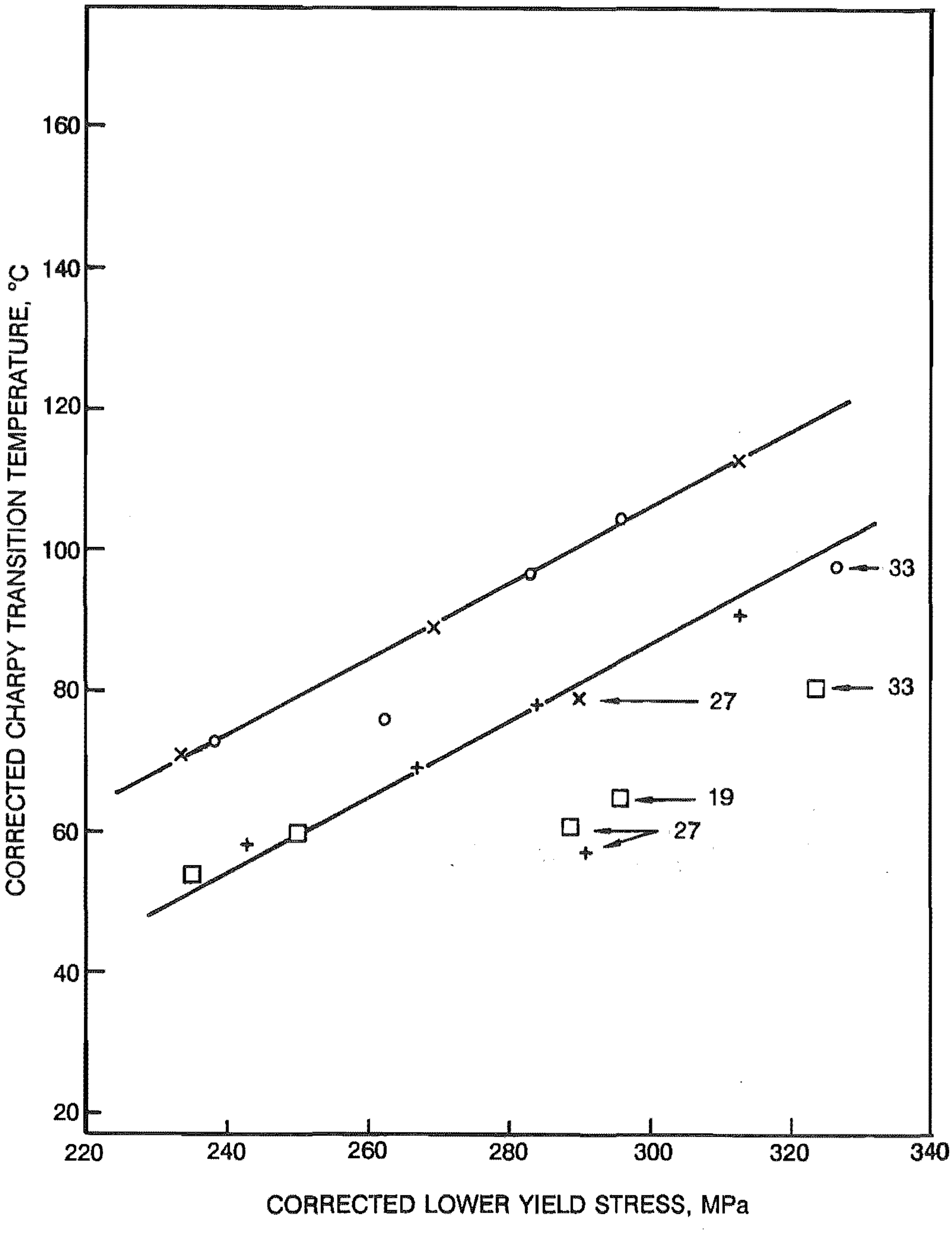

Figure 5.11 Correlation between corrected Charpy transition temperature and corrected lower yield stress - Sample Set 1.

(o) Approximate rolling temperature of 1100 °C, fast cooling rate applied.
(x) Approximate rolling temperature of 1100 °C, slow cooling rate applied.
(□) Approximate rolling temperature of 1000 °C, fast cooling rate applied.
(+) Approximate rolling temperature of 1000 °C, slow cooling rate applied.

temperature and corrected lower yield stress), the relationship being a function of a third variable, namely the rolling temperature of the steel. (The plotted points fall into two linear curves, each one related to a specific rolling temperature, ie. CCTT = 63 + 0.66 x CLYS °C at a rolling temperature of approximately 1100 °C and CCTT = 43 + 0.54 x CLYS °C at a rolling temperature of approximately 1000 °C). The most probable cause of this dependence on rolling temperature is grain orientation caused by rolling. Parameters such as pearlite laminae spacing can be ignored as this is effected by composition and cooling rate, but is independent of rolling temperature. The effect of grain orientation has been found to produce enhanced mechanical properties in the direction of rolling, but also a greater propensity for failure by cleavage under an applied stress normal to the direction of rolling [12]. In a charpy test piece, for the samples under consideration, failure by cleavage is under an applied stress parallel to the direction of rolling. Shear stresses along the test piece, however, can produce delamination parallel to the direction of rolling ahead of a propagating cleavage crack. These delaminations "blunt" the advancing crack, and result in retardation of the propagation of the crack. The net result of this is that the fracture mode transition temperature of the steel is lowered.

The scatter of points on figure 5.11 appears random in nature. No explanation can be offered for this anomaly, other than it may be related to strain induced precipitation during rolling in the austenite phase.

The effect of cooling rate appears to have a small and inconsistent effect on the fracture mode transition temperature of the samples considered in figure 5.10, no obvious trend being apparent. Retarding the cooling rate of the samples would produce precipitate coarsening, and thus a loss of precipitation strengthening. This would lower the fracture mode transition temperature of the samples. A set of charpy test pieces were prepared from sample set 2 to determine the effect of cooling rate on the fracture mode transition temperature by measuring the effect of bar diameter on this property (see tables 3.5 and 4.3). The larger the bar diameter, the slower the cooling rate, and vice versa. Sample 50A, rolled at approximately 1100 °C and fast cooled, was used as the sample for a bar diameter of 12mm, as this sample has a similar alloy composition and thermo-mechanical history to the other samples measured. Figure 5.12 shows the correlation between Charpy transition temperature (T_{27}) and bar diameter. From this figure it can be seen that there is a significant increase in the transition temperature as the cooling rate of the samples decreases. However, if a correction is made for the effects of ferrite grain size (table 4.1) and free interstitial nitrogen (table 4.5), it is found that cooling rate has a minimal effect on the transition temperature of these samples. It can be postulated that cooling rate has only a minor coarsening effect on the precipitate strengthening of the ferrite lattice. This is shown in figure 5.13. This result indicates that despite the retarded cooling rate of the larger bars, the cooling rate of the samples was still high enough to prevent significant solute diffusion through the ferrite matrix, preventing the coarsening of the precipitates during cooling.

Further charpy tests were carried out with samples from sample set 2 to evaluate any significant differences between Charpy transition temperatures measured using standard 10.0mm x 10.0mm test pieces, and sub-standard 7.5mm x 10.0mm test pieces. Correlation between the two would give significance to the results obtained for sample set 1. The results of these tests are shown on figure 5.14. The temperatures shown on this figure are all based on a 27 joule energy level. It can be seen from the figure that a linear relationship exists between the results for the two different sizes of test pieces, indicating that a 7.5mm sub-standard test piece can be used in the place of 10mm standard test piece for measuring the Charpy transition temperature of these vanadium micro-alloyed steels (and probably any low carbon steel). This correlation is independent of the cross sectional area of

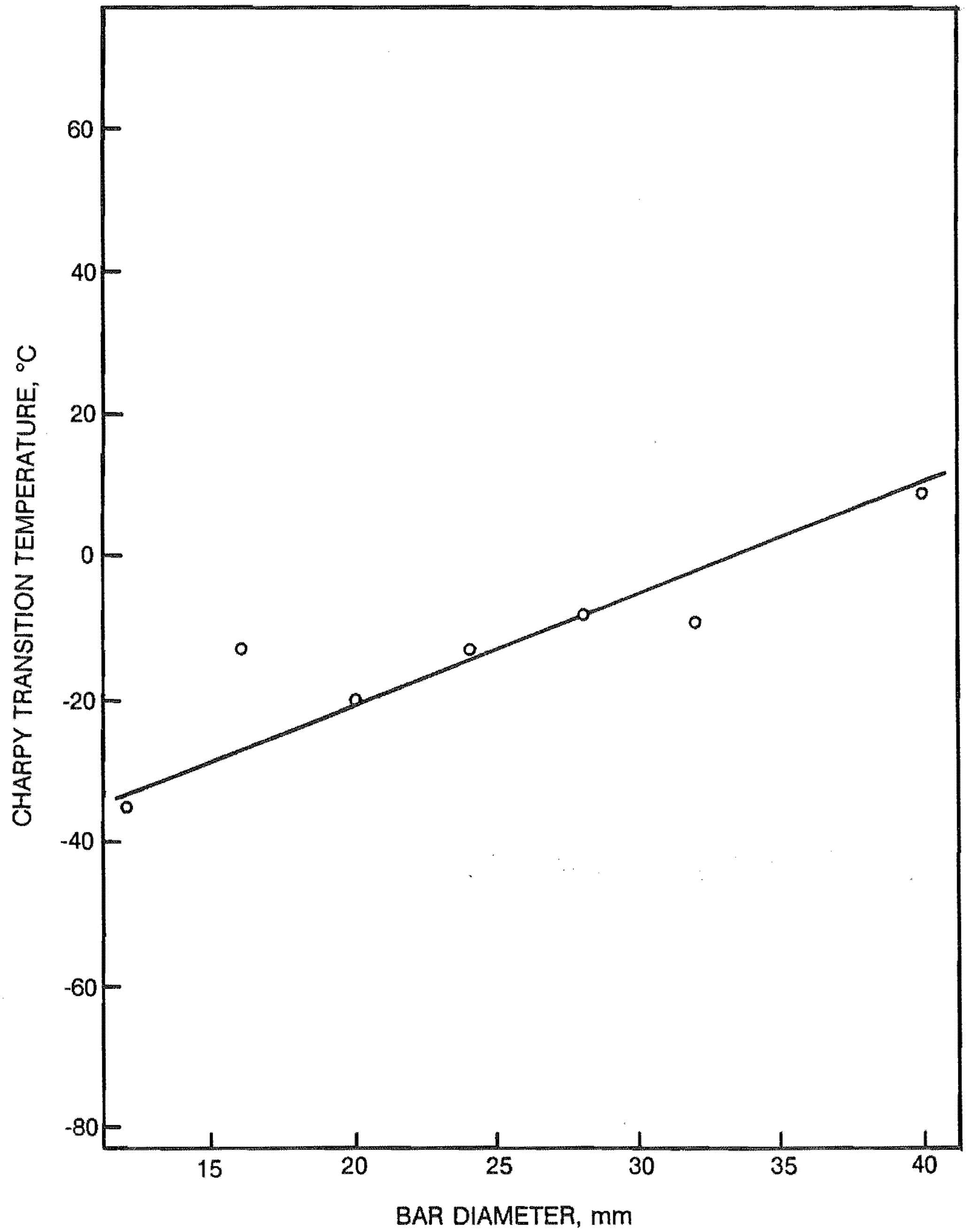

Figure 5.12 Charpy transition temperature as a function of bar diameter.

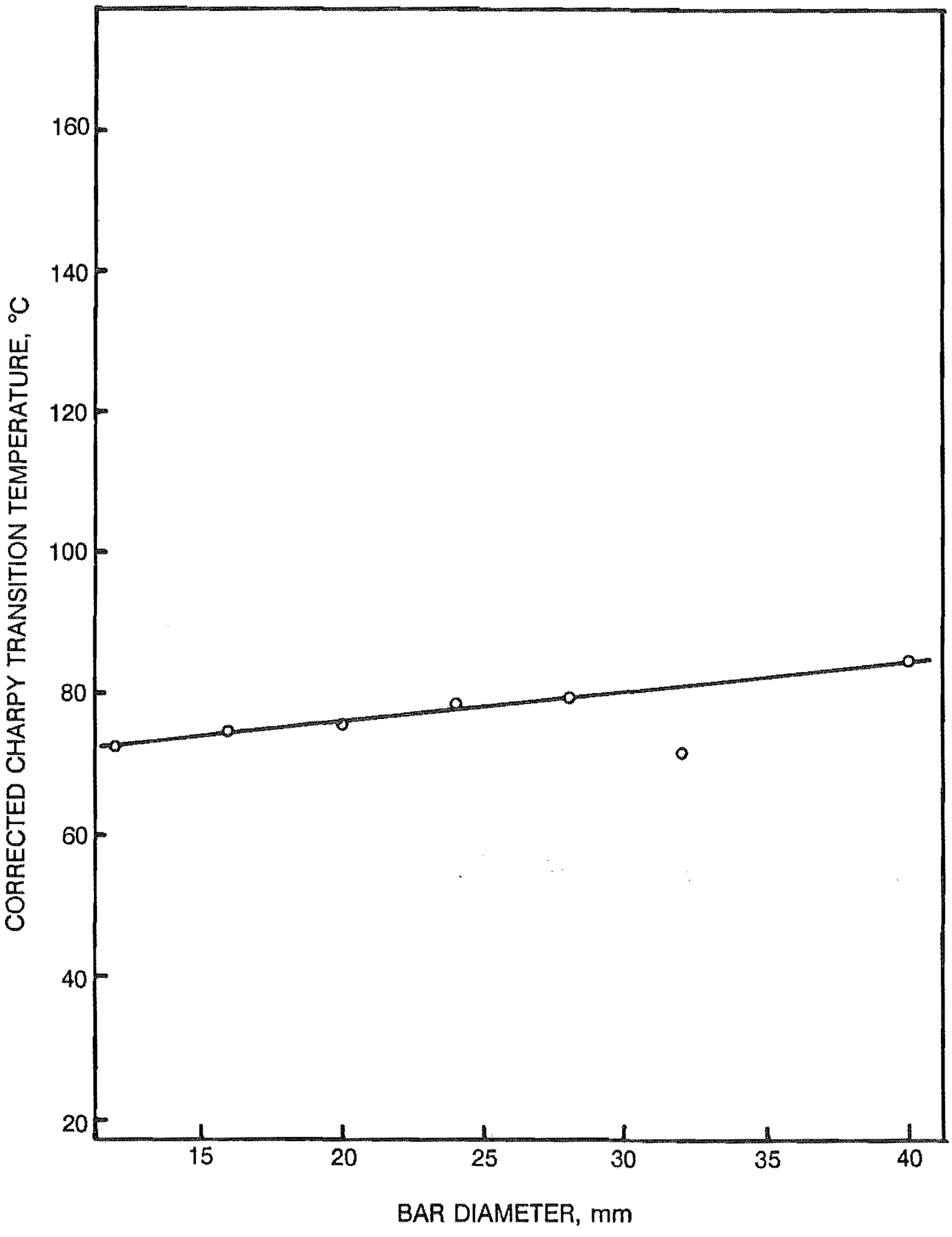

Figure 5.13 Corrected Charpy transition temperature as a function of bar diameter.

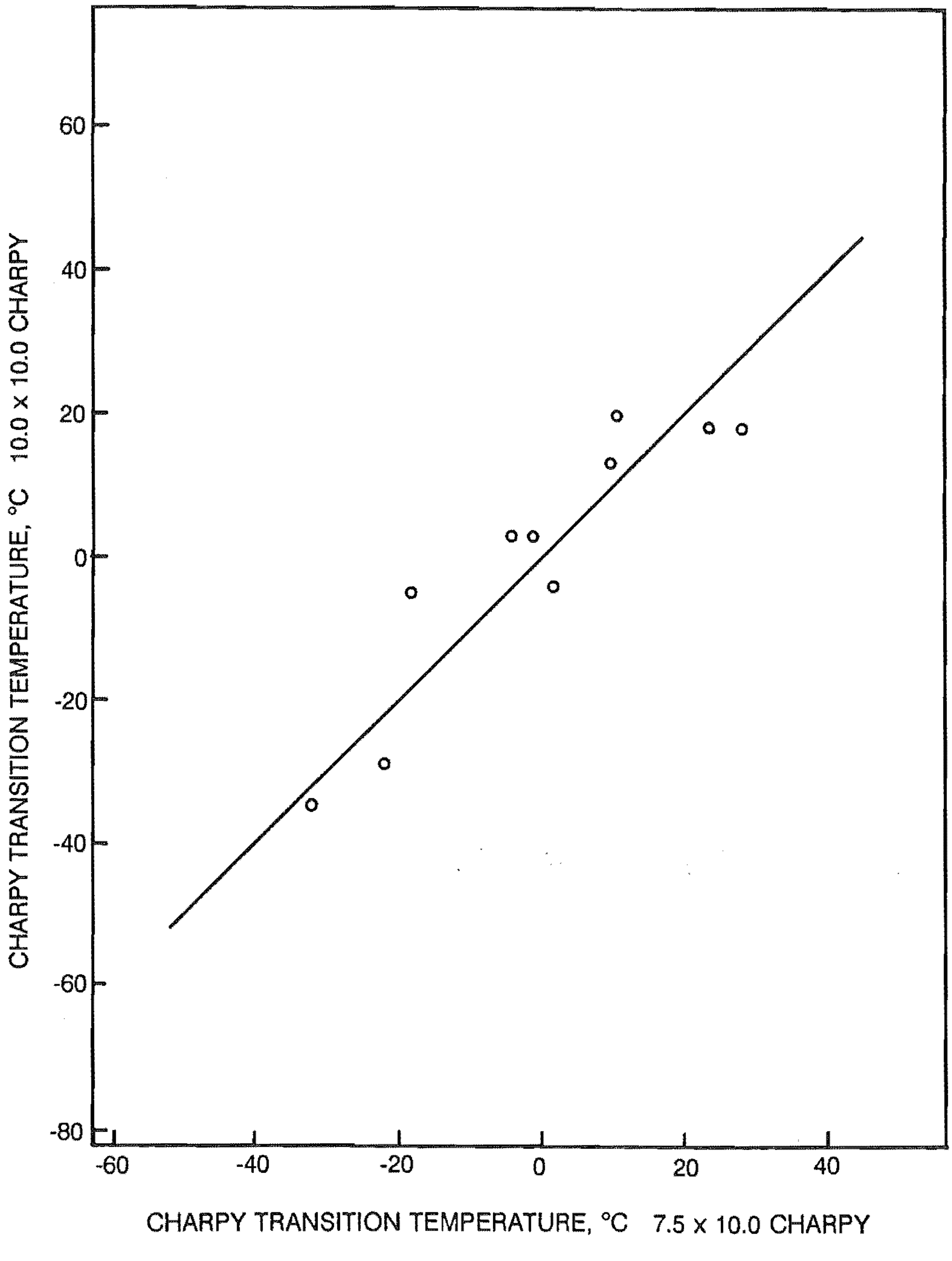

<u>Figure 5.14</u> Charpy transition temperature - correlation of standard and sub-standard charpy test pieces.

the sub-standard test piece when a energy level of 27 joules is used to define the transition temperature. This is in agreement with work done by Towers [65].

5.4 Strain Ageing Propensity.

The strain ageing characteristics of Sample Set 1 were measured to evaluate the levels of "free" interstitial nitrogen in the samples. This indirect method of evaluation was used as a reference for the direct measurement of interstitial nitrogen by mineral acid dissolution, which is discussed in section 5 of this chapter.

Strain ageing propensity is defined as an index ΔY, where:

$$\Delta Y = \sigma_{LYS\ aged} - \sigma_{0.05}$$

$\sigma_{LYS\ aged}$ = lower yield stress after ageing.
$\sigma_{0.05}$ = flow stress at a strain of 0.05, prior to aging.

The results for the strain ageing index of Sample Set 1 are plotted on figure 5.15, in MPa, as a function of total vanadium concentration. It can be seen from the figure that once a vanadium concentration of 0.06 wt. % is achieved, the level of strain ageing drops to less than 15 MPa. Erasmus suggests that this indicates a interstitial nitrogen concentration of less than 0.0013 wt. % and relates to stage one strain ageing [61]. The samples with vanadium concentrations above 0.06 wt. % can, therefore, be considered to be free of interstitial nitrogen, and therefore not susceptible to strain ageing [43].

Stoichiometry would indicate that all the samples were free of interstitial nitrogen, as all samples contain sufficient vanadium to precipitate all of the nitrogen as VN [19]. However, in figure 5.15 it can be seen that the samples with a vanadium concentration of 0.04 wt. %, exhibit significant levels of strain ageing. Excessive levels of vanadium, above stoichiometry, are therefore required to limit the degree of strain ageing experienced by the steel after plastic deformation. In the case of sample set 1, an atomic ratio of 1.8:1 (V:N) is required to ensure the strain ageing propensity of the steel is acceptably low.

The strain ageing index for the samples in sample set 2 are included in table 4.2. Most of the samples have similar vanadium and nitrogen concentrations to sample 50 of sample set 1, and show similar degrees of strain ageing. It would appear, therefore, that the slower cooling rate of these samples has not decreased their strain ageing propensity, despite the greater time available for the diffusion of nitrogen through the structure. The only samples to show a lower degree of strain ageing were those samples which had an atomic ratio of greater than 1.8:1 (V:N). It can therefore be stated that composition is more significant than cooling rate in determining the strain ageing propensity of a steel.

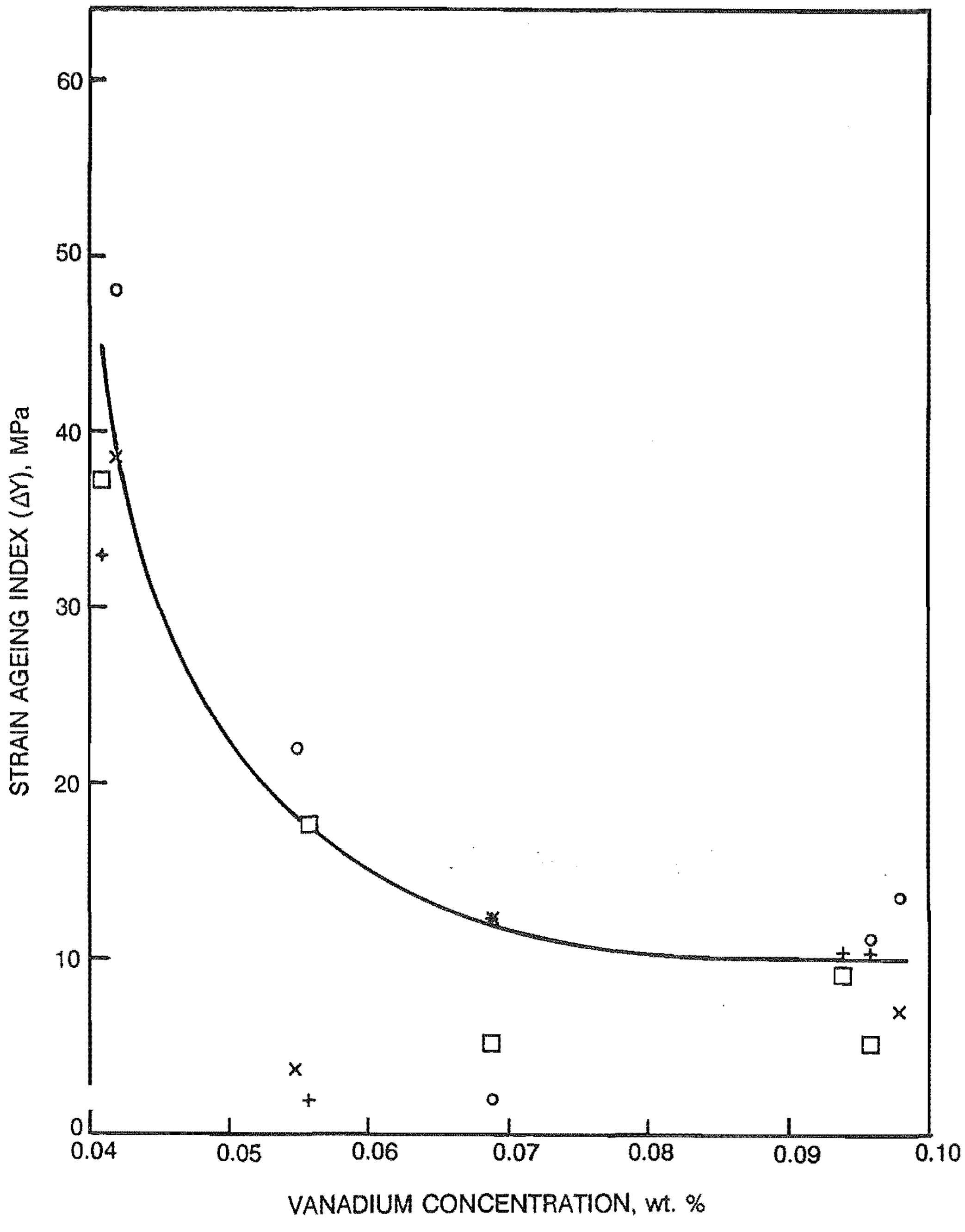

Figure 5.15 Strain ageing index ΔY as a function of total vanadium concentration - Sample Set 1.

(o)	Approximate rolling temperature of 1100 °C, fast cooling rate applied.
(×)	Approximate rolling temperature of 1100 °C, slow cooling rate applied.
(□)	Approximate rolling temperature of 1000 °C, fast cooling rate applied.
(+)	Approximate rolling temperature of 1000 °C, slow cooling rate applied.

5.5 Nitrogen Analysis.

Nitrogen analysis was carried out on all the samples reported in this project using a technique in which the steel samples were dissolve in a dilute solution of H_2SO_4 [63]. The method is detailed in appendix A. The result of this dissolution is that the nitrogen in the steel sample can be divided into two parts. One part is the acid soluble nitrogen. This contains all the "free" nitrogen in the solution, which is responsible for the strain ageing propensity of the samples. The other part is the acid insoluble nitrides. These are nitrides in the sample which are chemically stable under the attack of the acid, being primarily vanadium nitride (VN) in this instance.

The results for this "standard" nitrogen analysis are given in tables 4.4 and 4.5. It can be seen from these tables that the concentration of soluble nitrogen in the samples is approximately 200 % greater than the concentration of the insoluble nitrides. This is an unusual result, considering that most of the samples have a low strain ageing propensity (see figure 5.15). It was therefore considered that the dissolution technique in the analysis of the samples was producing inaccurate results, dissolving a portion of the acid insoluble nitrogen. This portion is then included in the soluble portion of the analysis. It was suspected that the high cooling rate of the samples under consideration had produced precipitates which were a lot finer than the precipitates in the samples which were used in the development of this analysis technique. The lower relative stability of these precipitates causing their breakdown under the acid attack. An alteration to the analysis technique was thus required.

In the "standard" analysis technique, the samples were dissolved in 20% v/v H_2SO_4 at 100 °C. It was considered that this dissolution was too harsh, and therefore it was decided to reduce the acid concentration to 5% v/v, and to do the dissolution at room temperature. Under these condition the entropy of the solution was too low, such that the dissolution did not proceed. To alleviate this problem it was decided to use electrolysis to dissolve the sample. This required the sample to be made anodic in the solution, with an inert cathode being present to complete the current circuit. The layout of this "cell" is shown in figure 5.16. It consists of a 250 ml beaker containing 200 mls of acid. A rod anode of the sample stands in the middle of the beaker, the dimensions of the rod being 10mm diameter; 80mm long. A screw at the top of the anode holds a wire from the positive pole of the current source. The cathode is made of 316 stainless steel, is 35mm high, and covers the circumference of the beaker. It sits submerged in the acid, with the exception of a tab which protrudes above the acid and is connected to a wire from the negative pole of the current source. The beaker sits in a tray of water, this being a heat sink.

To ensure a good contact with the current source, the anode was made to protrude out above the solution. The sample dissolved was therefore the change in the weight of the anode. The reaction at the anode is: $Fe \rightarrow Fe^{++} + 2e^-$. The cathode was made of 316 stainless steel, and had a larger surface area than the anode to speed the reaction. Platinum was not used for the cathode for cost reasons. As long as the "cell" is wired correctly, the cathode is inert to the solution. The reaction at the cathode is: $2H^+ + 2e^- \rightarrow H_2$ (gas).

Both the anode and cathode were cleaned and weighed before being placed in the acid. This cleaning was done first with acetone, and then with distilled water. This will eliminate contamination of the acid with nitrogen containing compounds carried on the anode or cathode. It is also essential to keep control over contaminants in either the solutions or glassware, as the nitrogen concentration is measured in parts per million.

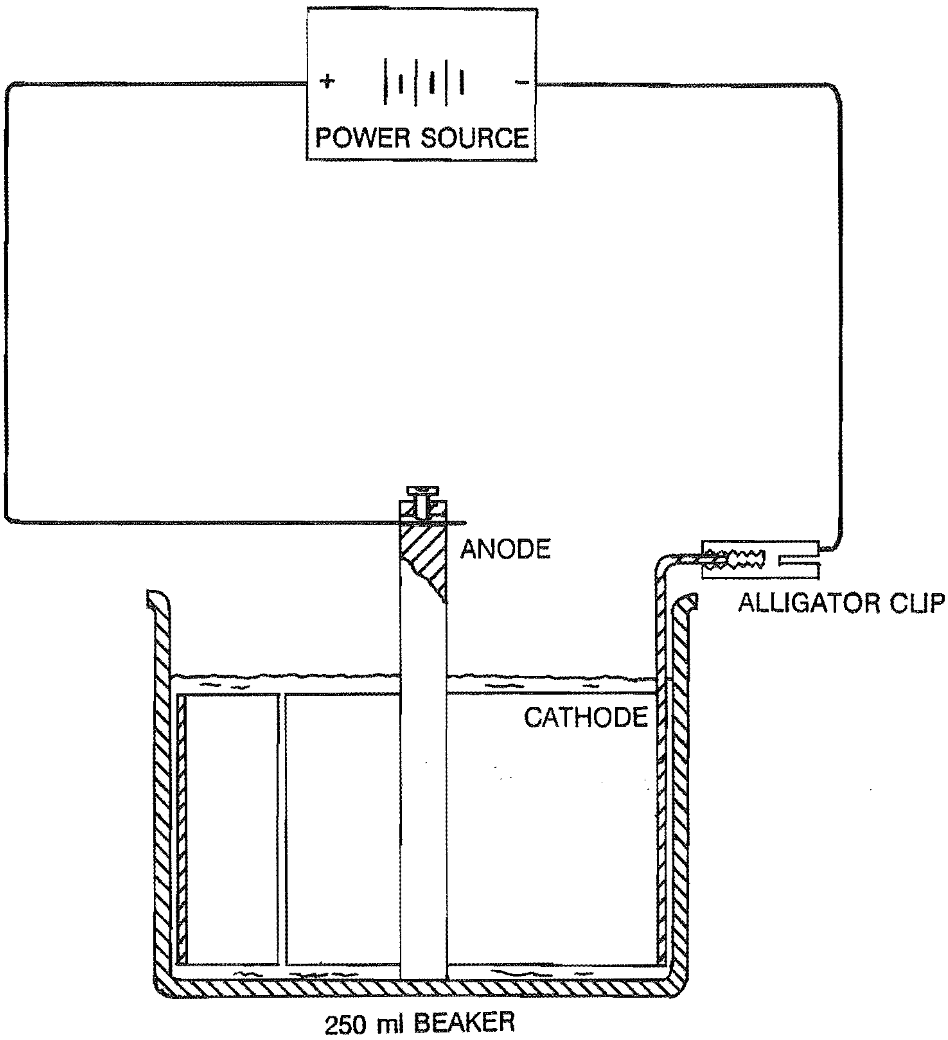

Figure 5.16 Dissolution cell - alternate nitrogen analysis.

A current density on the anode of 1.3 amps/cm^2 was used to drive the reaction (voltage approximately 2 volts). This resulted in approximately 2 grams of sample being dissolved in two hours. If larger current densities were used, gas began to evolve at the anode, halting the dissolution.

During the dissolution, the reaction at the anode became passive as a dark film built up on the anode. This may happen at any time, and results in the dissolution being halted. When this happened, the current density on the anode was increased to 5.1 amps/cm^2 (10 volts) for 15 seconds, and then returned to 1.3 amps/cm^2. This produced a gas evolution at the anode, cleaning off the film, and allowing the dissolution to proceed.

After two hours the sample was removed from the acid and rinsed with distilled water. The rinsings were added to the solution in the beaker. All sediment adhering to either the anode or cathode when removed was rinsed off and included in the solution in the beaker, as these sediments contain nitride precipitates.

This "alternative" method of nitrogen analysis is detailed in Appendix B.

The results of this "alternate" nitrogen analysis technique are given in tables 4.4 and 4.5 for sample set 1 and sample set 2 respectively. These values of free nitrogen were used for the corrections to the lower yield strength, tensile strength, and charpy transition temperature mentioned earlier in this chapter. Large differences in the measured value of N_{sol} can be seen when comparing the analysis techniques.

A major problem with this technique is that some of the sediment adhering to the sample anode and the cathode cannot be easily rinsed off when these are removed from the solution. The accuracy of the result can therefore be questioned. To evaluate the severity of this error two other samples were analysed using the "alternative" method. One was a plain carbon steel with no micro-alloy addition, the other a titanium micro-alloyed steel. These samples had been furnace cooled to induce large precipitates and had previously measured soluble/insoluble nitrogen proportions. The results of this analysis are shown in figure 5.17. A sample from sample set 1 (27A) was also analysed many times to check on the consistency of the analysis. These results are shown in figure 5.18. The results of these experiments showed that the soluble portion of the nitrogen in the samples was always measured accurately and was repeatable. This was not true for the insoluble portion. The true insoluble portion of the nitrogen in the sample was then obtained by measuring the total nitrogen concentration of the sample by the "standard" analysis technique, and then subtracting the soluble portion of the nitrogen in the sample, as defined by this new "alternate" analysis technique. Though this involves a double analysis of the sample, it should be considered that a) the soluble (free) nitrogen concentration is often the more important concentration to measure, and can thus be done in a single analysis; and b) the analysis technique is straight forward, and a relatively easy way of obtaining some very important parameters in relation to the nitrogen concentration of the steel.

It should be also noted that as this "alternate" analysis technique has shown the "standard" analysis technique to be inaccurate under certain conditions, it casts doubt on its own accuracy. It cannot be stated that this new analysis technique does not dissolve any of the fine precipitates present in the ferrite matrix during dissolution. If this is the case, then it can only be stated that this "alternative" analysis technique provides a closer indication as to the true free nitrogen concentration of a steel sample.

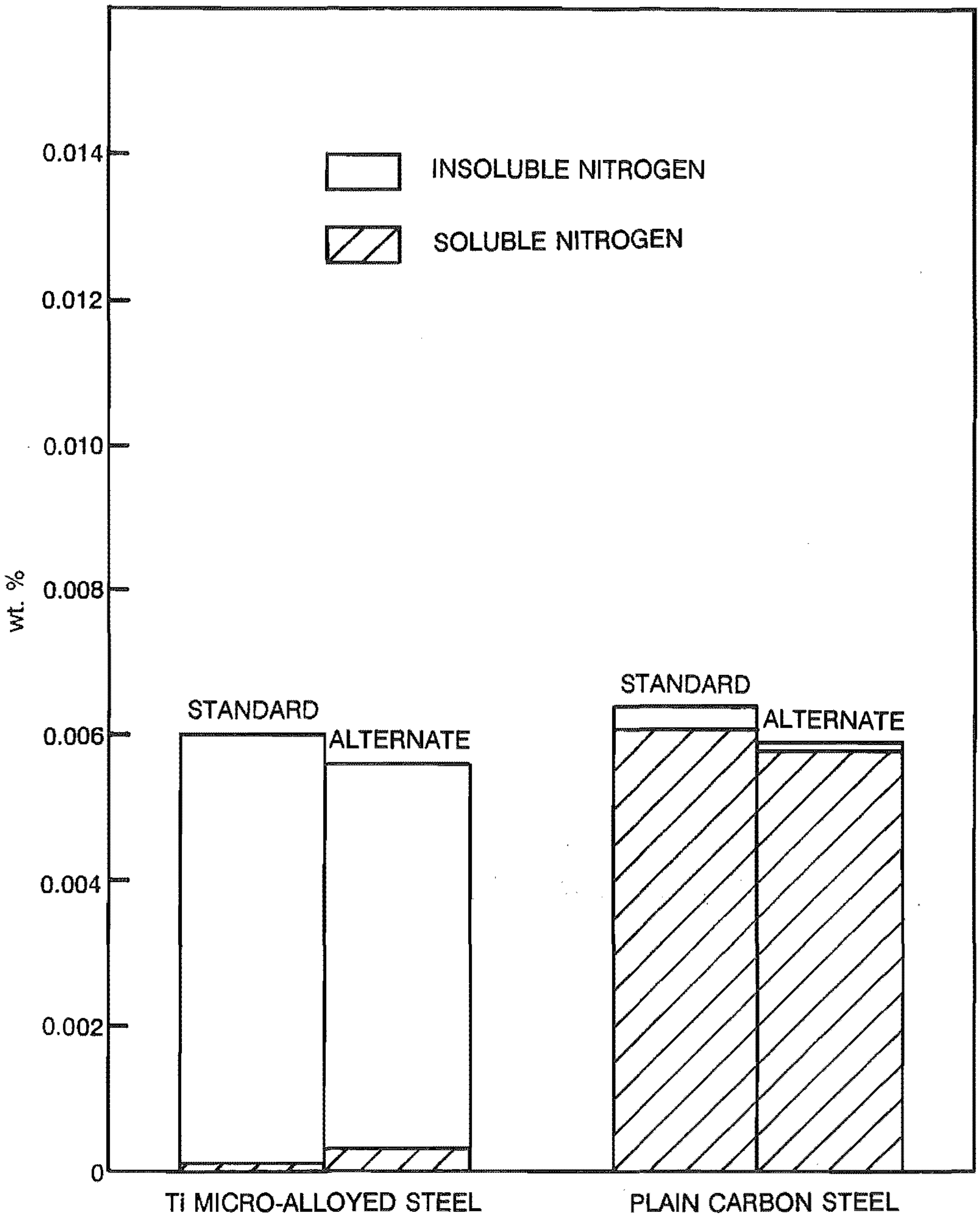

Figure 5.17 Comparison between the "alternate" analysis technique and the "standard" analysis technique when determining the nitrogen content of a titanium micro-alloyed steel, and an unalloyed low carbon steel.

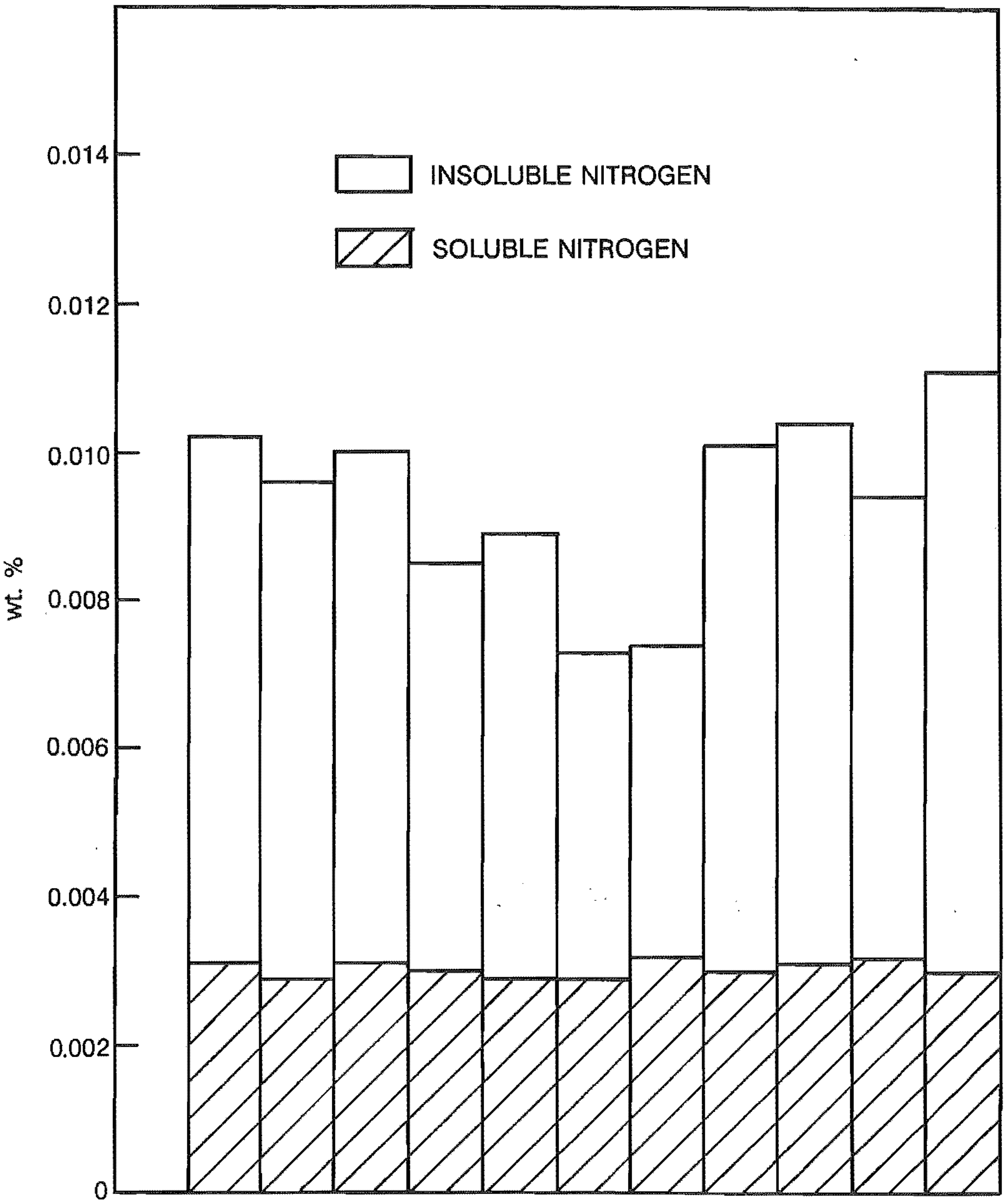

Figure 5.18 Repeatability of results for the "alternate" nitrogen analysis technique - results for the analysis of sample 27A from sample set 1.

Chapter 6.

Conclusions.

The addition of vanadium as a micro-alloy to a low carbon steel can dramatically enhance the mechanical properties of the steel. For example, the addition of 0.1% wt. vanadium to a 0.22 carbon, 1.16 manganese steel can produce a steel with a lower yield stress exceeding 580 MPa, a tensile strength exceeding 730 MPa, and ductility exceeding 25% elongation. To maximise the returns from a micro-alloying addition of vanadium, however, care has to be taken to ensure the thermo-mechanical treatments applied to the steel are optimised. To do this, the following points relating to the inter-relationship between steel chemistry, the thermo-mechanical processing of the steel, and the final mechanical properties of the steel should be noted.

The ferrite grain size of a vanadium micro-alloyed steel is significantly influenced by the cooling rate of the steel after rolling in the austenite phase. In the case where a multi-pass rolling schedule is carried out above the "recrystallisation stop" temperature of the steel, and where the level of micro-alloying is low such that strain induced precipitation of vanadium nitride does not occur during rolling, the post rolling cooling rate is the primary factor influencing the ferrite grain size of the steel. A large steel cross-section will, therefore, require a cooling rate equivalent to that of a small cross-section to maintain the same ferrite grain size under these rolling conditions.

A fine austenite grain structure can be obtained by multi-pass rolling above the "recrystallisation stop" temperature of the steel if rapid cooling is applied to the steel after rolling. Rolling below the "recrystallisation stop" temperature of the steel may also produce a fine ferrite grain size, via ferrite transformation from a severely deformed austenite grain structure. This is mechanically undesirable, however, as high rolling loads result with no advantage in terms of ferrite grain refinement.

Precipitation of vanadium nitride may be strain induced in a vanadium micro-alloyed steel at rolling temperatures below the equilibrium precipitation temperature of the nitride in the steel. This precipitation may or may not be desirable. If these precipitates are allowed to coarsen during post precipitation thermo-mechanical treatments, the precipitation strengthening of the steel will be decreased. This loss of strengthening is in proportion to the loss of micro-alloy from solution in the austenite since there is then a reduction in precipitation in the ferrite phase. If this austenite precipitation remain fine, however, it can enhance the tensile properties of the steel.

Reducing rolling temperatures to assist strain induced precipitation of vanadium nitride (assuming solubility requirements are satisfied) will increase the rolling loads of the rolling mill. However, this reduction in rolling temperature will have the desirable effect of lowering the fracture mode transition temperature of the steel, as measured by the Charpy impact test. This is caused by rolling induced grain orientation parallel to the direction of rolling.

The coarsening rate of vanadium carbo-nitride precipitates has been found to be purely dependent on the steel chemistry, and is independent of the rolling temperature and cooling rate of the steel. If the atomic ratio of vanadium to nitrogen in the steel is above approximately 2:1, precipitates which form in the ferrite phase during cooling become carbon rich, and coarsen more rapidly than would be the case if the precipitates were nitrogen rich. Precipitate coarsening severely decreases precipitate strengthening of the steel. Enhanced nitrogen concentrations must, therefore, be produced in vanadium micro-alloyed steels with high vanadium concentrations to maximise the precipitation strengthening.

Steel chemistry is also primarily responsible for the strain aging propensity of a vanadium micro-alloyed steel. The effects of rolling temperature and cooling rate have been found to be of minimal significance. To ensure sufficient vanadium is available in solution to precipitate with all "free" interstitial nitrogen in solution in the steel, a atomic ratio of vanadium to nitrogen of greater than 1.8:1 was found to be required.

The measurement of the "free" interstitial nitrogen concentration in a steel is becoming increasingly more important in predicting the mechanical behaviour. This analysis is based on the dissolution of a steel sample in dilute sulphuric acid, the resulting solution containing the "free" interstitial nitrogen, and the insoluble fraction containing nitrogen in the form of stable nitride precipitates present in the steel. It has been found that the accuracy of this nitrogen analysis is a function of the size of micro-alloy precipitates present in the steel. If a distribution of very fine precipitates is present in the steel, as was the case in this work, extreme care had to be taken to ensure that some of these nitride precipitates are not dissolved, and thus included in the "free" nitrogen fraction.

Chemical nitrogen analysis of a steel should not be regarded as producing an absolute measurement of the concentration of "free" interstitial nitrogen. Its accuracy is purely dependant on the micro-structure of the steel being analysed. This accuracy can be improved, however, by cross-referencing chemical nitrogen analysis with the strain aging propensity of the steel. In the case of a micro-alloyed steel, this would provide a more certain indication of the effectiveness of the alloy in precipitating with nitrogen in solution in the steel.

Chapter 7.

Recommendations.

It is recommended that separate chemistry and thermo-mechanical processing routes be produced for each bar diameter. If possible, these parameters should be further altered to optimise the mechanical properties of their product for specific customer requirements.

Considering first the tensile properties of the bars, micro-alloy concentrations in the bars should be made leaner, the vanadium concentration being only that which is required to meet minimum mechanical specifications. The primary strengthening mechanism of the steel should be grain refinement, through high rolling temperatures and accelerated cooling after rolling. In the case where a high degree of grain refinement cannot be obtained by thermo-mechanical processing, higher levels of micro-alloying should be used, such that strain induced precipitation is present during the cooling of the steel to prevent ferrite grain growth. This may require higher vanadium and nitrogen levels than are presently being used, depending on the grain refinement that can be obtained by accelerated cooling.

In the case where the fracture mode transition temperature of the steel is of great importance to a customer, the rolling temperature of the steel should be reduced. This reduction in rolling temperature is limited to the safe working loads on the rolling mill, and will have the effect of reducing roll life.

It is further recommended that the nitrogen concentration of the steel be altered along with the vanadium concentration, such that the atomic ratio of vanadium to nitrogen between 1.8:1 and 2:1. This will prevent precipitate coarsening during processing of the steel, thereby reducing tensile properties. This will also minimise the strain aging propensity of the steel. In the case where a customer requires a non-stain aging steel, and it is not possible to lower the total nitrogen concentration of the steel, the micro-alloy concentration should be increased, the higher cost of the steel being overcome by a premium selling price.

In the case of a reinforcing steel, it is recommended that a lean vanadium alloyed steel be used, which has been rolled through a multi-stand rolling schedule at high temperatures (approximately 1100 °C) and fast cooled to ambient temperatures. It should have a V:N atomic ratio between 1.8:1 and 2:1, and enhanced alloy additions of both vanadium and nitrogen where cooling is not adequate to acquire a fine ferrite grain structure.

References.

1. Woodhead, J.H. and Keown, S.R., Conf. Proc. HSLA Steels '85, Beijing, China, 1985, p.15.

2. Honeycombe, R.W.K., Metal Science, vol.14, 1980, p.201.

3. Parsons, S.A. and Edmonds, D.V., Materials Science & Tech., vol.3, 1987, p.894.

4. Meyer, L., Strassburger, C. and Schneider, C., Ref.1, p.29.

5. Ratnaraj, R., Ph.D Thesis, University of Canterbury, 1990.

6. Balliger, N.K. and Honeycombe, R.W.K., Metal. Trans. A., vol.11A, 1980, p.421.

7. Irvine, K.J., Pickering, F.B. and Gladman, T., J.I.S.I., 1967, p.161.

8. Gladman, T. and Delieu, D., Metal Science, vol.8, 1974, p.167.

9. Akben, M.G. and Jonas, J.J., Conf. Proc. Technology and Applications of HSLA Steels, Pennsylvania, USA, 1983, p.149.

10. Sage, A.M., Ref.1, p.657.

11. Yamamoto, S., Ouchi, C. and Osuka, T., Conf. Proc. Thermomechanical Processing of Microalloyed Austenite, Pennsylvania, USA, 1981, p.613.

12. Gladman, T., Delieu, D. and McIvor, I.D., Conf. Proc. Microalloying '75, New York, USA, 1976, p.32.

13. Pickering, F.B., Ref.9, p.1.

14. Roberts, W., Ref.9, p.33.

15. Pickering, F.B., Ref 12, p.9.

16. Platts, G.K., Vassiliou, A.D. and Pickering, F.B., The Metallurgist and Materials Technologist, 1984, p.447.

17. Pickering, F.B., Ref.1, p.305.

18. Woodhead, J.H., Conf. Proc. Vanadium in High Strength Steels, Chicago, USA, 1979, p.3.

19. Roberts, W. and Sandberg, A., Report IM-1489, Swedish Institute for Metals Research, Drottning, Sweden, 1980.

20. Meyer, L., Heisterkamp, F. and Mueschenborn, W., Ref.12, p.153.

21. Siwecki, T., Sandberg, A. and Roberts, W., Ref.9, p.619.

22. Tiitto, K., Fitzsimons, G. and DeArdo, A.J., Acta. Met., vol.31, 1983, p.1159.

23. Keown, S.R. and Wilson W.G., Ref.11, p.357.

24. Amin, R.K., Korchynsky, M. and Pickering, F.B., Metals Tech., vol.8, 1981, p.250.

25. Siwecki, T., Sandberg, A., Roberts, W. and Lagneborg, R., Ref.11, p.163.

26. Jaiswal, S. and McIvor, I.D., Materials Science & Tech., vol.1, 1985, p.276.

27. Honeycombe, R.W.K., Ref.1, p.243.

28. Baker, T.N., J.I.S.I., 1973, p.502.

29. Litivinenko, D.A., Ref.12, p.470.

30. Honeycombe, R.W.K., Trans. I.S.I. Japan, vol.20, 1980, p.139.

31. Balliger, N.K. and Honeycombe, R.W.K., Metal Science, vol.14, 1980, p.121.

32. Cuddy, L.J., Ref.11, p.129.

33. Amin, .K. and Pickering, F.B., Ref.11, p.1.

34. Amin, .K. and Pickering, F.B., Ref.11, p.377.

35. Smith, R.M., Chandra, T. and Dunne, D.P., Conf. Proc. RIS International Symp. on Metallurgy and Materials Science, 1981, p.371.

36. Ianc, P.P. and Dragan, N.I., Ref.11, p.361.

37. Kaspar, R., Distl, J.S., Braag, K., Klaar, H.J., Zeislmair, U., Steel Res., 1987, p.271.

38. Engl, B. and Kaup, K., Ref.11, p.467.

39. Roberts, W., Sandberg, A., Siwecki, T. and Werlefors, T., Ref.9, p.67.

40. Cuddy, L.J. and Raley, L.J., Metal. Trans. A, vol.14A, 1983, p.1989.

41. Crowther, D.N., Mohamed, Z. and Mintz, B., Metal. Trans. A, vol.18A, 1987, p.1929.

42. Akben, M.G., Weiss, I. and Jonas, J.J., Acta. Met., vol.29, 1981, p.111.

43. Heikkinen, V.K. and Boyd, J.D., Canadian Metal. Quarterly, vol.15, 1976, p.219.

44. Umemoto, M., Zing Hai Guo, Tamura, I., Materials Science & Tech., vol.3, 1987, p.249.

45. Falco, M., Parrini, C. and Pozzi, A., Metal. Italia, vol.67, 1975, p.376.

46. Crooks, M.J., Garratt - Reed, A.J., Vander Sande, J.B., Owen, W.S., Metal. Trans. A, vol.13A, 1982, p.1347.

47. DeArdo, A.J., Conf. Proc. Accelerated Cooling of Austenite, Pennsylvania, USA, 1985, p.97.

48. Cochrane, R.C. and Morrison, W.B., Metals Tech., 1981, p.458.

49. Gray, J.M. and DeArdo, A.J., Ref.1, p.83.

50. Law, N.C., Parsons, S.A., Howell, P.R., Edmonds, D.V., Materials Science & Tech., vol.3, 1987, p.642.

51. Yan, Z.Q., Zhang, W.X. and Zhang, Y.M., Ref.1, p.299.

52. Lin, H.R. and Hendrickson, A.A., Metal. Trans. A, vol.19A, 1980, p.421.

53. Korchynsky, M., Conf. Proc. Mechanical Working and Steel Processing XVIII, Toronto, Canada, 1980, p.39.1.

54. Pradhan, R., Ref.9, p.193.

55. Lis, A. and Lis, J., Conf. Proc. Electron Microscopy 8th European Congress, Budapest, Hungary, 1984, p.803.

56. Stephenson, E.T., Karchner, G.H. and Stark, P., Trans. ASM, vol.57, 1964, p.208.

57. White, M.J. and Owen, W.S., Metal. Trans. A, vol.11A, 1980, p.597.

58. Ramakrishna, D. and Gupta, S.P., Materials Science & Eng., 1987, p.1347.

59. Erasmus, L.A., J.I.S.I., 1964, p.128.

60. Cottrell, A., "An Introduction to Metallurgy", Edward Arnold, 1967, IBSN:0.7131.2510.1.

61. Erasmus, L.A. and Pussegoda, L.N., Metal. Trans. A, vol.11A, 1980, p.231.

62. Hundy, B.B., J.I.S.I., 1954, p.34.

63. Standard Methods of Analysis, The United Steel Companies Ltd., 1951, Sheffield.

64. Irvine, K.J., J.I.S.I., 1969, p.837.

65. Towers, O.L., Metal Construction, 1986, p.171R.

Appendix A.

Standard Method of Nitrogen Analysis.

Nitrogen in steel may be in one of two forms - as "free" interstitial nitrogen or combined as a stable precipitate with such micro-alloying elements as titanium, vanadium, zirconium.

When a sample of steel micro-alloyed with one of these elements is dissolved in dilute sulphuric acid, the nitride precipitates remain undissolved, due to their high stability. By separating the undissolved precipitates from the solution of acid, sulphates, ferrous ions, and dissolved "free" nitrogen, the insoluble portion of the nitrogen in the sample can be determined, the soluble portion being contained in the solution.

Details of the method are:

A. Preparation of Solutions:

1. Ammonia free distilled water is to be used for all solutions.

2. Sulphuric acid: Add 200 mls of low nitrogen H_2SO_4 slowly to flask containing 800 mls of distilled water. This operation should be done in a fume cupboard.

3. Sodium hydroxide: Add 500 gms of NaOH to one litre of distilled water, and heat slowly to dissolve. Add one gram of Devarda's alloy. Allow to cool and settle, then decant into a bulk storage container.

4. Ammonia standard solution: Dissolve 0.669 gms of NH_3Cl in 100 mls of distilled water. Take 10 mls of this solution and further dilute to one litre. 1 ml of this solution contains 0.0000175 gms of nitrogen.

5. Nesslers reagent: To a solution of 23 gms of KI dissolved in 100 mls of distilled water add a solution of 11 gms of $HgCl_2$ dissolved in 220 mls of distilled warm water until a permanent orange colour is obtained. Add a solution of 58 gms of NaOH dissolved in 100 mls of distilled water. Allow to stand over night, and then decant into a dark bottle through hardened filter paper. Keep stoppered and out of the light.

6. Boric acid: Dissolve 2 gms of Boric acid in one litre of distilled water.

7. Barium chloride: Dissolve 20 gms of $BaCl_2$ in one litre of distilled water.

B. Calibration of Nesslers Reagent:

1. Select 20 clean 100 mls bottles, and weigh each of them. Add 5 mls of boric acid solution to each. Add increasing amounts of ammonia solution to each bottle (ie. 0 mls to the first bottle, 2 mls to the second, 4 mls to the third, 6 mls to the fourth, and so on) recording the volume added to each. Add distilled water to each bottle to bring their fluid weight to 90 gms. Add 2 mls of Nesslers reagent to each bottle, shake and allow to sit for 10 minutes. Using a colourimeter, determine the optical intensity of each solution. Plot colour intensity against the volume of ammonia solution in each bottle.

C. Sample Analysis.:

1. Prepare fine drillings of the sample. The drill and sample should be cleaned with acetone first to ensure the drillings are clean and free of grease. Do not overheat the sample during drilling, as this may alter the nitrogen morphology.

2. Accurately weigh out 3.5 grams of drillings into a round bottom conical flask, noting the exact weight. To this 50 mls of sulphuric acid solution (20%) is added, the flask stoppered, and placed over a boiling water bath, producing a constant head of steam at 100 °C. The bath should be kept in a fume cupboard. The flask, containing the drillings, is left over the water bath for 45 minutes, being agitated every 15 minutes to remove hydrogen bubbles adhering to the drillings. Remove the flask and allow to cool. Do not over heat the flask or leave it over the water bath for longer than 45 minutes, as this may cause some of the insoluble nitride precipitates to be dissolved. Prepare a reference "blank" solution by following the whole analysis procedure without adding a sample to a conical flask. This "blank" will show any nitrogen contamination of the solutions or apparatus.

3. Transfer all the contents of each conical flask into a large glass centrifuge tube, rinsing the inside of the flask with distilled water to ensure all the contents are transferred. Centrifuge at 3000 rpm for 5 minutes. Ensure that the centrifuge is balanced before centrifuging, or the vibrations from the out of balance forces in the centrifuge may cause the centrifuge tube to break, and the sample will be lost. When the centrifuge has stopped add 2 mls of barium chloride solution (forming white $BaSO_4$ precipitate) and again centrifuge at 3000 rpm for 5 minutes. This is to flocculate all particles to the bottom of the centrifuge tube. When centrifuge has stopped, carefully decant the clear solution into a small bottle, rinsing the centrifuge tube carefully with distilled water, making sure the material at the bottom of the tube is not disturbed. This clear solution contains the soluble (ie. "free" interstitial) nitrogen. It also contains less stable nitrides, such as aluminium nitride, which have been dissolved.

4. Rinse the insoluble residue out of the bottom of the centrifuge tube into the original round bottom conical flask with distilled water. Use as little distilled water as possible. Attach a splash head, and add 9 mls of concentrated sulphuric acid. Heat over a Bunsen burner, while supporting the glassware in a retort stand, until all the water has been boiled away. This point is reached when the solution starts to change colour. It will also "pop" when fumes that have

condensed in the splash head drip back into the flask. The $BaSO_4$ precipitate which was also transfered to the flask will not dissolve. All the water must be removed to ensure that the nitride precipitates are completely broken down and dissolved in the acid. When no more water remains in solution extinguish the Bunsen and allow to cool. Add 40 mls of distilled water to the flask, via the splash head. Rinse the inside and connecting taper of the splash head with distilled water, draining the rinsings into the flask. This cloudy solution contains all the insoluble nitrides (ie. the nitrogen combined in a precipitate with the micro-alloying elements present).

5. Condition distillation apparatus (figure A.1) by adding 100 mls of sodium hydroxide solution to the distillation chamber (A) via the funnel (B), the funnel tap should be open. Rinse the funnel with distilled water, collecting the rinsings in the distillation chamber. Close the funnel tap. Light the burner to boil the distilled water in the reservoir (C). When steam starts to flow through the tap at the base of the drain (D) close the drain tap so that steam flows to the distillation chamber. This will cause the solution in the distillation chamber to boil. Allow to boil for 10 minutes then extinguish the burner. Condensation of the steam between the distilled water reservoir and the distillation chamber causes the contents of the distillation chamber to be drawn through to the drain. The tap at the base of the drain (D) can now be opened to expel the solution.

6. Pour the solution containing the soluble nitrogen into the funnel (B) of the steam distillation apparatus. Rinse both the solution bottle and the funnel with distilled water, draining the rinsings into the funnel. The funnel tap should be open, so that the solution and distilled water rinsings drain into the distillation chamber (A). Add 100 mls of sodium hydroxide solution via the funnel again rinsing the funnel with distilled water. Close the funnel tap. Light the burner to boil the distilled water in the reservoir (C). When steam starts to flow through the tap at the base of the drain (D) close the drain tap so that steam flows to the distillation chamber. This will cause the solution in the distillation chamber to boil, releasing steam, and nitrogen in the form of ammonia, which pass through to the condenser tube (E). The condensate is collected in a small bottle containing 5 mls of boric acid solution. The end of the condenser should be submerged in the boric acid solution to prevent the release of any ammonia which is still gaseous after passing through the condenser tube. Continue collecting condensate until the bottle contains 70-80 mls. Remove the bottle and extinguish the burner. Condensation of the steam between the distilled water reservoir and the distillation chamber causes the "used" solution to be drawn through to the drain. The tap at the base of the drain (D) can now be opened to expel the solution. Repeat this process with the solution containing the insoluble nitrides.

7. Add distilled water to the bottles of condensate to bring their fluid weight to 90 gms. Prepare a zero ammonia solution and zero the colourimeter. Add 2 mls of Nesslers reagent to each bottle, shake and allow to stand for 15 minutes. Measure the optical intensity of each solution, and determine the equivalent ammonia concentration of the solution from the calibration curve for the reagent. Determine the nitrogen concentration of each sample by dividing the weight of nitrogen in the sample (1 ml of ammonia solution = 0.0000175 gms) by the weight of the sample that was dissolved.

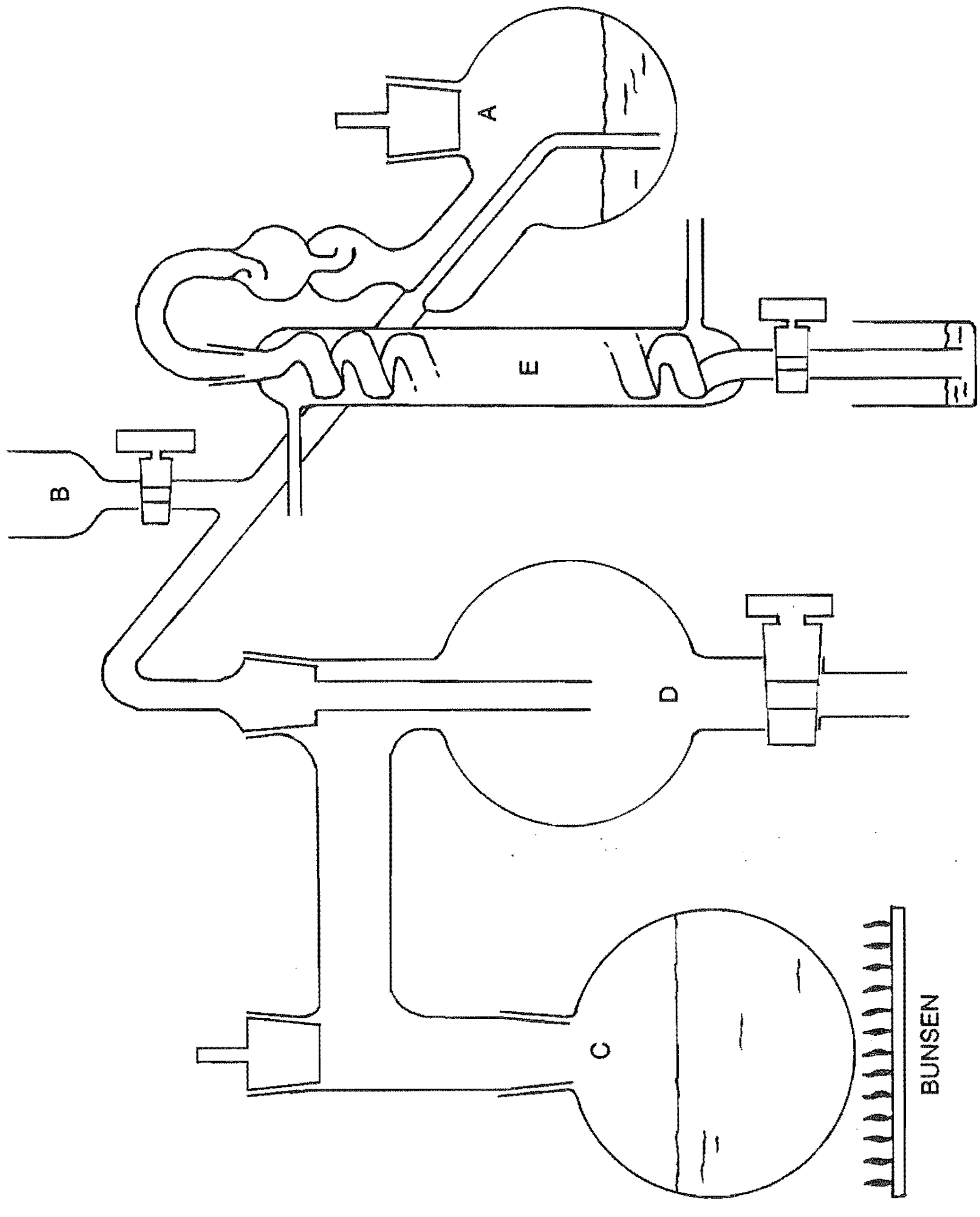

Figure A.1 Steam distillation apparatus for determination of nitrogen in steel.

Appendix B.

Alternate Method of Nitrogen Analysis.

This method was developed to compensate for the inaccuracies arising from the standard method during the analysis of a vanadium micro-alloyed steel which had a very fine precipitate size. Use of the standard method proved to dissolve these fine precipitates, including the nitrogen in the acid soluble fraction of the nitrogen. The success of this alternate method is that the dissolution of the steel sample is not as strong as is the case for the standard method.

Details of the method are:

A. Preparation of Solutions:

1. Ammonia free distilled water is to be used for all solutions.

2. Sulphuric acid: Add 10 mls of low nitrogen H_2SO_4 slowly to flask containing 200 mls of distilled water. This operation should be done in a fume cupboard.

3. Sodium hydroxide: Add 500 gms of NaOH to one litre of distilled water, and heat slowly to dissolve. Add one gram of Devarda's alloy. Allow to cool and settle, then decant into a bulk storage container.

4. Ammonia standard solution: Dissolve 0.669 gms of NH_3Cl in 100 mls of distilled water. Take 10 mls of this solution and further dilute to one litre. 1 ml of this solution contains 0.0000175 gms of nitrogen.

5. Nesslers reagent: To a solution of 23 gms of KI dissolved in 100 mls of distilled water add a solution of 11 gms of $HgCl_2$ dissolved in 220 mls of distilled warm water until a permanent orange colour is obtained. Add a solution of 58 gms of NaOH dissolved in 100 mls of distilled water. Allow to stand over night, and then decant into a dark bottle through hardened filter paper. Keep stoppered and out of the light.

6. Boric acid: Dissolve 2 gms of Boric acid in one litre of distilled water.

7. Barium chloride: Dissolve 20 gms of $BaCl_2$ in one litre of distilled water.

B. Calibration of Nesslers Reagent:

1. Select 20 clean 100 mls bottles, and weigh each of them. Add 5 mls of boric acid solution to each. Add increasing amounts of ammonia solution to each bottle (ie. 0 mls to the first bottle, 2 mls to the second, 4 mls to the third, 6 mls to the fourth, and so on) recording the volume

added to each. Add distilled water to each bottle to bring their fluid weight to 90 gms. Add 2 mls of Nesslers reagent to each bottle, shake and allow to sit for 10 minutes. Using a colourimeter, determine the optical intensity of each solution. Plot colour intensity against the volume of ammonia solution in each bottle.

C. <u>Sample Analysis:</u>

1. Machine the sample into an rod shaped anode, preferably of dimensions: diameter 10mm; length 80mm. A small transverse hole with a connecting threaded axial hole are required at one end to allow the attachment of a wire (see figure B.1). The sample should then be cleaned with acetone and accurately weighed.

2. Form a cathode from 316 stainless steel to fit around the inner circumference of a 250 ml beaker to a hight of 35mm, with the exception of a small tab, which rises to a hight of 70mm (see figure B.1). Clean the cathode with acetone.

3. Rinse the cathode in distilled water and place in a clean 250 ml beaker. Attach a wire to the tab of the cathode using an alligator clip. Using a small screw, attach a wire to the anode. Rinse the anode in distilled water, and stand it in the center of the beaker. Connect the wires to a power source, the cathode being connected to the negative pole, the anode being connected to the positive pole. Place the beaker in a tray of water, 30mm deep. Ensure the wires are not in contact with the water.

4. Add 200 mls of sulphuric acid solution (5%) to the beaker, and turn the power source on to 2 volts. Leave the anode to dissolve in the acid for two hours. If the reaction begins to slow, or halts, due to a black build up on the surface of the anode, increase the voltage to 10 volts for five seconds, then return the setting to 2 volts.

5. After two hours turn power source to 10 volts for 15 seconds, and then turn it off. Disconnect the anode an cathode wires from the power source. Carefully remove both the anode and cathode from the solution, rinsing both with distilled water as this is done, the rinsings being collected in the beaker. Try to rinse off all adhering particles.

6. Clean the anode with acetone and weigh. Calculate the difference in weight, this being the weight of sample dissolved in the acid solution. Clean the cathode.

7. Transfer all the contents of the beaker into 4 large glass centrifuge tubes, rinsing the inside of the beaker with distilled water to ensure all the contents are transfered. (This may have to be repeated later if the centrifuge tubes cannot hold all the solution.) Centrifuge at 3000 rpm for 5 minutes. Ensure that the centrifuge is balanced before centrifuging, or the vibrations from the out of balance forces in the centrifuge may cause the centrifuge tube to break, and the sample will be lost. When the centrifuge has stopped add 2 mls of barium chloride solution (forming white $BaSO_4$ precipitate) and again centrifuge at 3000 rpm for 5 minutes. This is to flocculate all particles to the bottom of the centrifuge tube. When centrifuge has stopped, carefully decant the clear solution into small bottles, rinsing the centrifuge tube carefully with

distilled water, making sure the material at the bottom of the tube is not disturbed. This clear solution contains the soluble (ie. "free" interstitial) nitrogen. It also contains less stable nitrides, such as aluminium nitride, which have been dissolved. If all the solution was unable to fit into the centrifuge tubes, repeat the process using the same centrifuge tubes, being careful not to disturb the material at the bottom of the tube. The centrifuge tubes will then have a double layer of material at the bottom before proceeding to the next stage.

8. Rinse the insoluble residue out of the bottom of the centrifuge tubes into two round bottom conical flask with distilled water. Use as little distilled water as possible. Attach a splash head to each, and add 9 mls of concentrated sulphuric acid. Heat over a Bunsen burner, while supporting the glassware in a retort stand, until all the water has been boiled away. This point is reached when the solution starts to change colour. It will also "pop" when fumes that have condensed in the splash head drip back into the flask. The $BaSO_4$ precipitate which was also transfered to the flask will not dissolve. All the water must be removed to ensure that the nitride-precipitates are completely broken down and dissolved in the acid. When no more water remains in solution extinguish the Bunsen and allow to cool. Add 40 mls of distilled water to each flask, via the splash head. Rinse the inside and connecting taper of each splash head with distilled water, draining the rinsings into the flask. This cloudy solution contains all the insoluble nitrides (ie. the nitrogen combined in a precipitate with the micro-alloying elements present).

9. Condition distillation apparatus (figure B.2) by adding 100 mls of sodium hydroxide solution to the distillation chamber (A) via the funnel (B), the funnel tap should be open. Rinse the funnel with distilled water, collecting the rinsings in the distillation chamber. Close the funnel tap. Light the burner to boil the distilled water in the reservoir (C). When steam starts to flow through the tap at the base of the drain (D) close the drain tap so that steam flows to the distillation chamber. This will cause the solution in the distillation chamber to boil. Allow to boil for 10 minutes then extinguish the burner. Condensation of the steam between the distilled water reservoir and the distillation chamber causes the contents of the distillation chamber to be drawn through to the drain. The tap at the base of the drain (D) can now be opened to expel the solution.

10. Pour all the solutions containing the soluble nitrogen into the funnel (B) of the steam distillation apparatus. Rinse both the solution bottle and the funnel with distilled water, draining the rinsings into the funnel. The funnel tap should be open, so that the solution and distilled water rinsings drain into the distillation chamber (A). Add 100 mls of sodium hydroxide solution via the funnel again rinsing the funnel with distilled water. Close the funnel tap. Light the burner to boil the distilled water in the reservoir (C). When steam starts to flow through the tap at the base of the drain (D) close the drain tap so that steam flows to the distillation chamber. This will cause the solution in the distillation chamber to boil, releasing steam, and nitrogen in the form of ammonia, which pass through to the condenser tube (E). The condensate is collected in a small bottle containing 5 mls of boric acid solution. The end of the condenser should be submerged in the boric acid solution to prevent the release of any ammonia which is still gaseous after passing through the condenser tube. Continue collecting condensate until the bottle contains 70-80 mls. Remove the bottle and extinguish the burner. Condensation of the steam between the distilled water reservoir and the distillation chamber causes the "used" solution to be drawn through to the drain. The tap at the base of the drain

(D) can now be opened to expel the solution. Repeat this process with solutions containing the insoluble nitrides.

11. Add distilled water to the bottles of condensate to bring their fluid weight to 90 gms. Prepare a zero ammonia solution and zero the colourimeter. Add 2 mls of Nesslers reagent to each bottle, shake and allow to stand for 15 minutes. Measure the optical intensity of each solution, and determine the equivalent ammonia concentration of the solution from the calibration curve for the reagent. Determine the nitrogen concentration of each sample by dividing the weight of nitrogen in the sample (1 ml of ammonia solution = 0.0000175 gms) by the weight of the sample that was dissolved.

The measurement of soluble nitrogen by this method is accurate and repeatable. This is not true for the soluble nitrogen. If an overall picture of the nitrogen morphology of the steel sample is required, it is recommended that both the standard and alternate techniques of analysis be used. Total nitrogen content can be given by the standard technique, soluble nitrogen by the alternate technique, and insoluble nitrogen can be calculated as the difference between these two values.

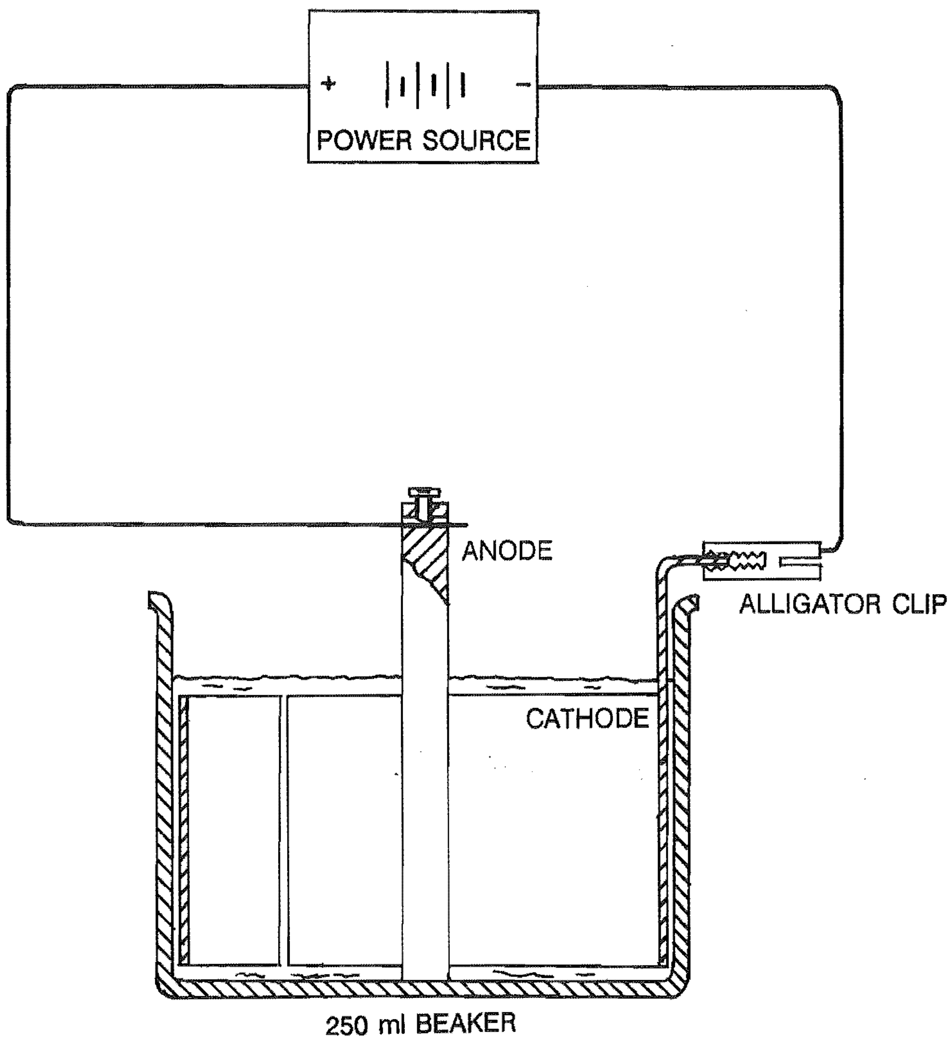

Figure B.1 Dissolution cell - alternate nitrogen analysis.

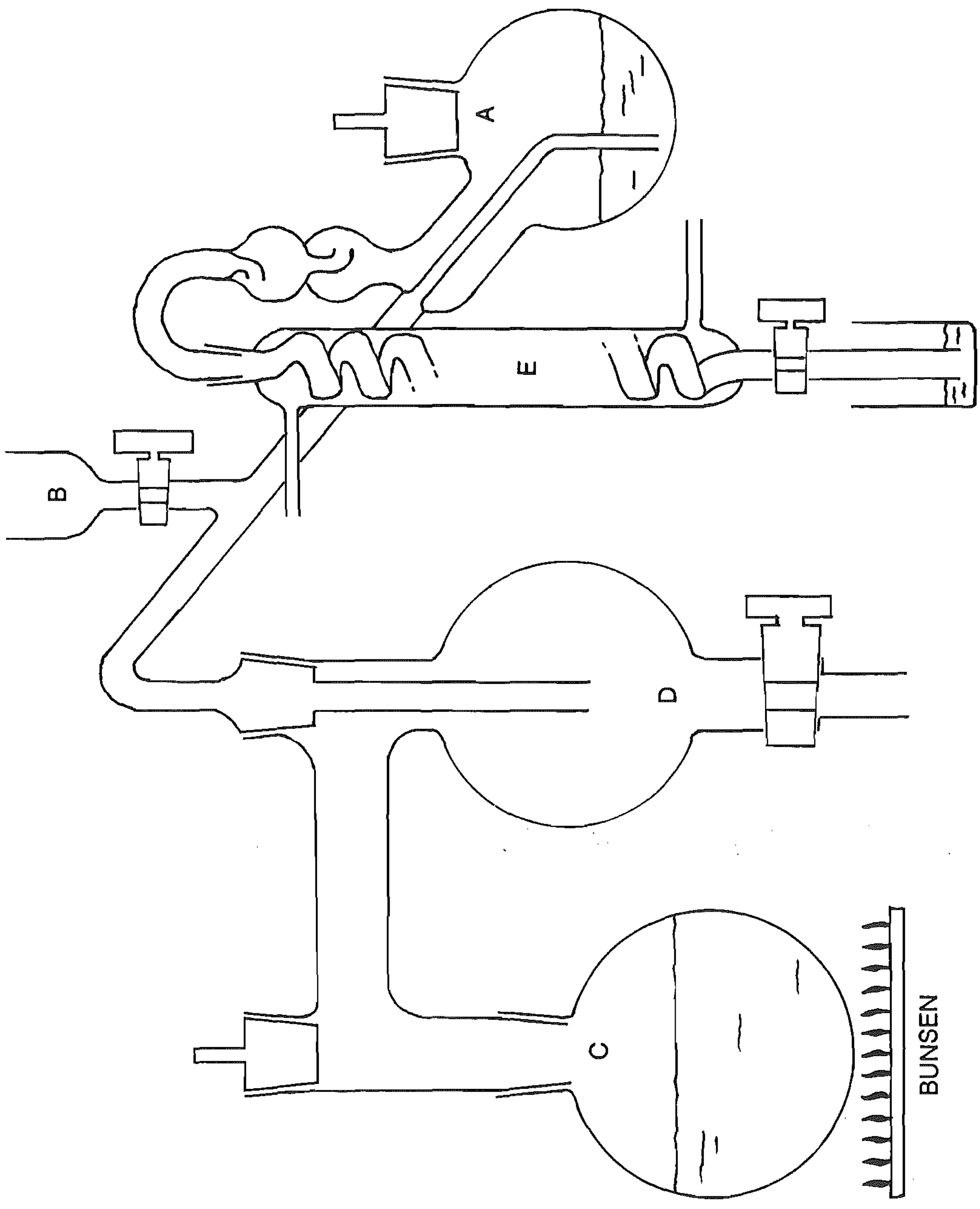

Figure B.2 Steam distillation apparatus for determination of nitrogen in steel.

Appendix C.

Charpy Transition Temperature Curves - Sample Set 1.

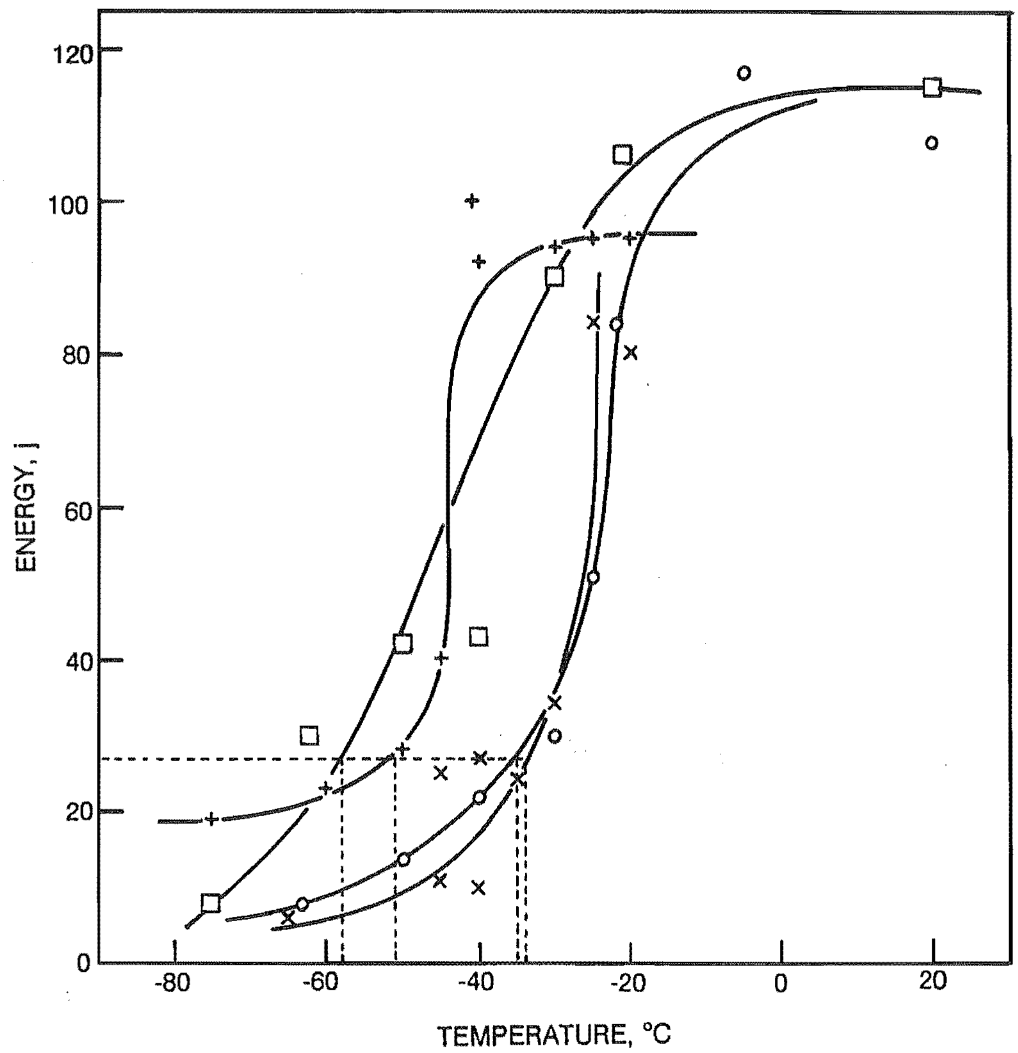

Sample 50.

(o) Approximate rolling temperature of 1100 °C, fast cooling rate applied.

(×) Approximate rolling temperature of 1100 °C, slow cooling rate applied.

(□) Approximate rolling temperature of 1000 °C, fast cooling rate applied.

(+) Approximate rolling temperature of 1000 °C, slow cooling rate applied.

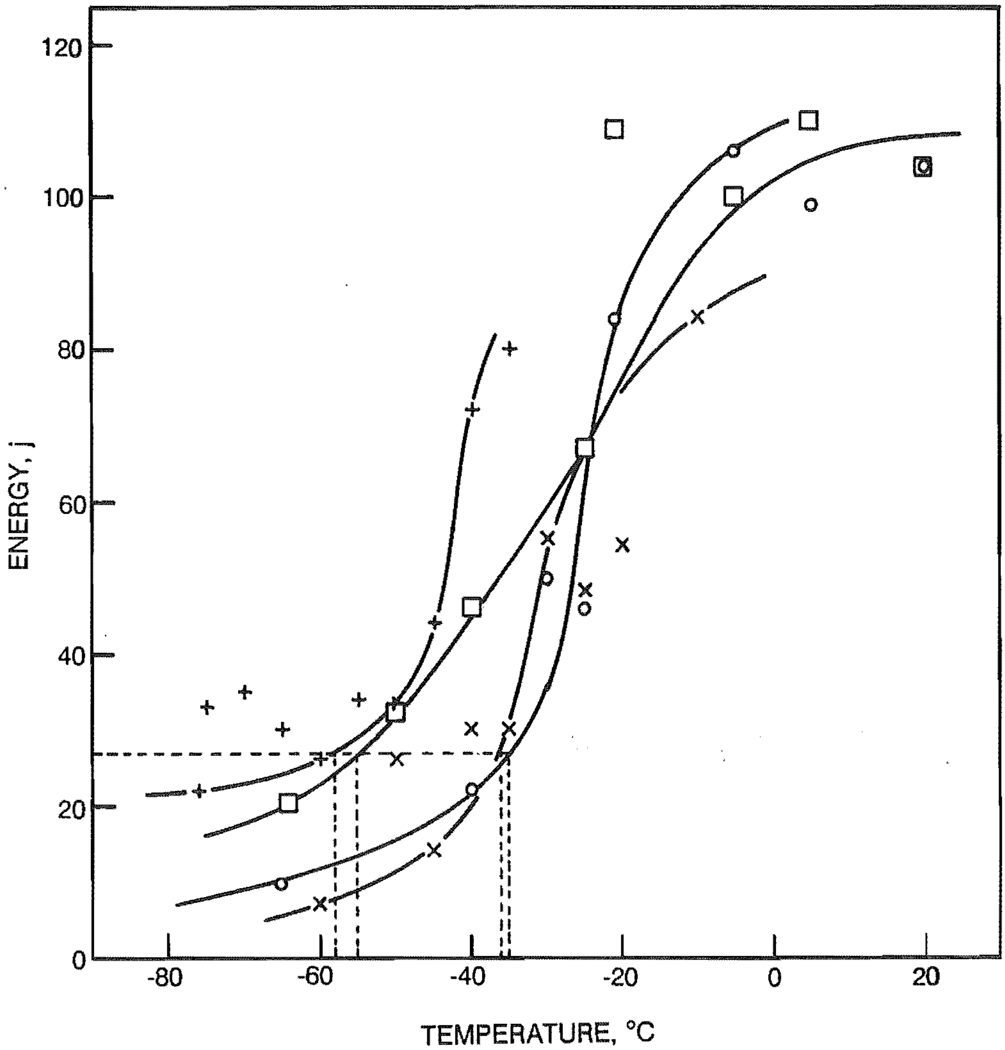

Sample 8.

(o) Approximate rolling temperature of 1100 °C, fast cooling rate applied.

(x) Approximate rolling temperature of 1100 °C, slow cooling rate applied.

(□) Approximate rolling temperature of 1000 °C, fast cooling rate applied.

(+) Approximate rolling temperature of 1000 °C, slow cooling rate applied.

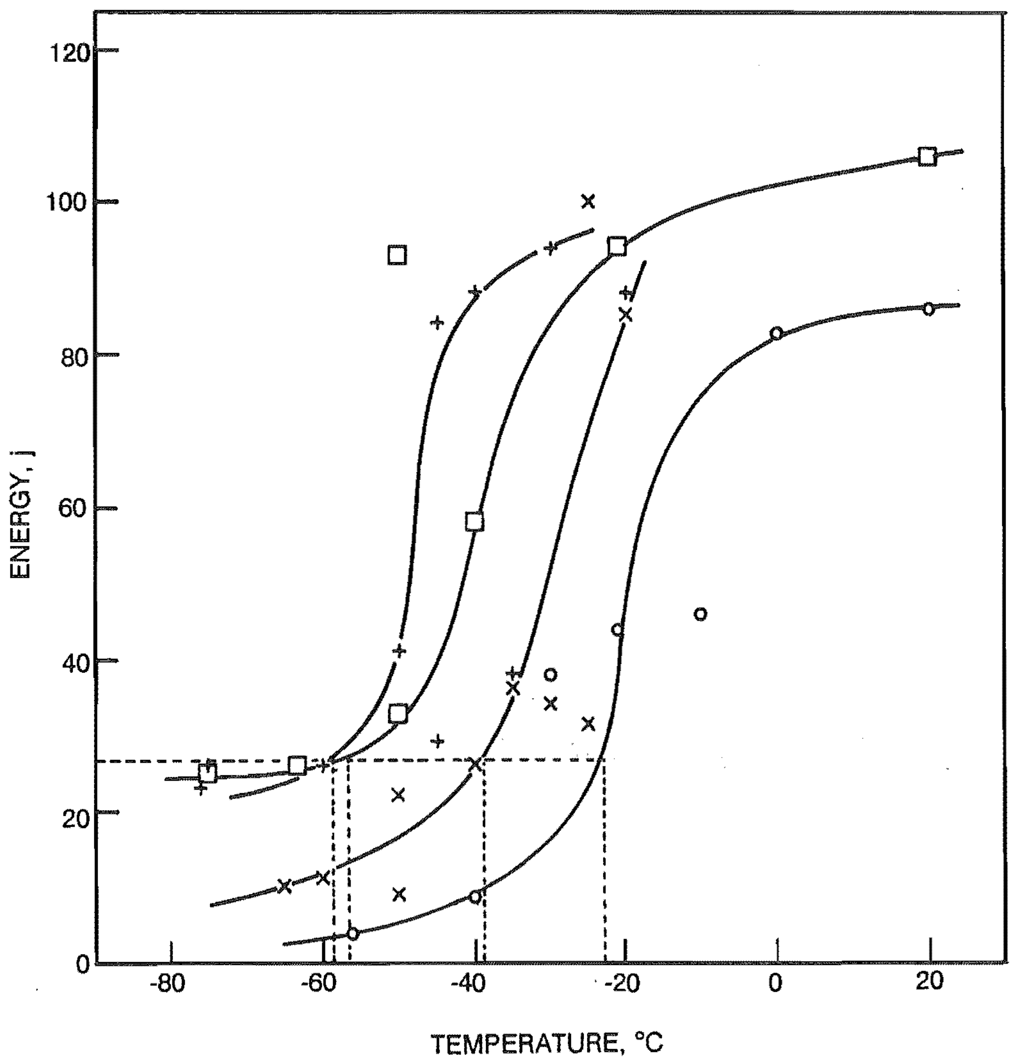

Sample 27.

(o) Approximate rolling temperature of 1100 °C, fast cooling rate applied.

(x) Approximate rolling temperature of 1100 °C, slow cooling rate applied.

(□) Approximate rolling temperature of 1000 °C, fast cooling rate applied.

(+) Approximate rolling temperature of 1000 °C, slow cooling rate applied.

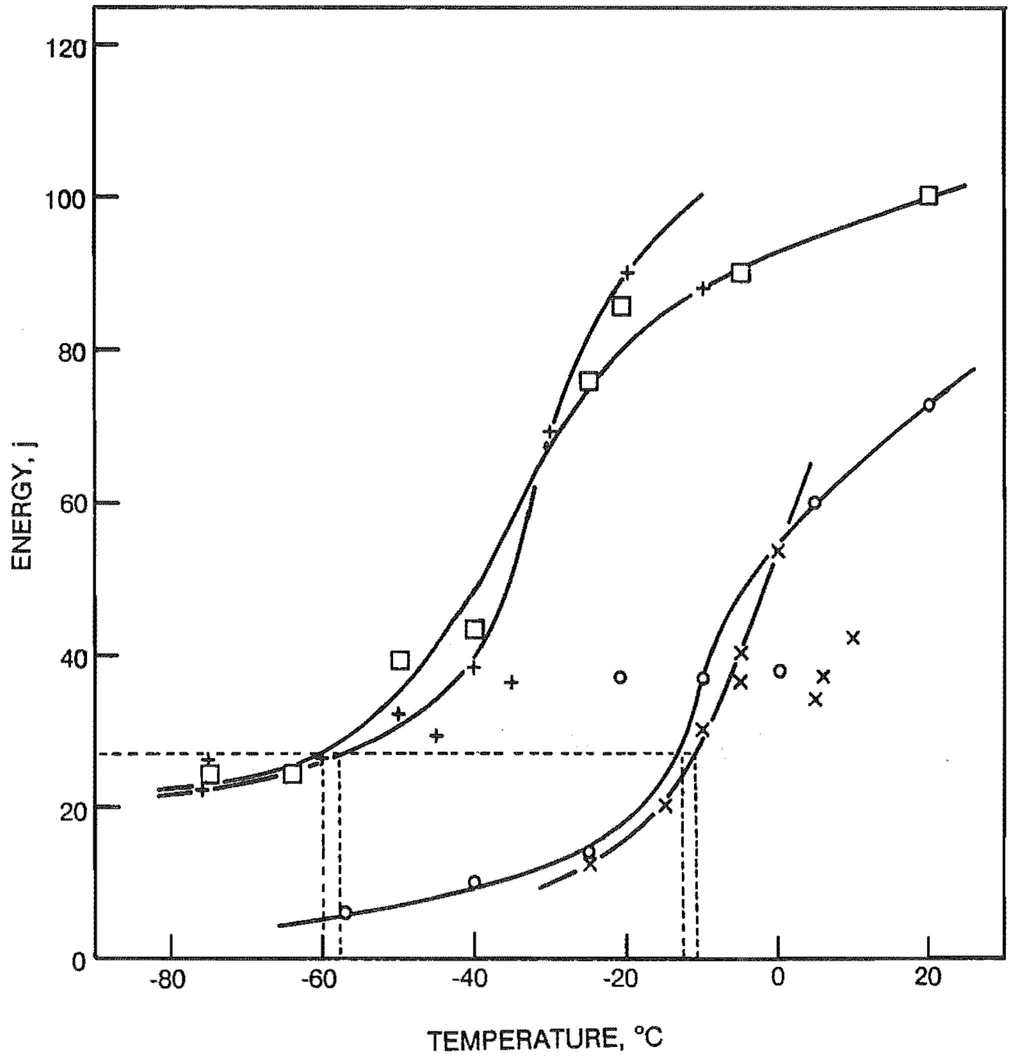

Sample 19.

(o) Approximate rolling temperature of 1100 °C, fast cooling rate applied.
(×) Approximate rolling temperature of 1100 °C, slow cooling rate applied.
(□) Approximate rolling temperature of 1000 °C, fast cooling rate applied.
(+) Approximate rolling temperature of 1000 °C, slow cooling rate applied.

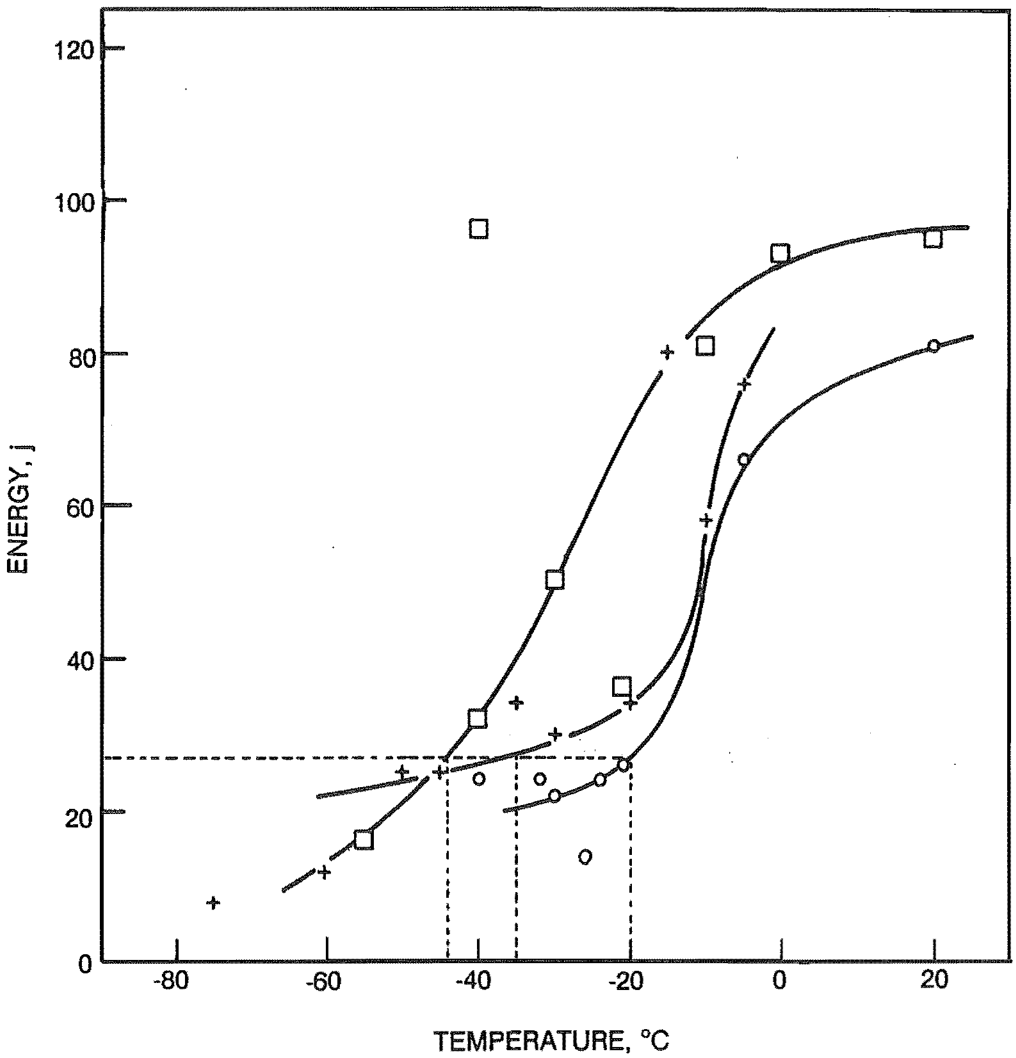

Sample 33.

(o) Approximate rolling temperature of 1100 °C, fast cooling rate applied.
(x) Approximate rolling temperature of 1100 °C, slow cooling rate applied.
(□) Approximate rolling temperature of 1000 °C, fast cooling rate applied.
(+) Approximate rolling temperature of 1000 °C, slow cooling rate applied.